Supplement of Earth Syst. Dynam., 9, 915–937, 2018
https://doi.org/10.5194/esd-9-915-2018-supplement

Earth System Dynamics
Open Access

Supplement of

Recent changes of relative humidity: regional connections with land and ocean processes

Sergio M. Vicente-Serrano et al.

Correspondence to: Sergio M. Vicente-Serrano (svicen@ipe.csic.es)

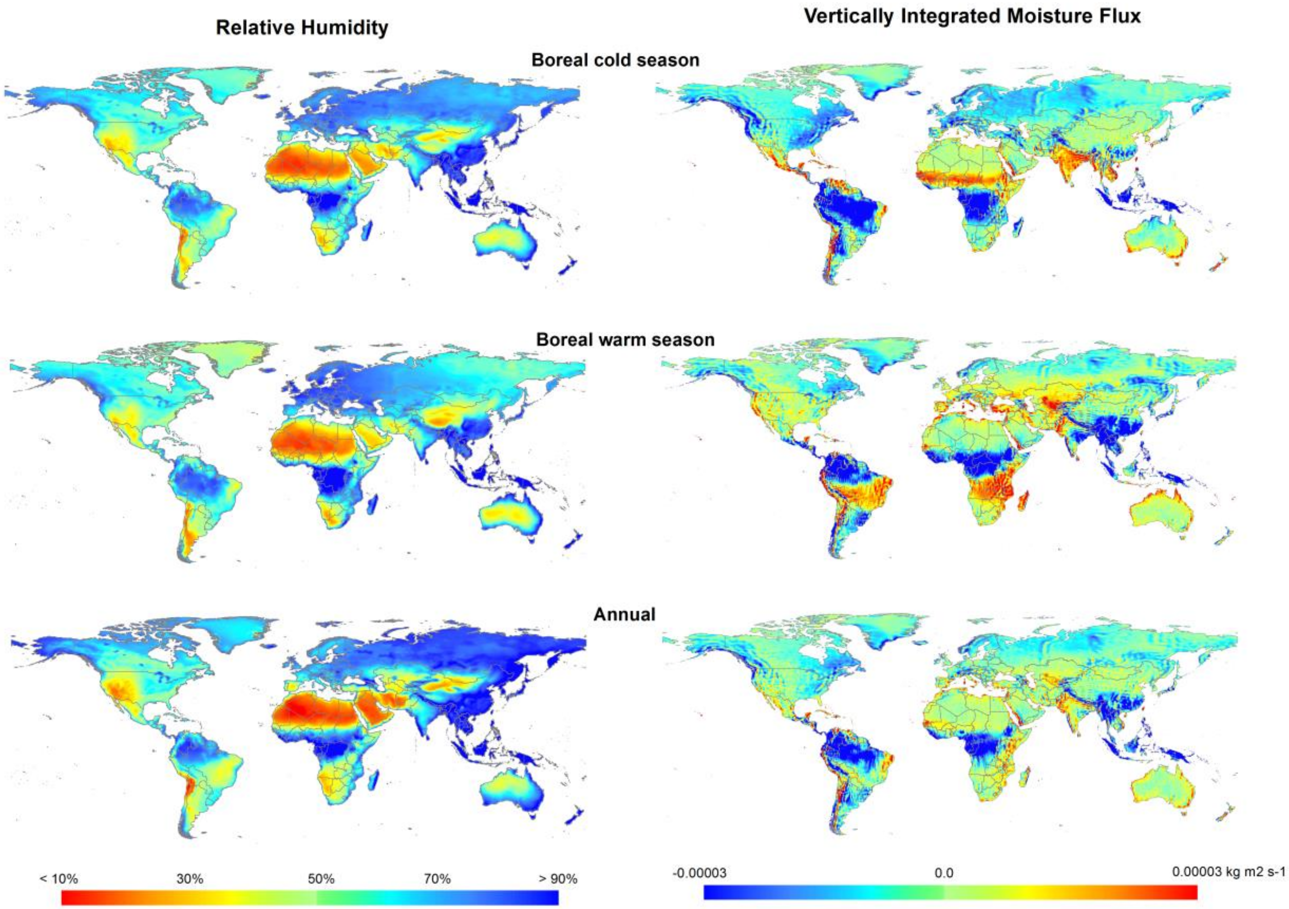

Figure S1. Annual and seasonal averages of RH and Vertically Moisture Flux (VMF) based on ERA-Interim dataset. RH shows higher average values over equatorial regions, Southeast Asia and the North Eurasia region. The lower values are recorded over tropical regions, mainly in the North Hemisphere. Spatial differences between the cold and warm seasons are very low. The annual pattern of the VIFM over continents shows that precipitation exceeds evaporation over the Intertropical Convergence Zone, Southeast Asia and the islands between the Pacific and Indian Oceans (Maritime continent), a great part of South America, Central America, Central Africa, and northward to 40ºN in the Northern Hemisphere. Evaporation is higher than precipitation over the main area of Australia, the Pacific coast of North America, Northeast Brazil, areas around the Mediterranean Sea, eastern coast of Africa and southwest Asia. Seasonally it is evident the poleward movement of the ITCZ during the hemispheric summer, and the change of the pattern over North America and Eurasian continent.

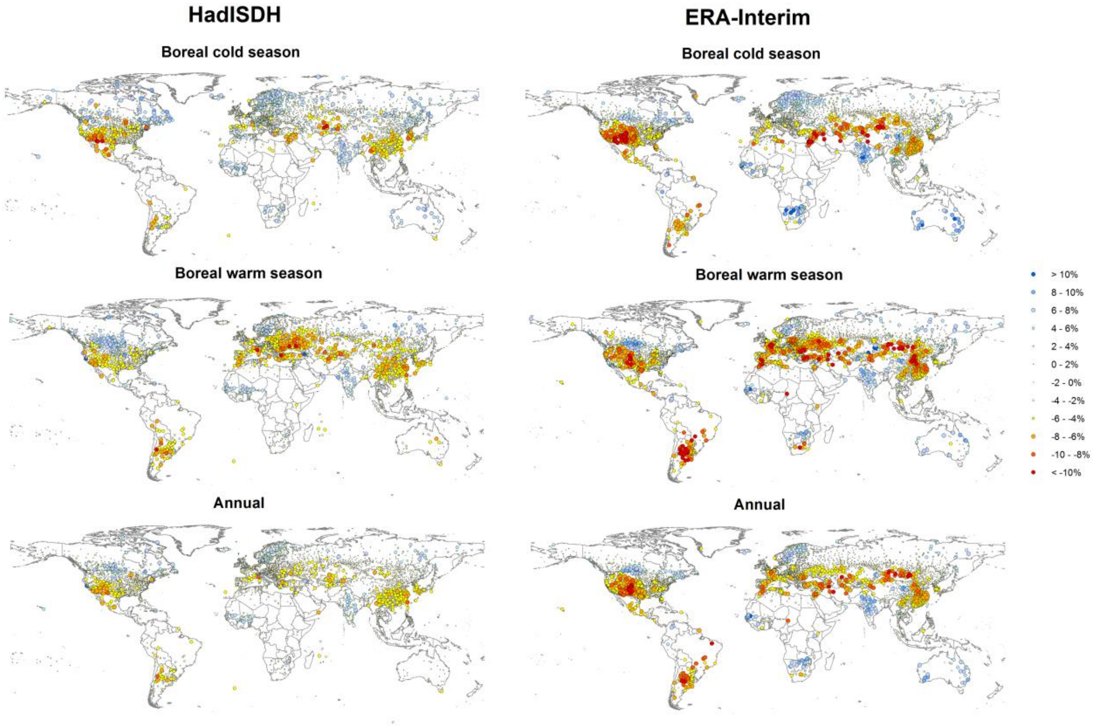

Figure S2: Spatial distribution of the magnitude of change of RH (% per decade) over the period 1979-2014 from HadISDH (left) and ERA-Interim dataset (right) considering the points with available HadISDH observatories. In the boreal cold season, the most marked decrease was observed in the Southwest and areas of Northeast North America, central Argentina, the Fertile Crescent region in western Asia, Kazakhstan, as well as in the eastern China and the Korea Peninsula. On the other hand, the dominant RH increase was recorded in larger areas, including most of Canada (mostly in the Labrador Peninsula), and large areas of North and central Europe and India. While the density of complete and homogeneous RH series is low, we found a dominant positive trend across the western Sahel and South Africa.

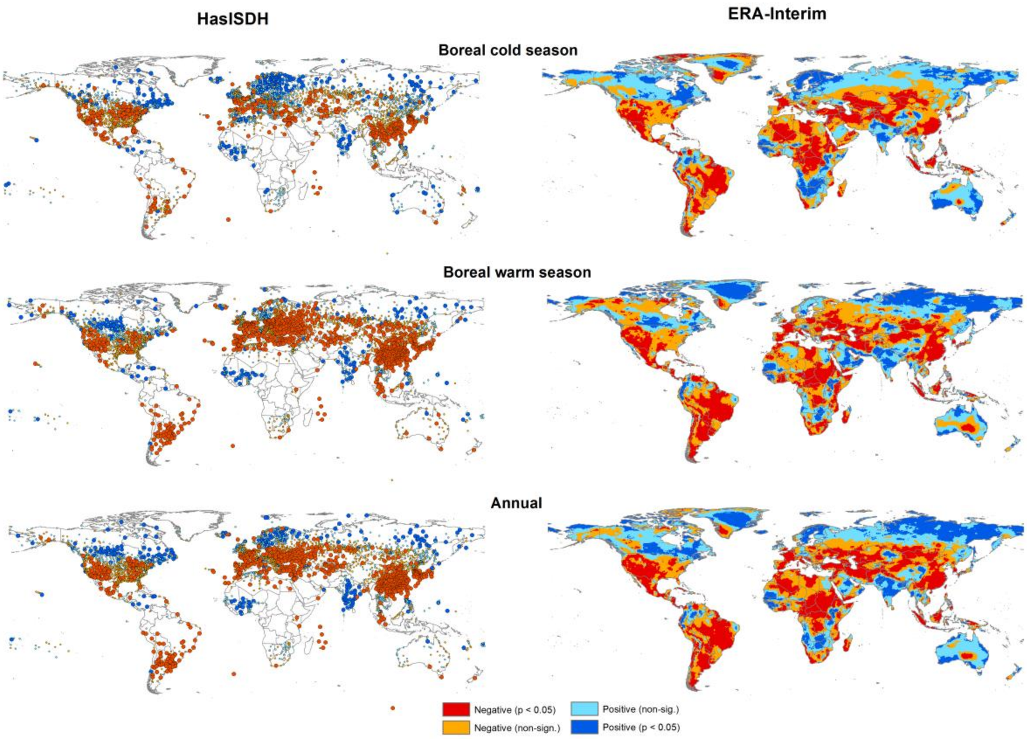

Figure S3. Annual and seasonal statistical significance of RH trend from HadISDH and ERA-Interim for 1979-2014.

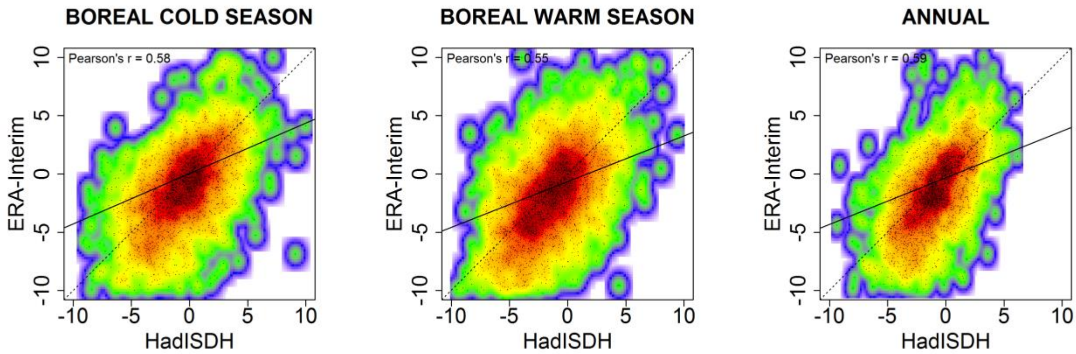

Figure S4: Scatterplots showing the global relationship between the magnitude of change in RH with HadISDH stations and ERA-Interim dataset at the seasonal and annual scales. Colors represent the density of points, with red color showing the highest density of points.

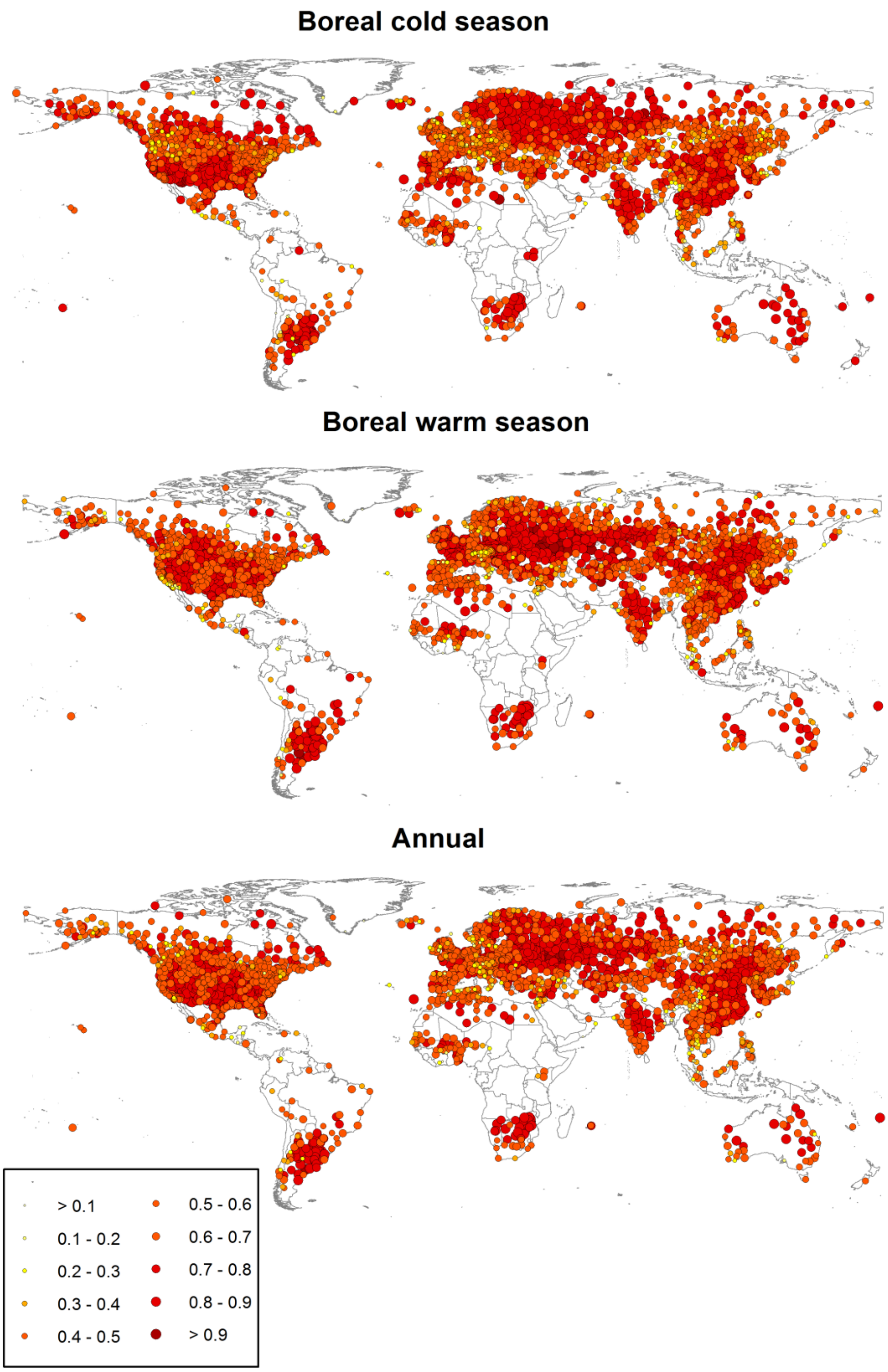

Figure S5. Spatial distribution of the Person's r between HadISDH and ERA-Interim RH at the seasonal and annual scales

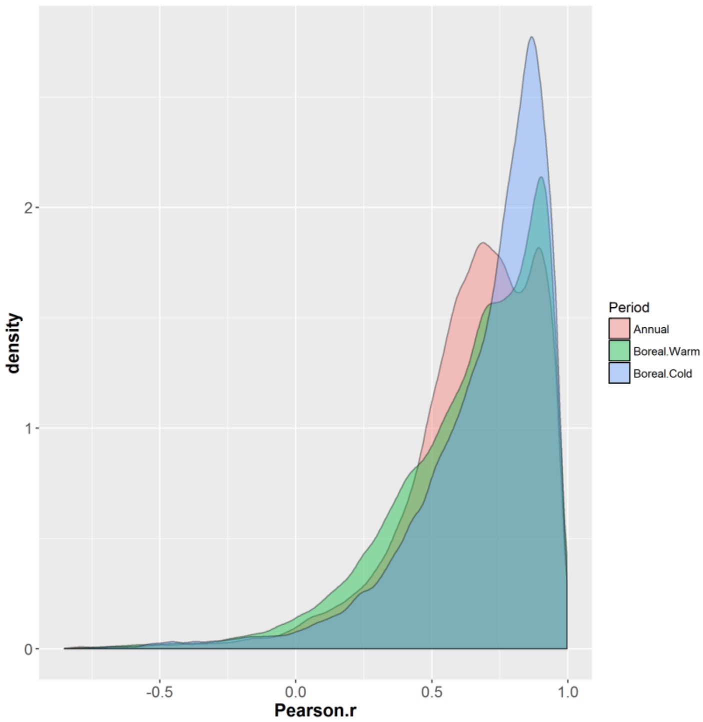

Figure S6. Frequency density plots of the Pearson's r coefficients between the HadISDH and ERA-Interim RH annually and seasonally.

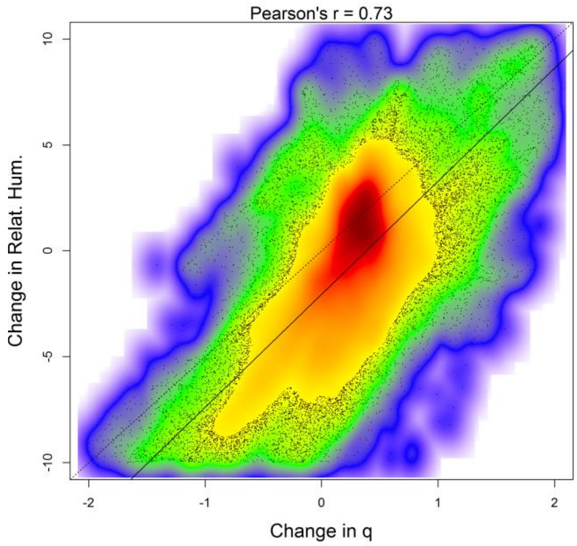

Figure S7: Scatterplot showing the global relationship between the annual magnitude of change in ERA-Interim q and the magnitude of change of RH. Colors represent the density of points with red color showing the highest density of points.

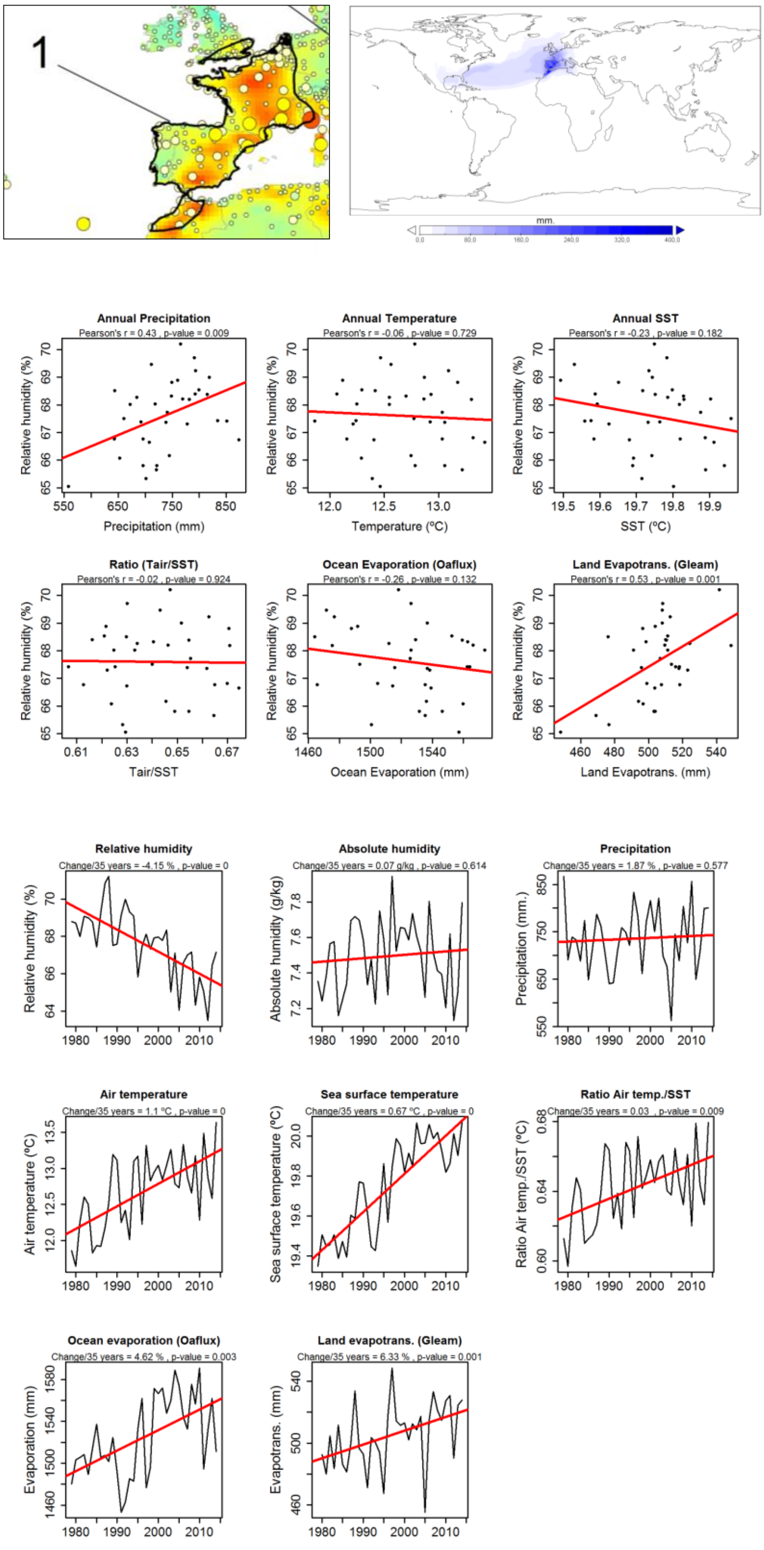

Figure S8: Top left: Annual RH humidity trends in the West Europe (region 1), top right: average E-P at the annual scale to identify the main humidity sources in the region. Center: Relationship between de-trended annual RH and de-trended annual variables between 1979 and 2014. Bottom: Annual evolution of the different variables corresponding to the West Europe region. The magnitude of change and signification of the trend is indicated for each variable.

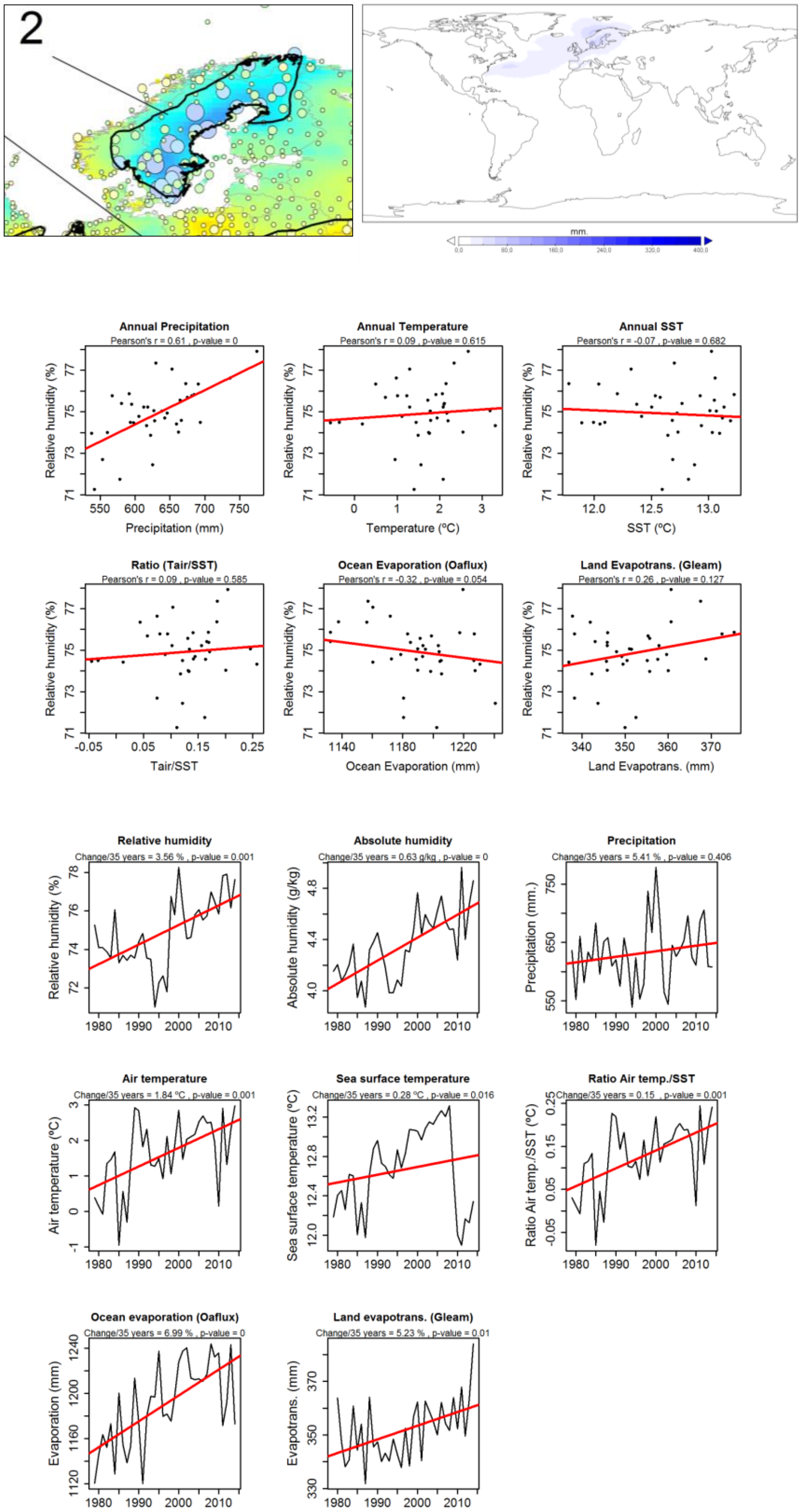

Figure S9: The same as Figure S8 but for Scandinavia (region 2).

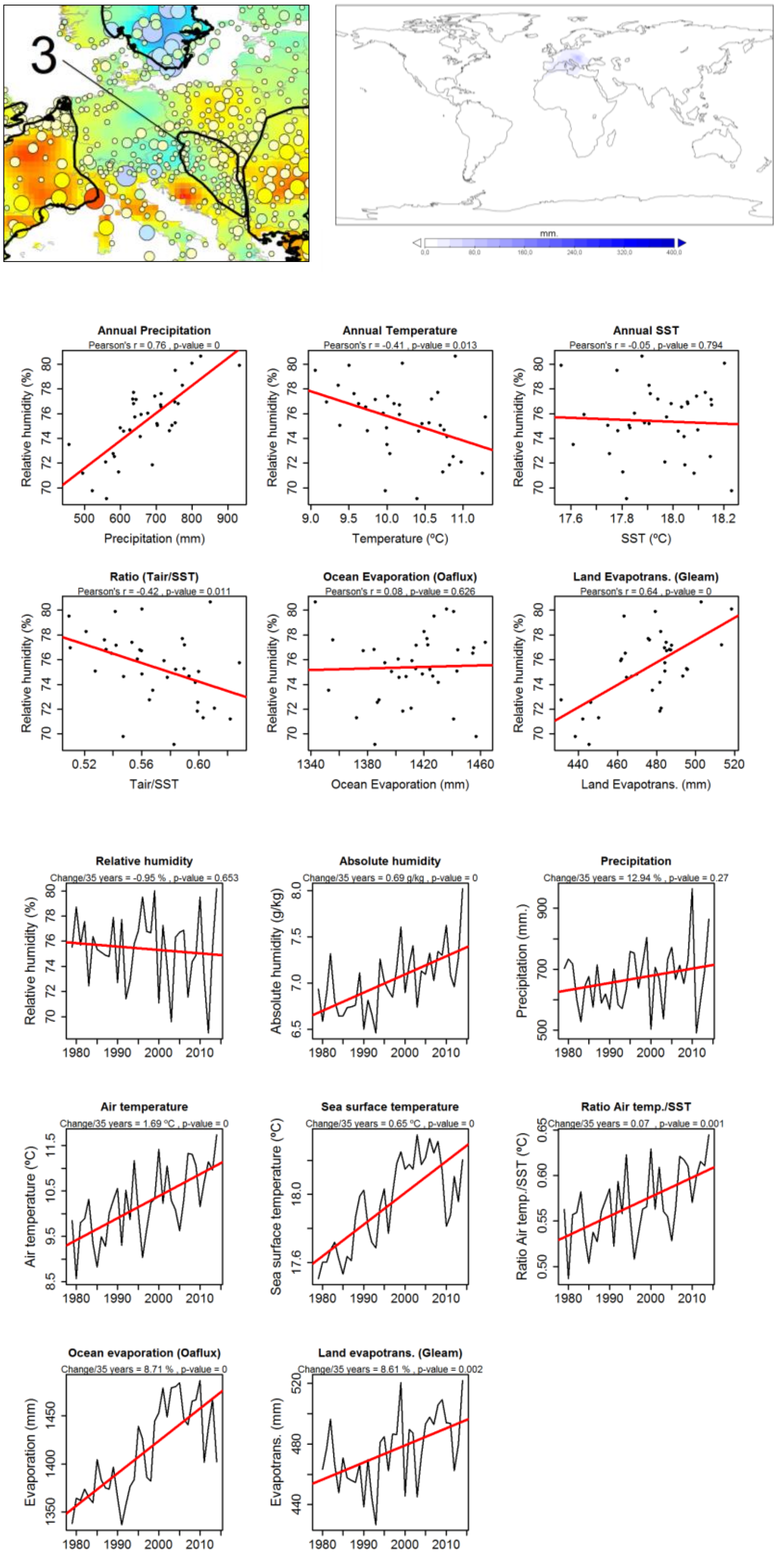

Figure S10: The same as Figure S8 but for Central-East Europe (region 3).

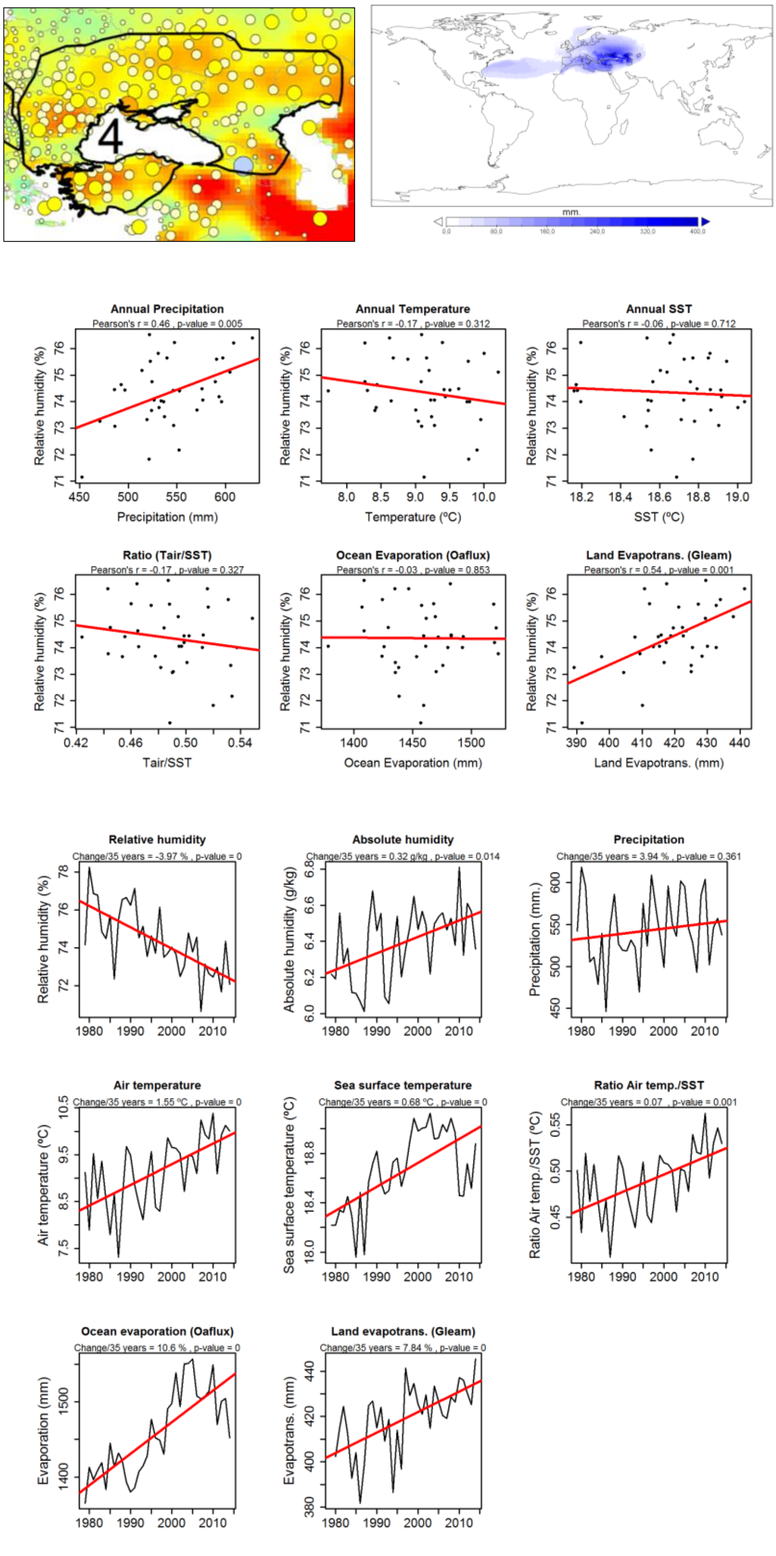

Figure S11: The same as Figure S8 but for South-East Europe and Turkey (region 4).

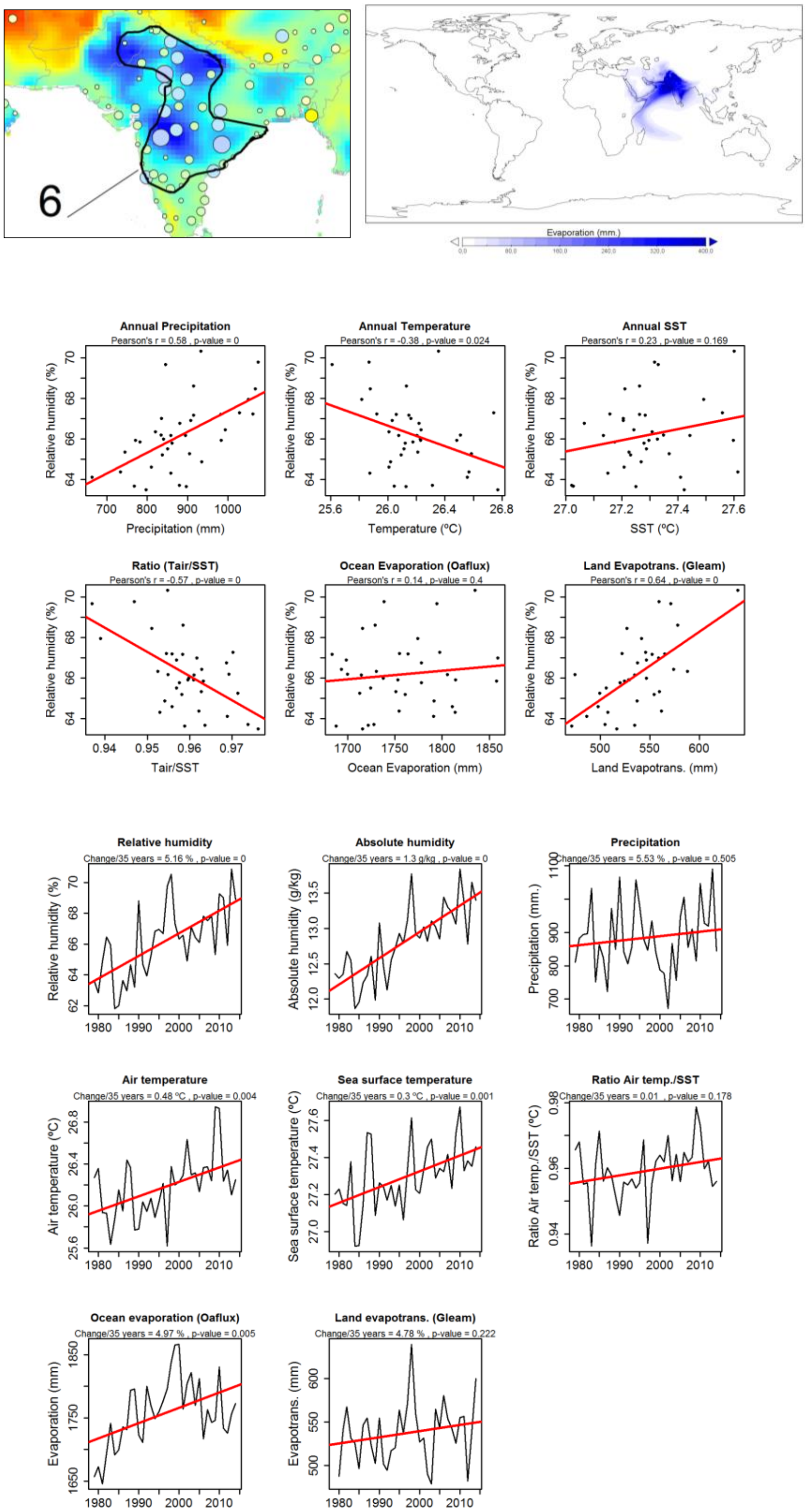

Figure S12: The same as Figure S8 but for India (region 6).

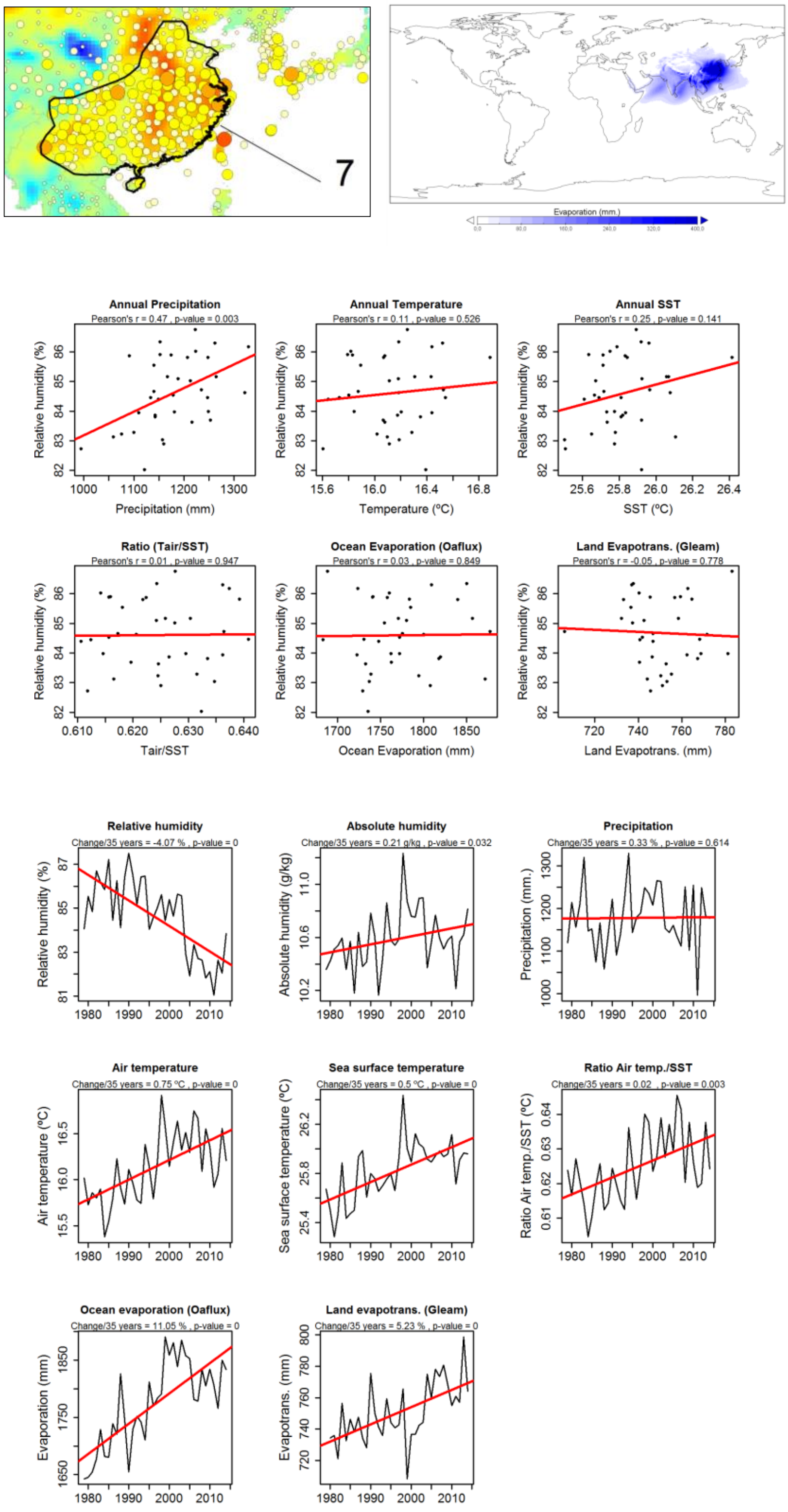

Figure S13: The same as Figure S8 but for East China (region 7).

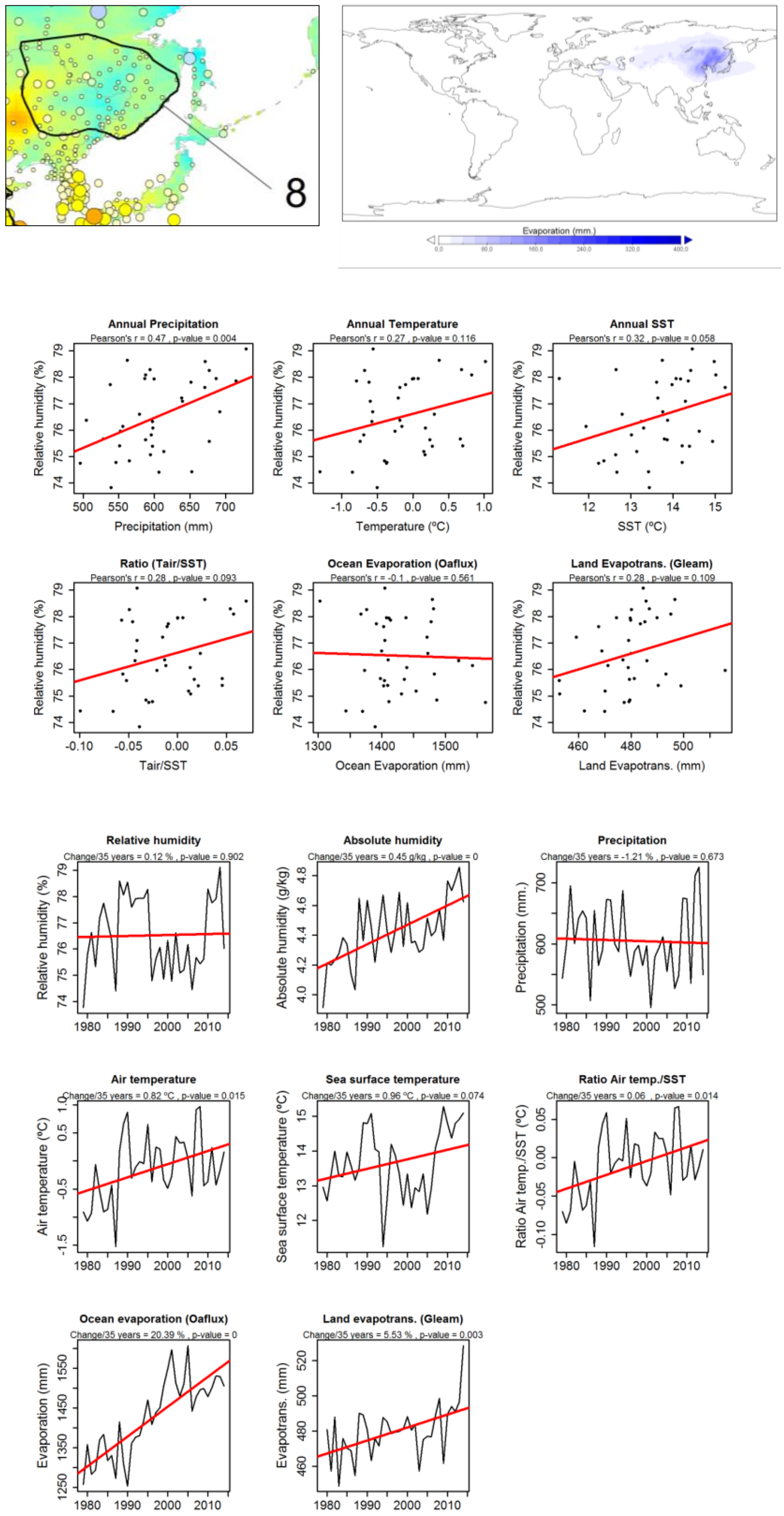

Figure S14: The same as Figure S8 but for North East Asia (region 8).

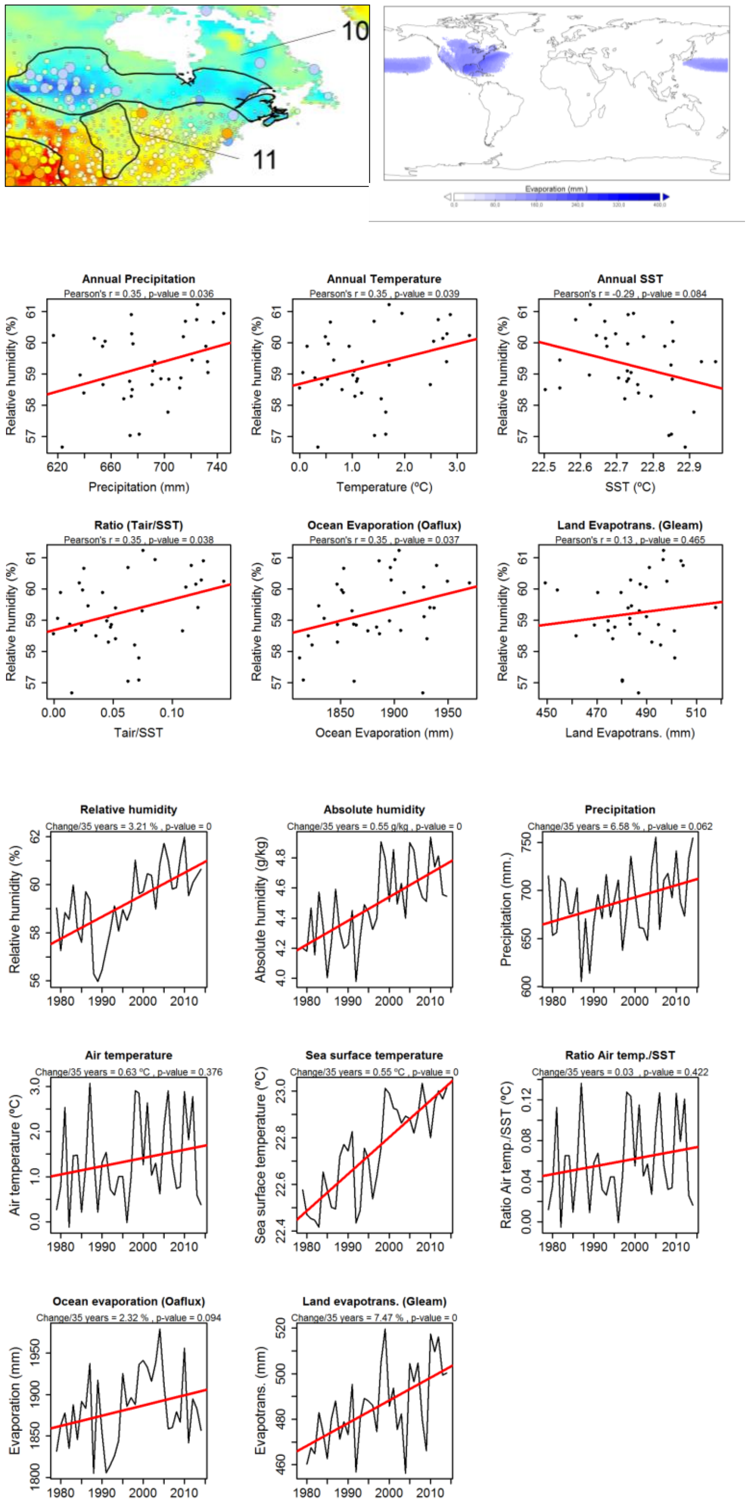

Figure S15: The same as Figure S8 but for Canada (region 10).

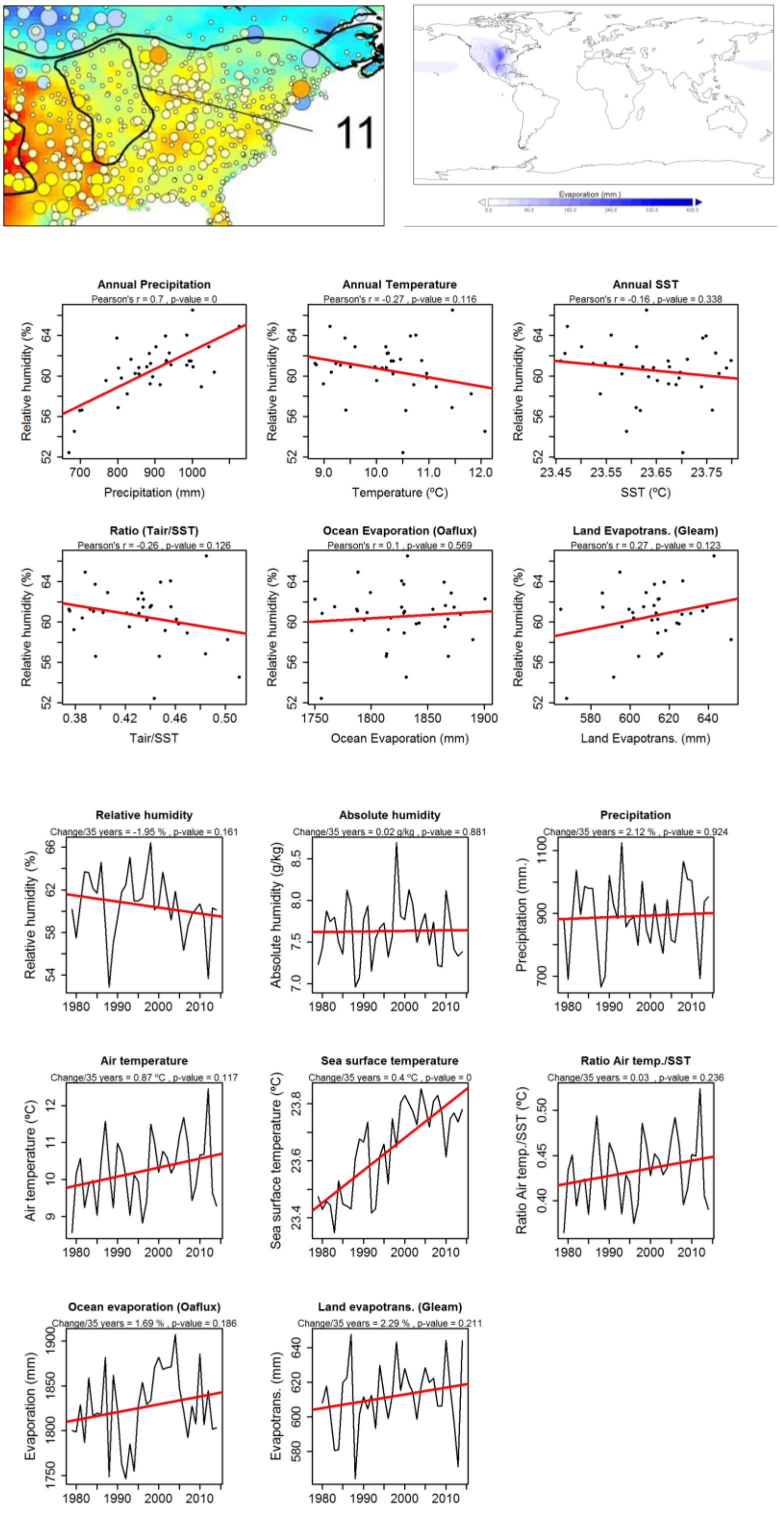

Figure S16: The same as Figure S8 but for central USA (region 11).

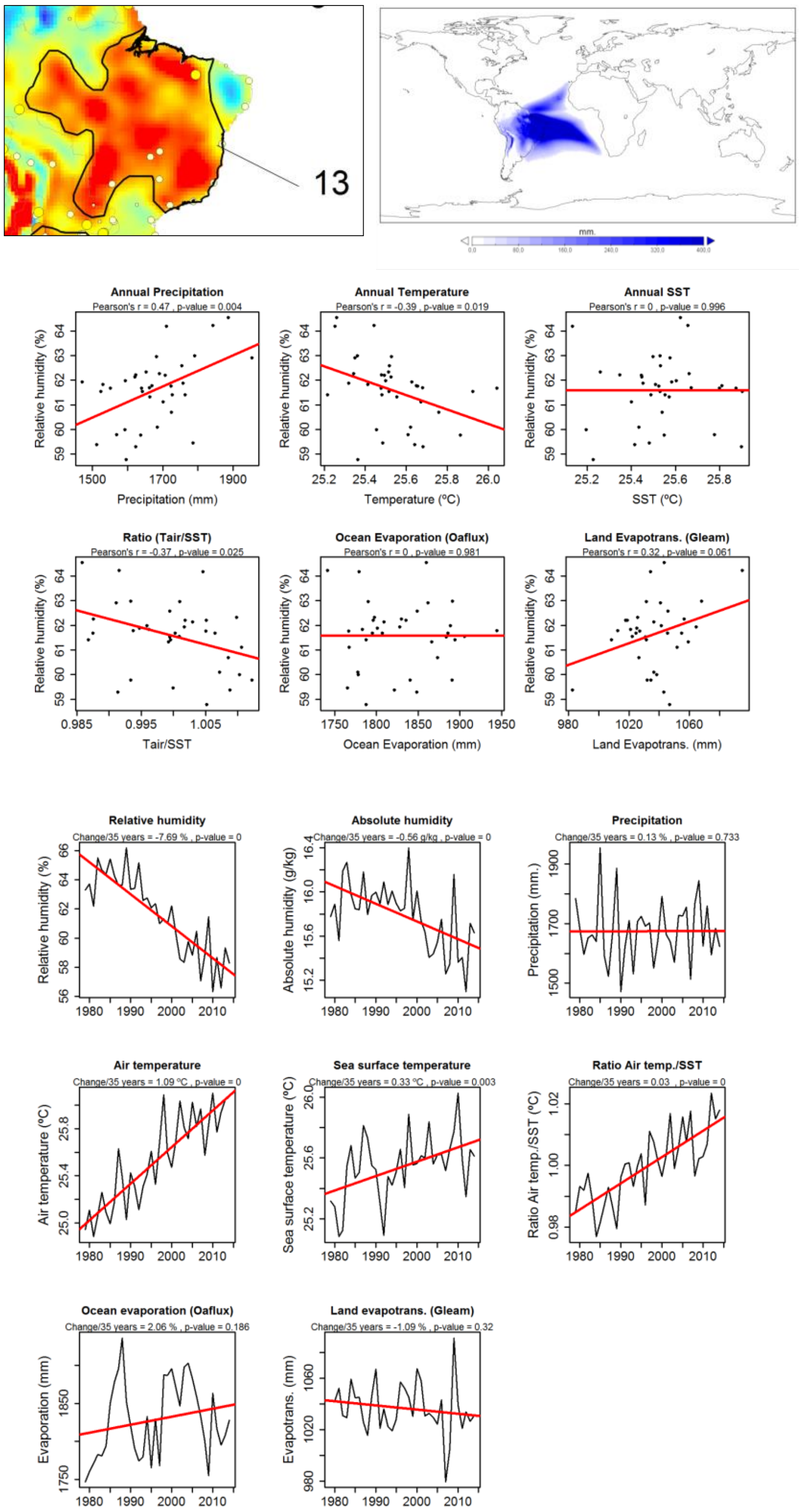

Figure S17: The same as Figure S8 but for Amazonian (region 13).

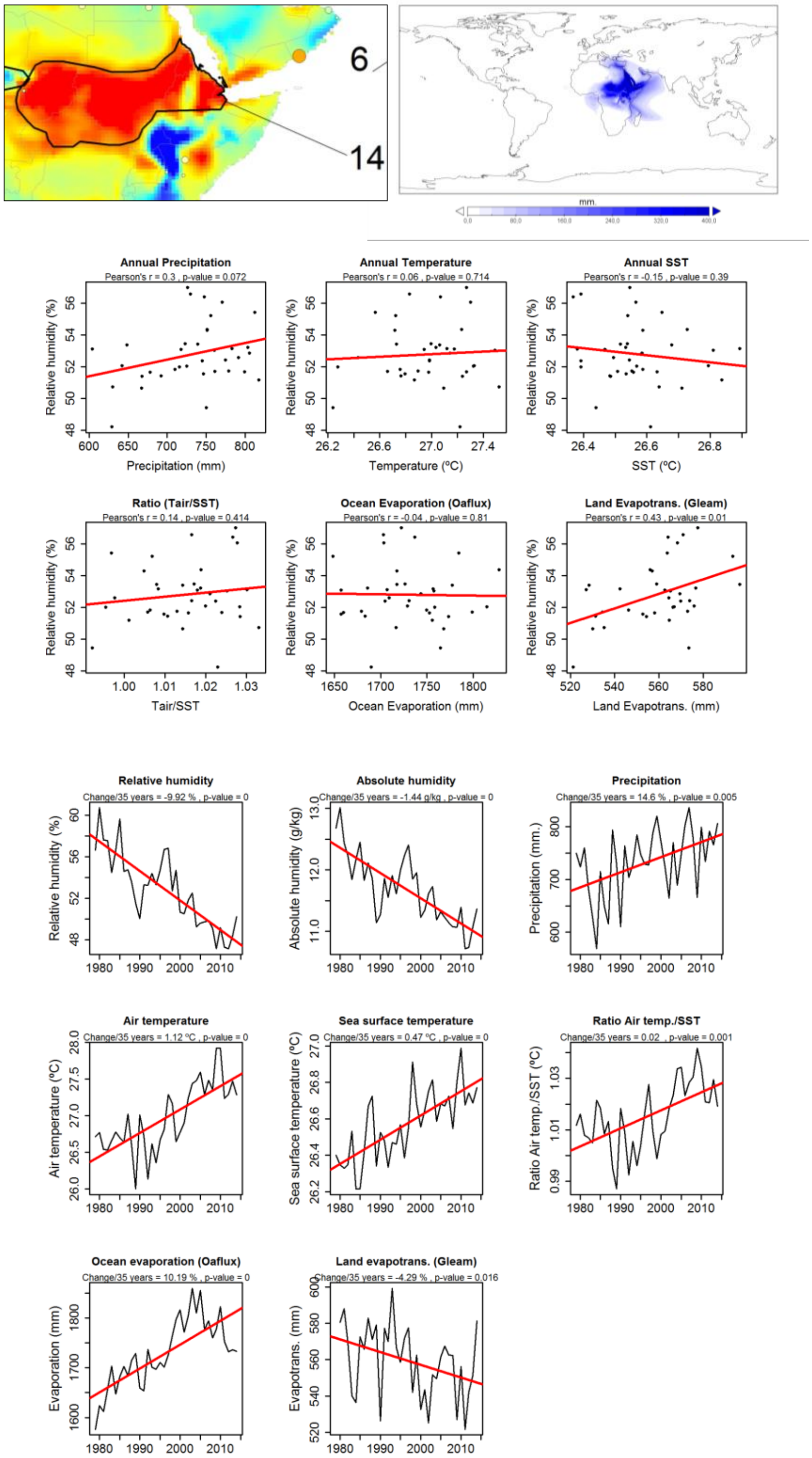

Figure S18: The same as Figure S8 but for East Sahel (region 14).

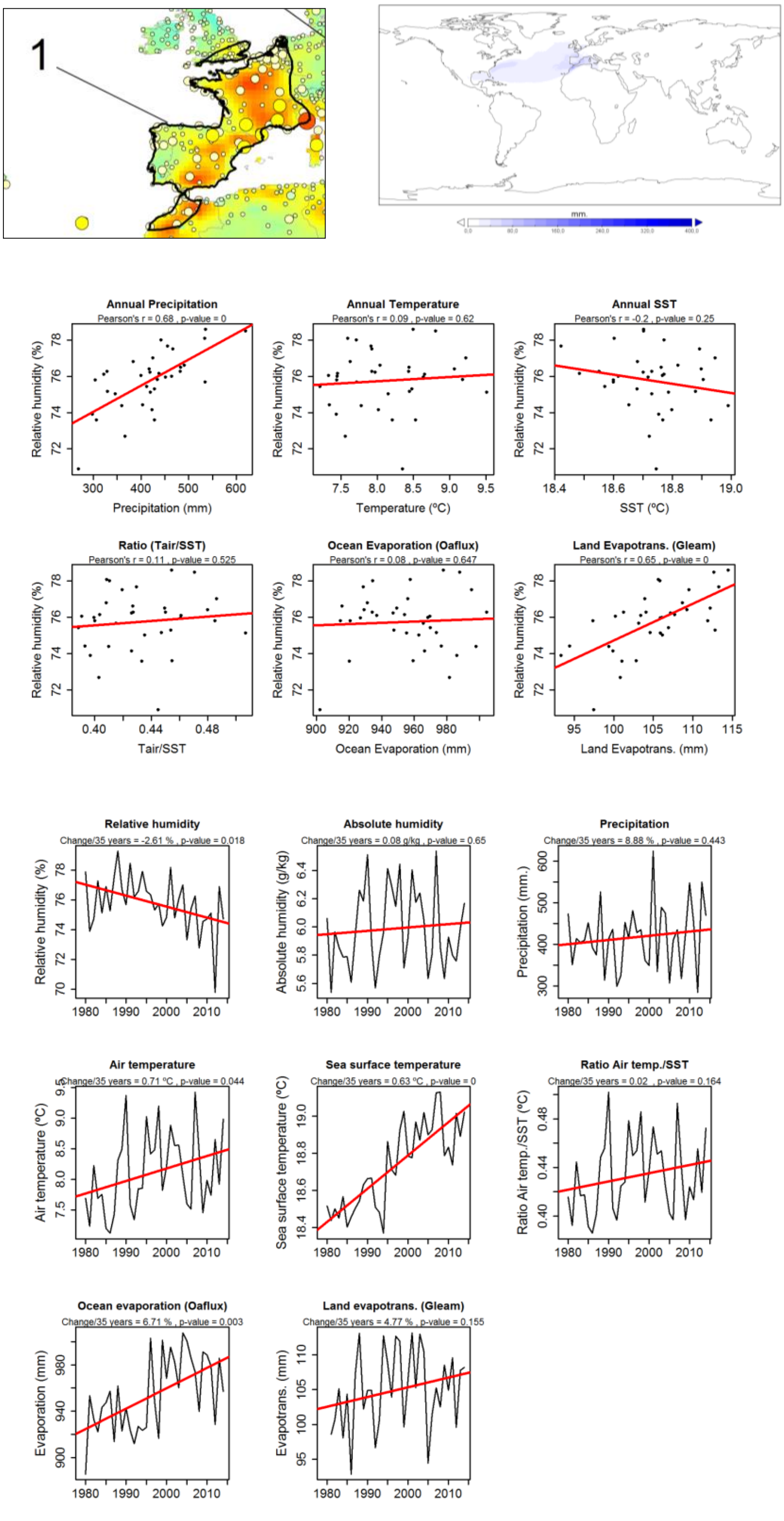

Figure S19: Top left: Boreal cold season RH humidity trends in West Europe (region 1), top right: average E-P in the boreal cold season to identify the main humidity sources in the region. Center: Relationship between de-trended cold season RH and de-trended cold season variables between 1979 and 2014. Bottom: Boreal cold season evolution of the different variables corresponding to West Europe region. The magnitude of change and signification of the trend is indicated for each variable.

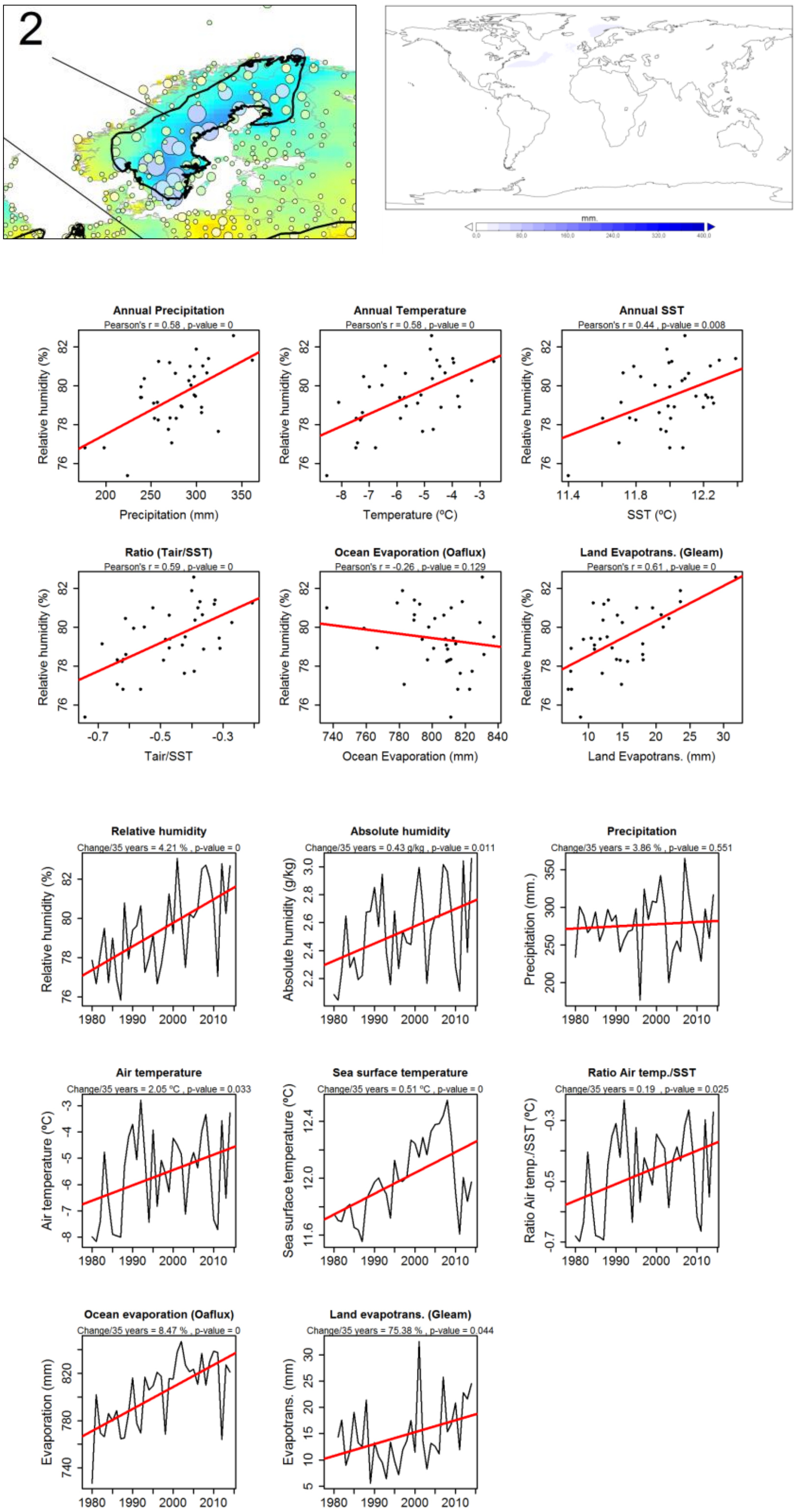

Figure S20: The same as Figure S19 but for Scandinavia (region 2).

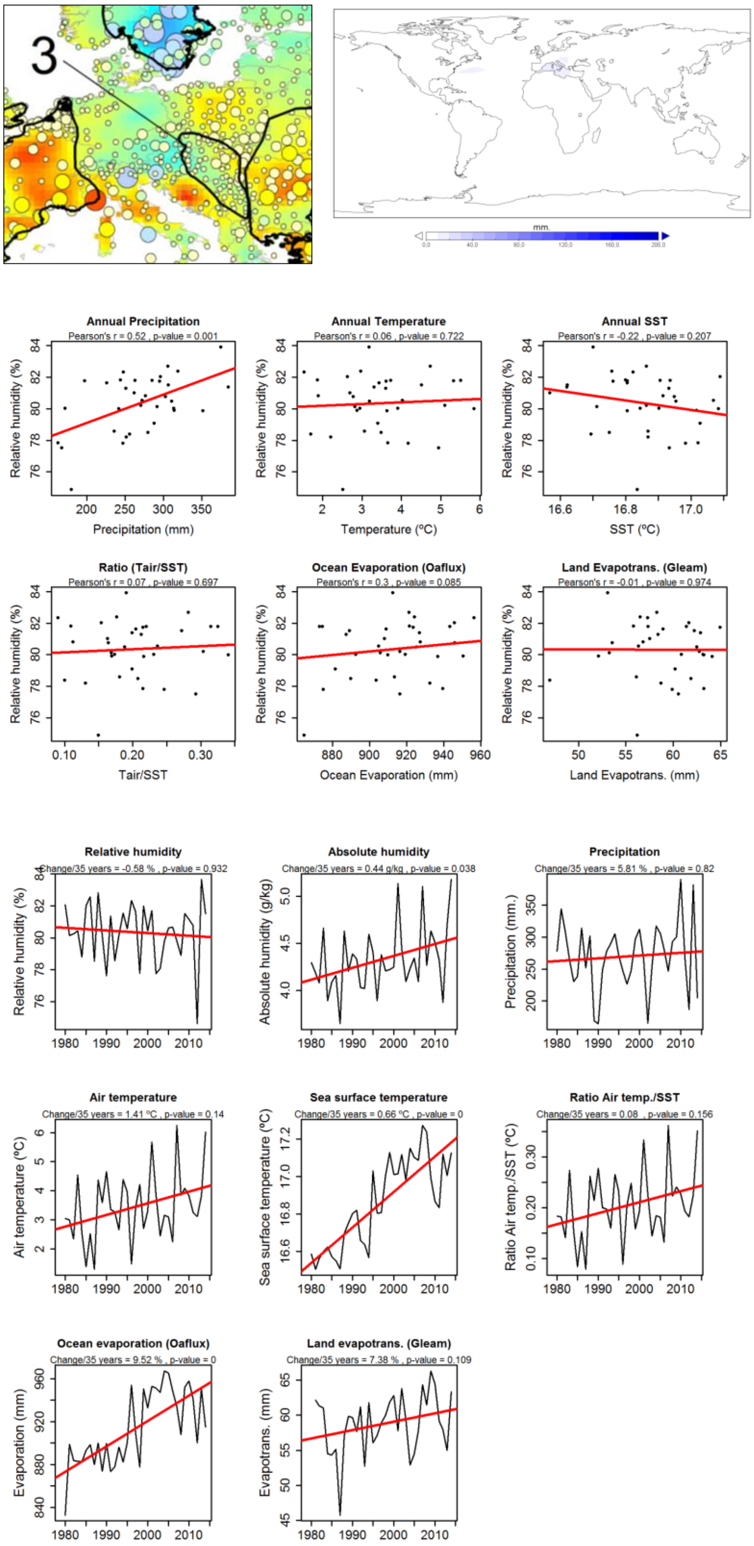

Figure S21: The same as Figure S19 but for Central-East Europe (region 3).

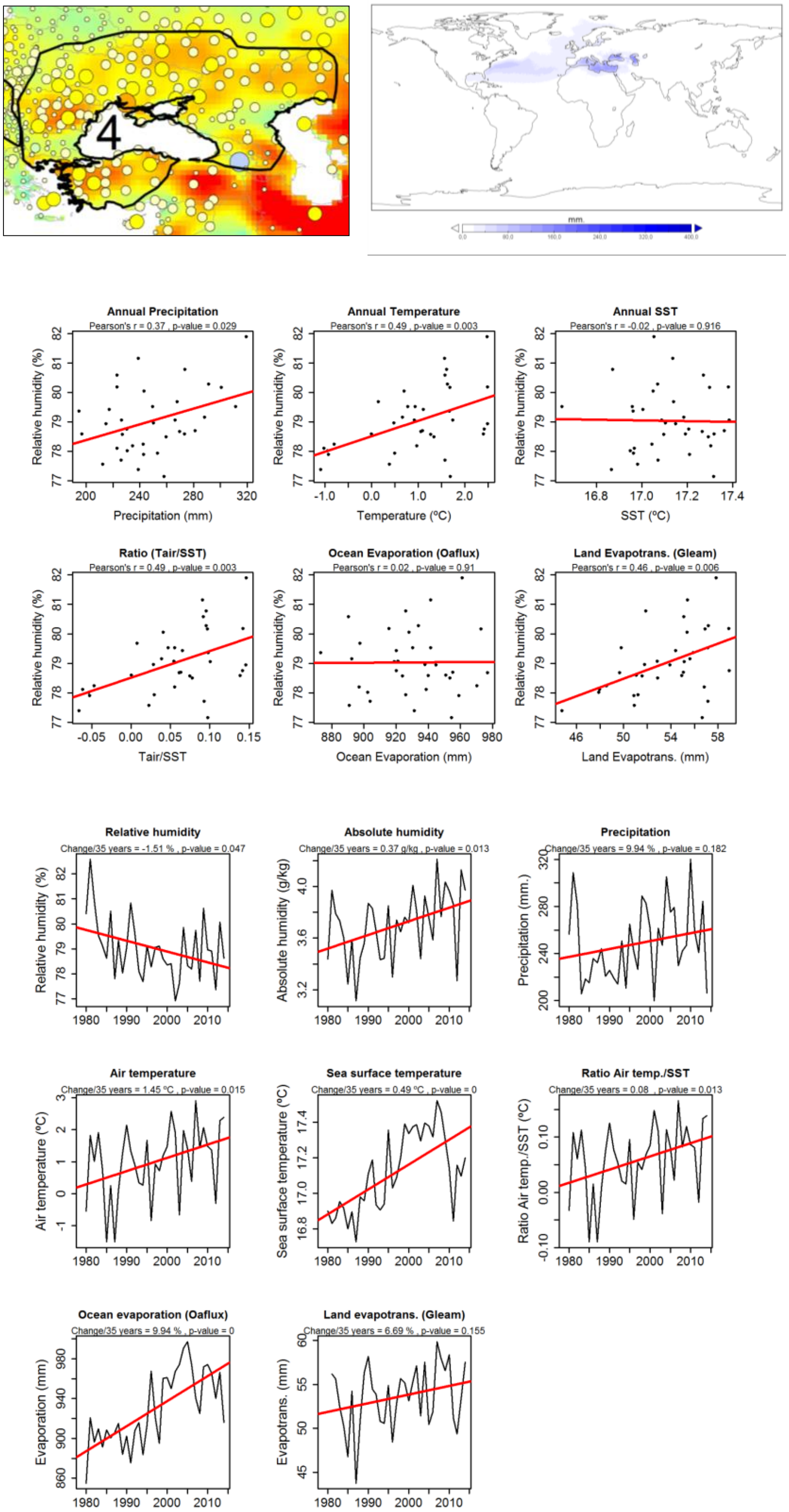

Figure S22: The same as Figure S19 but for South-East Europe and Turkey (region 4).

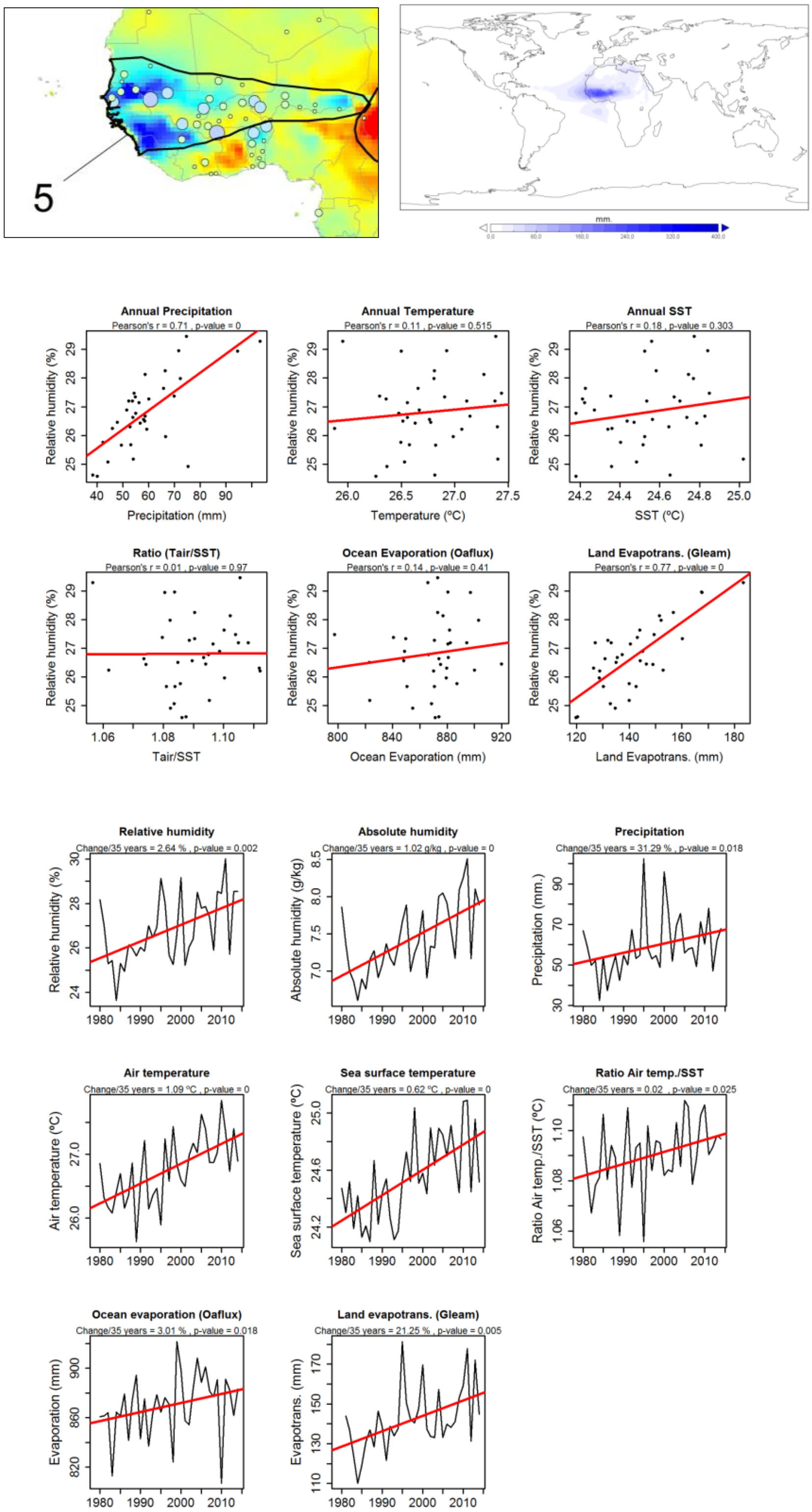

Figure S23: The same as Figure S19 but for West Sahel (region 6).

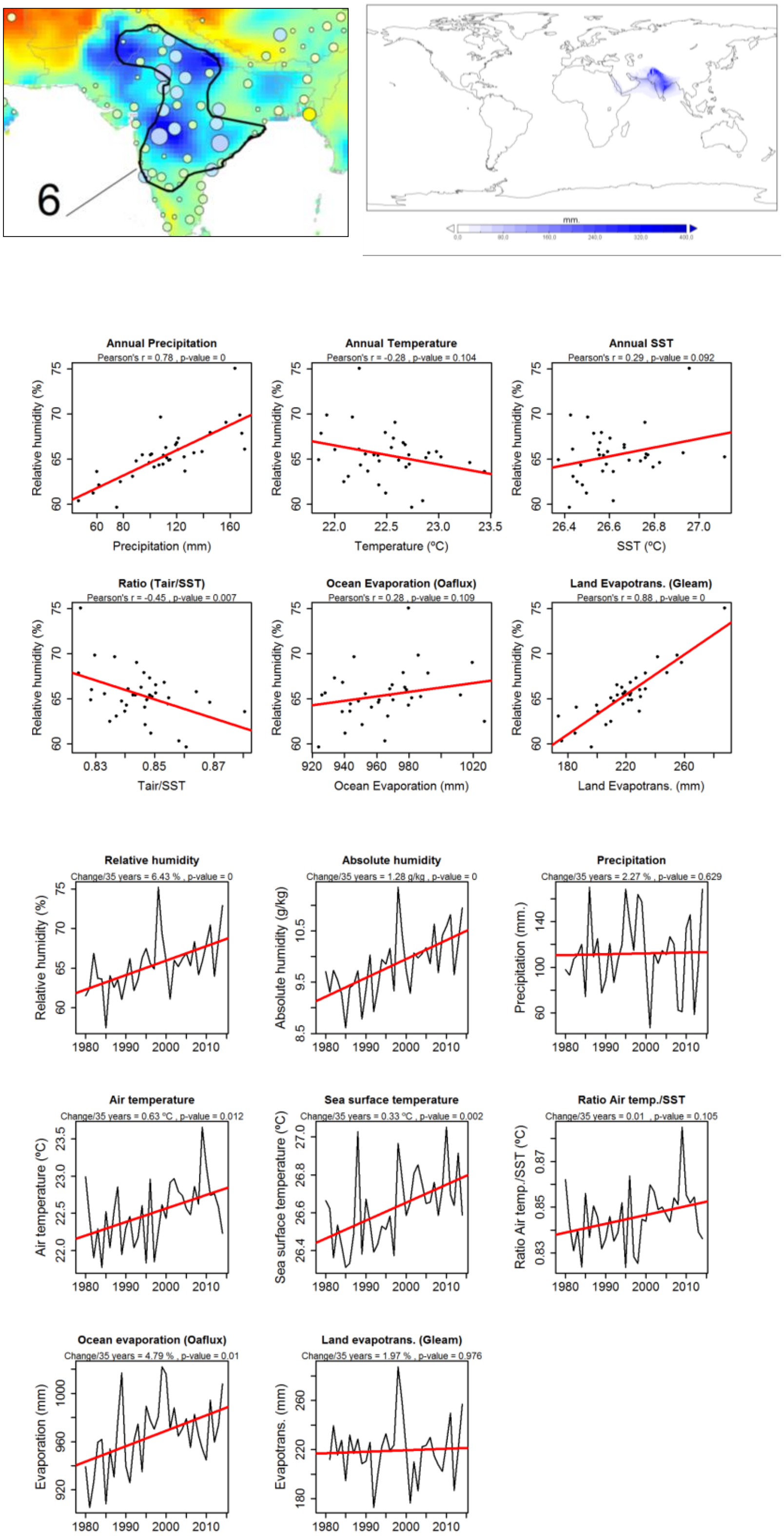

Figure S24: The same as Figure S19 but for India (region 6).

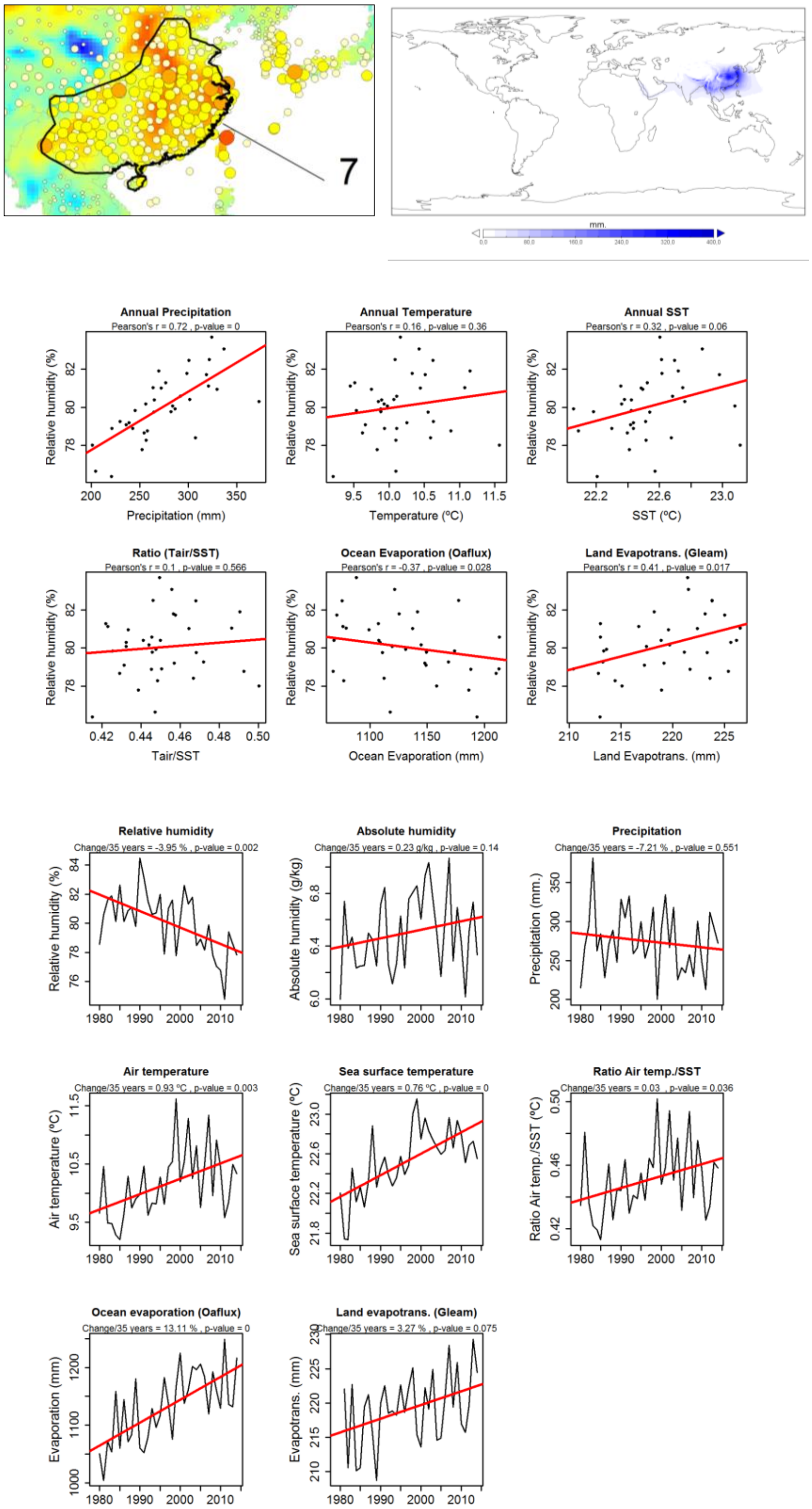

Figure S25: The same as Figure S19 but for East China (region 7).

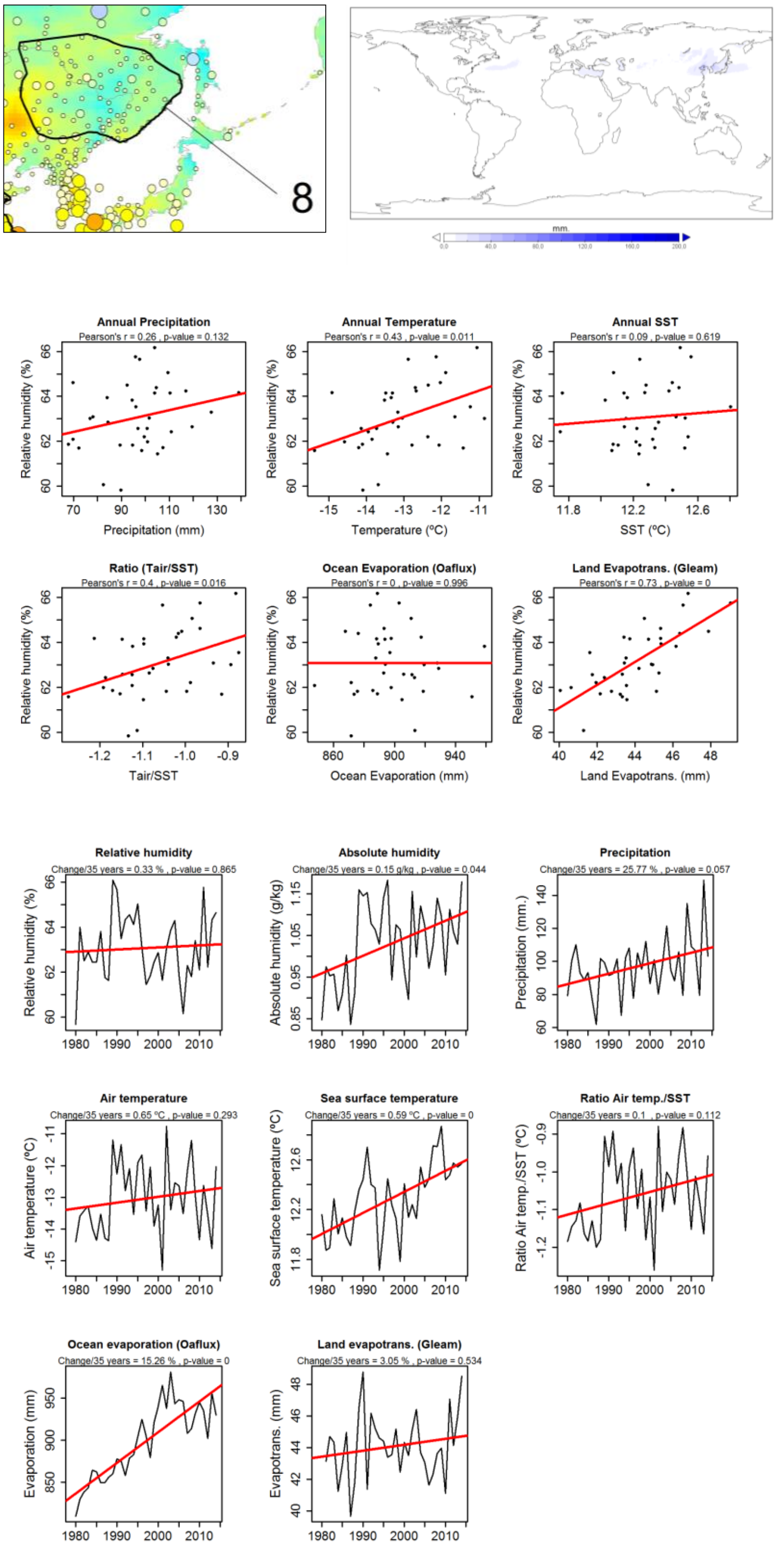

Figure S26: The same as Figure S19 but for North East Asia (region 8).

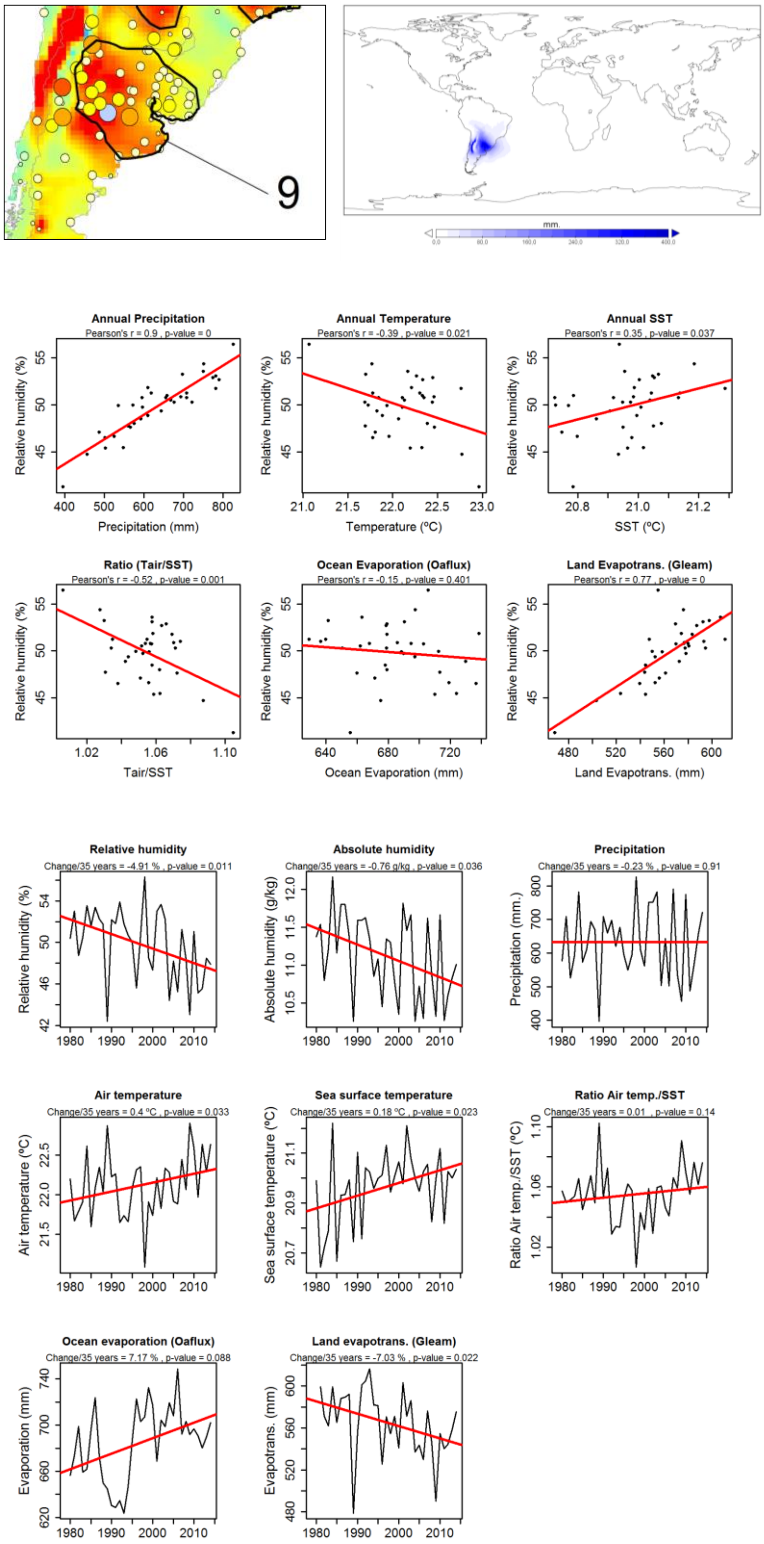

Figure S27: The same as Figure S19 but for La Plata (region 9).

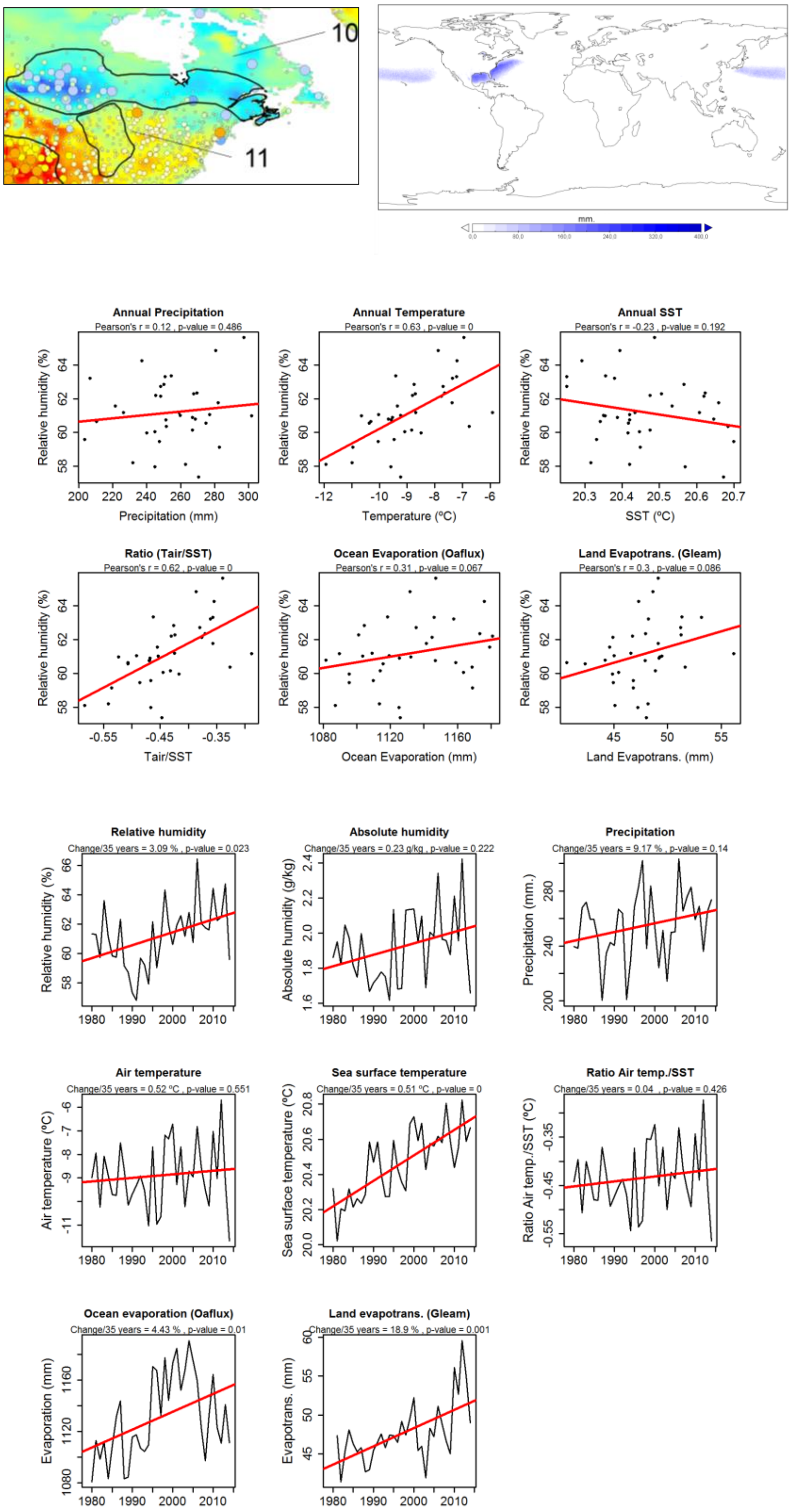

Figure S28: The same as Figure S19 but for Canada (region 10).

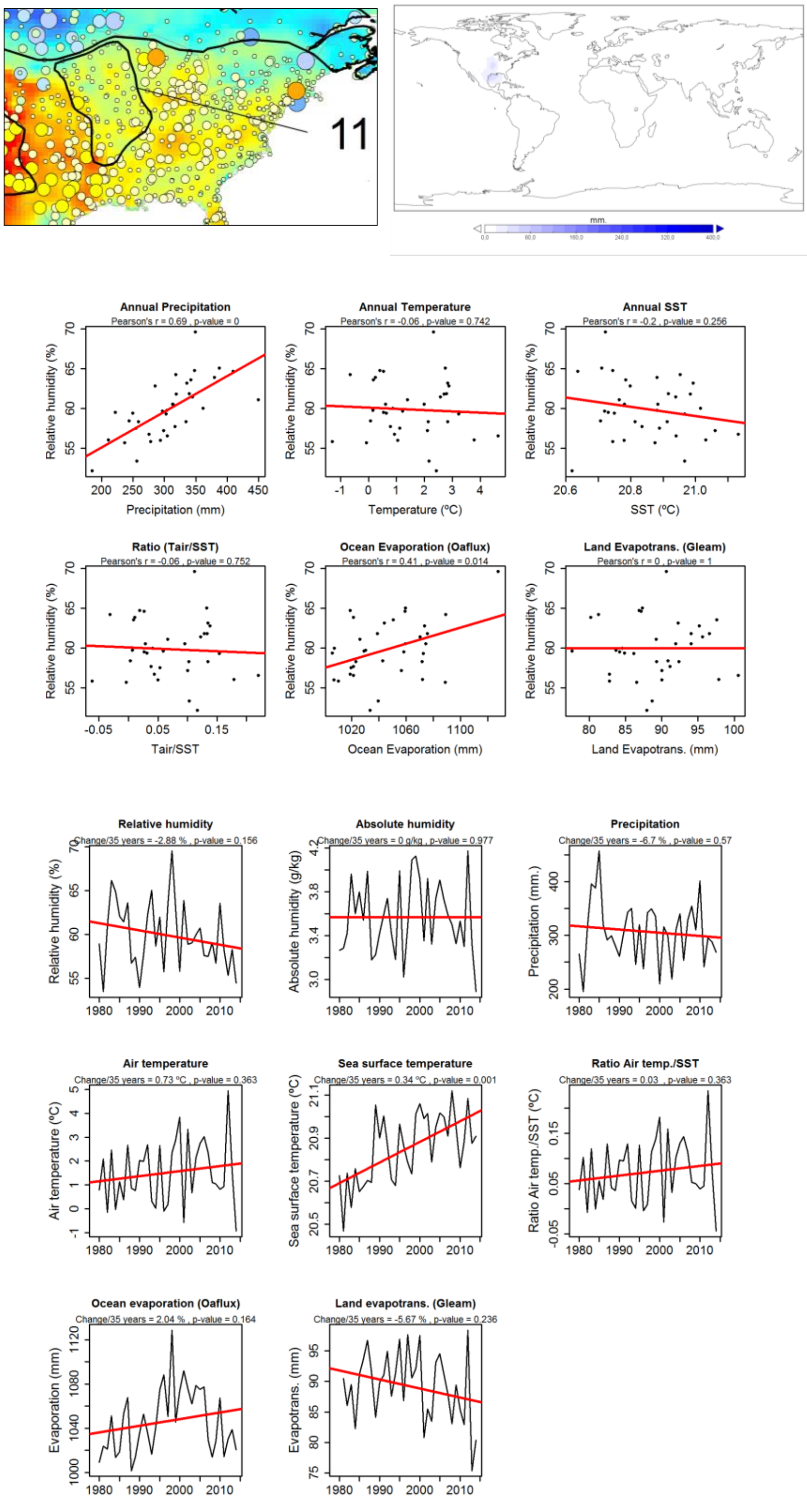

Figure S29: The same as Figure S19 but for central USA (region 11).

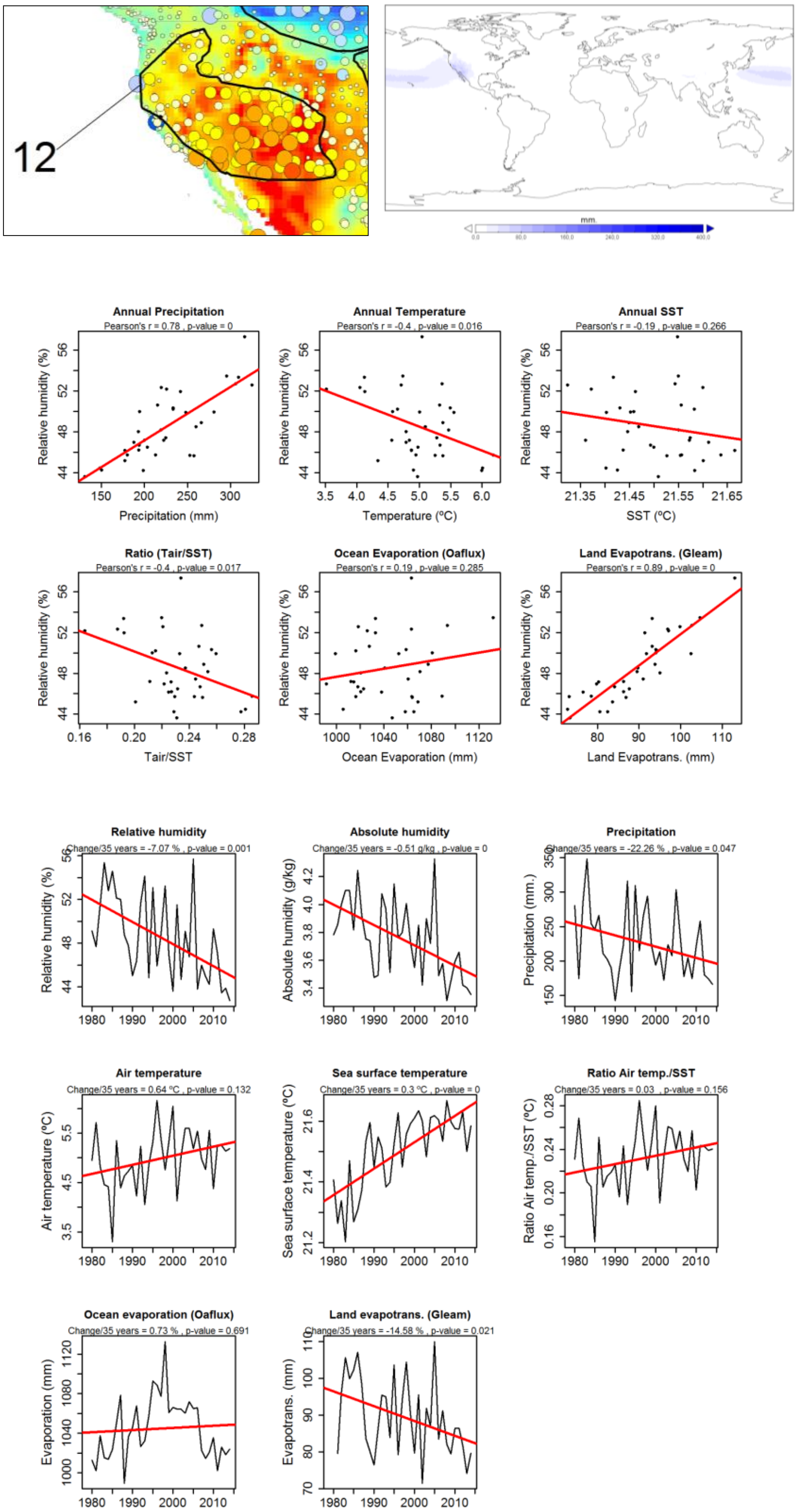

Figure S30: The same as Figure S19 but for West North America (region 12).

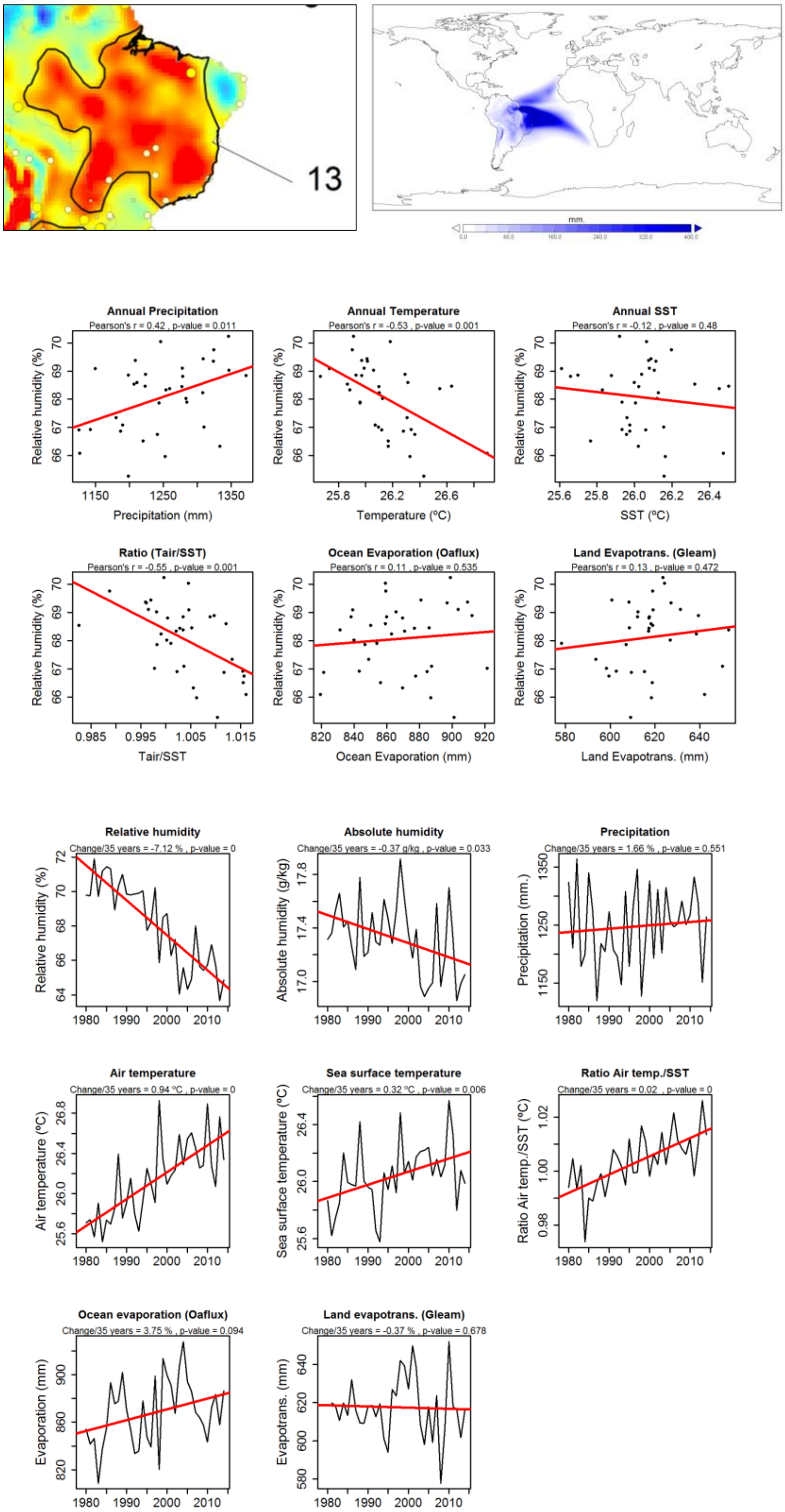

Figure S31: The same as Figure S19 but for Amazonian (region 13)

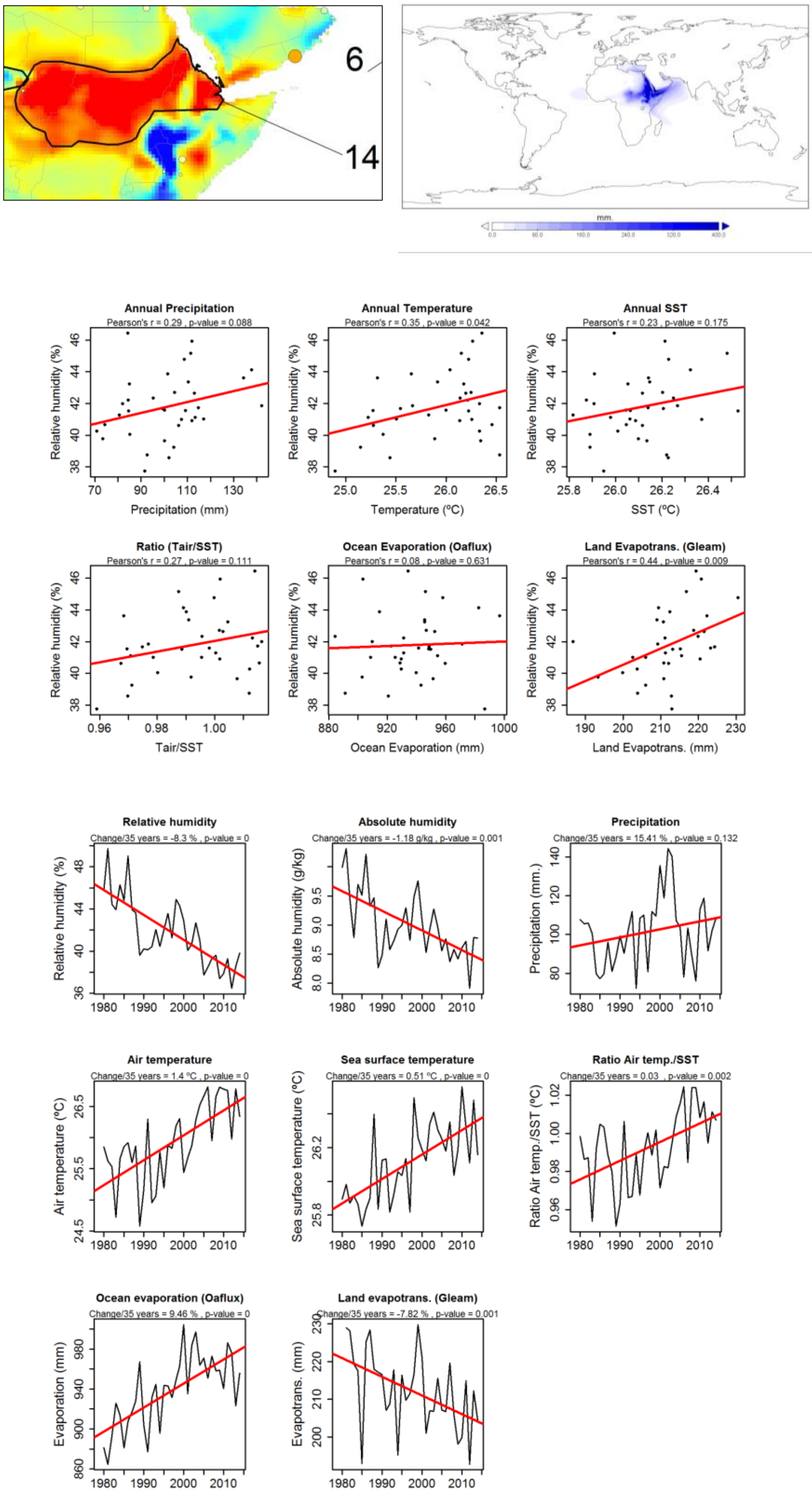

Figure S32: The same as Figure S19 but for East Sahel (region 14).

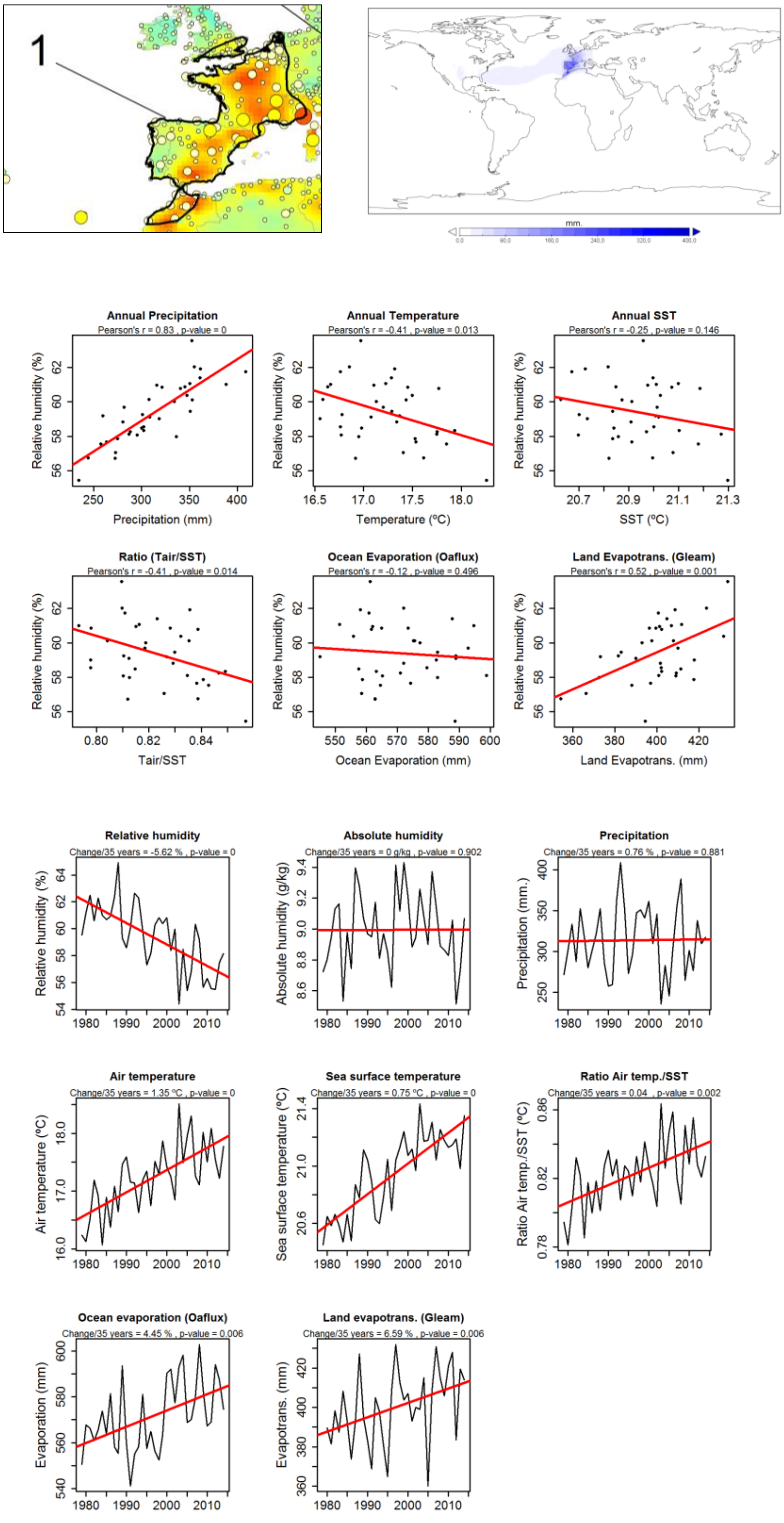

Figure S33: Top left: Boreal warm season RH humidity trends in West Europe (region 1), top right: average E-P in the boreal cold season to identify the main humidity sources in the region. Center: Relationship between de-trended boreal warm season RH and de-trended boreal warm season variables between 1979 and 2014. Bottom: Boreal cold season evolution of the different variables corresponding to West Europe region. The magnitude of change and signification of the trend is indicated for each variable.

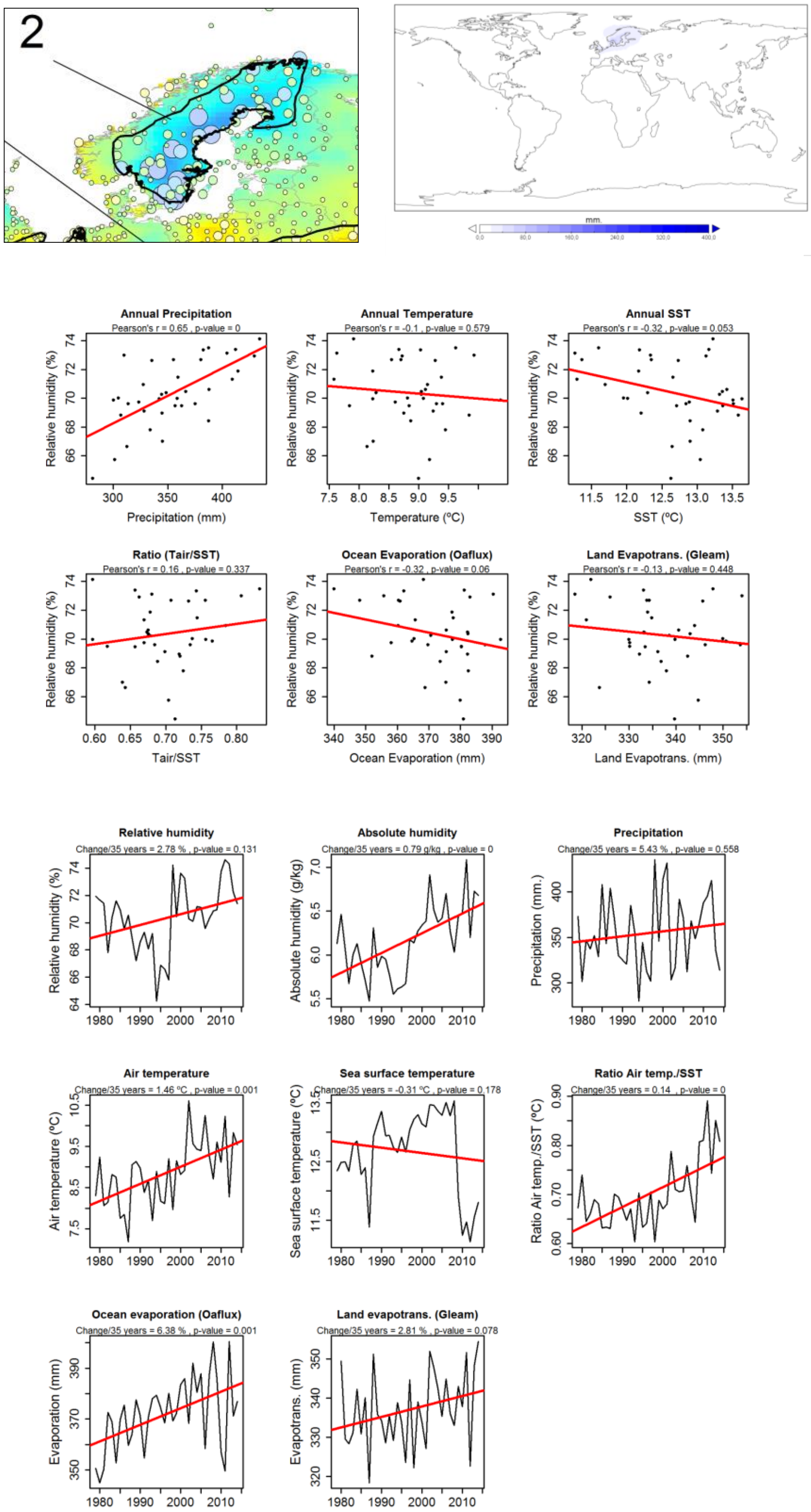

Figure S34: The same as Figure S33 but for Scandinavia (region 2).

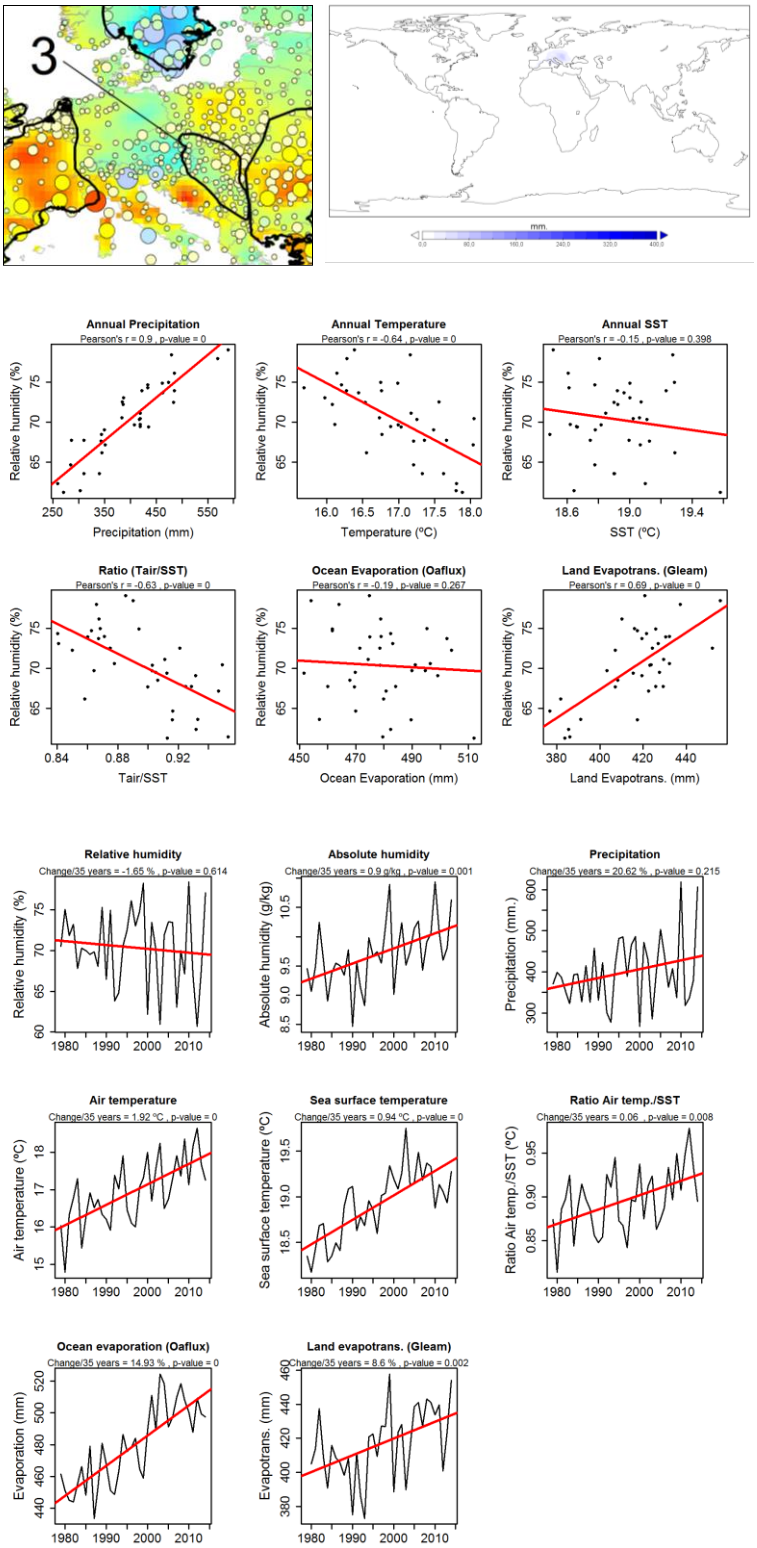

Figure S35: The same as Figure S33 but for Central-East Europe (region 3).

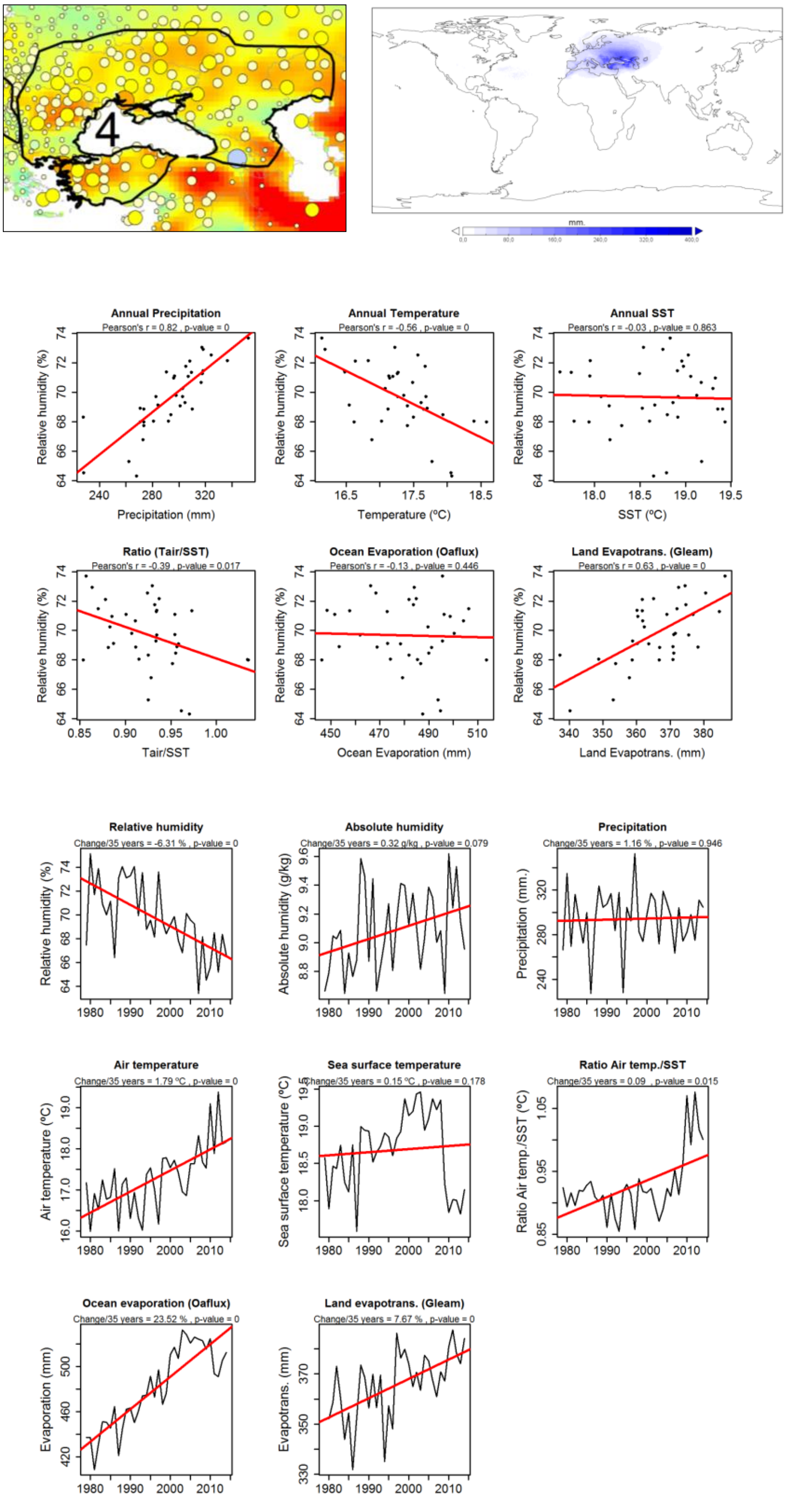

Figure S36: The same as Figure S33 but for South-East Europe and Turkey (region 4).

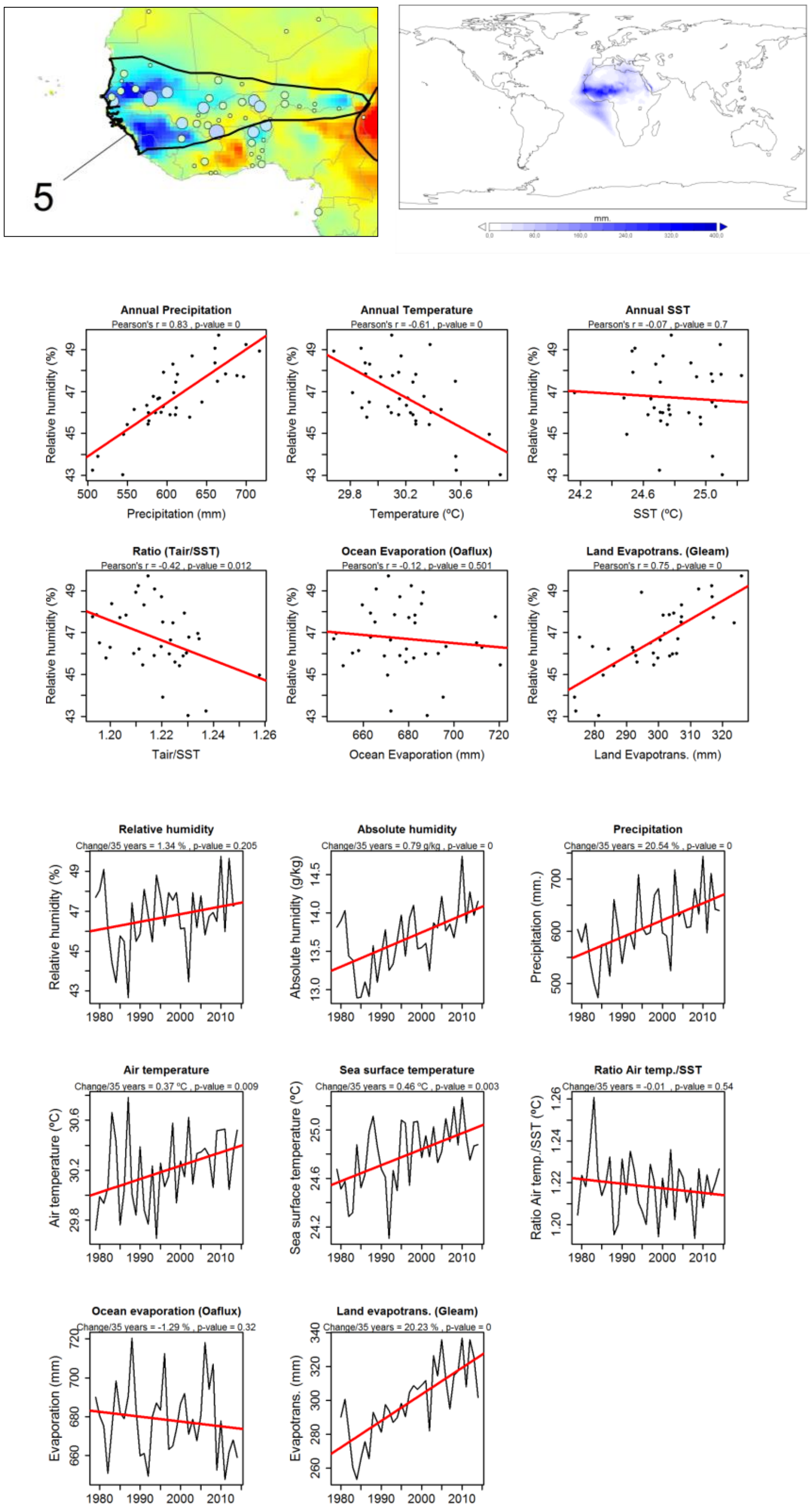

Figure S37: The same as Figure S33 but for West Sahel (region 6).

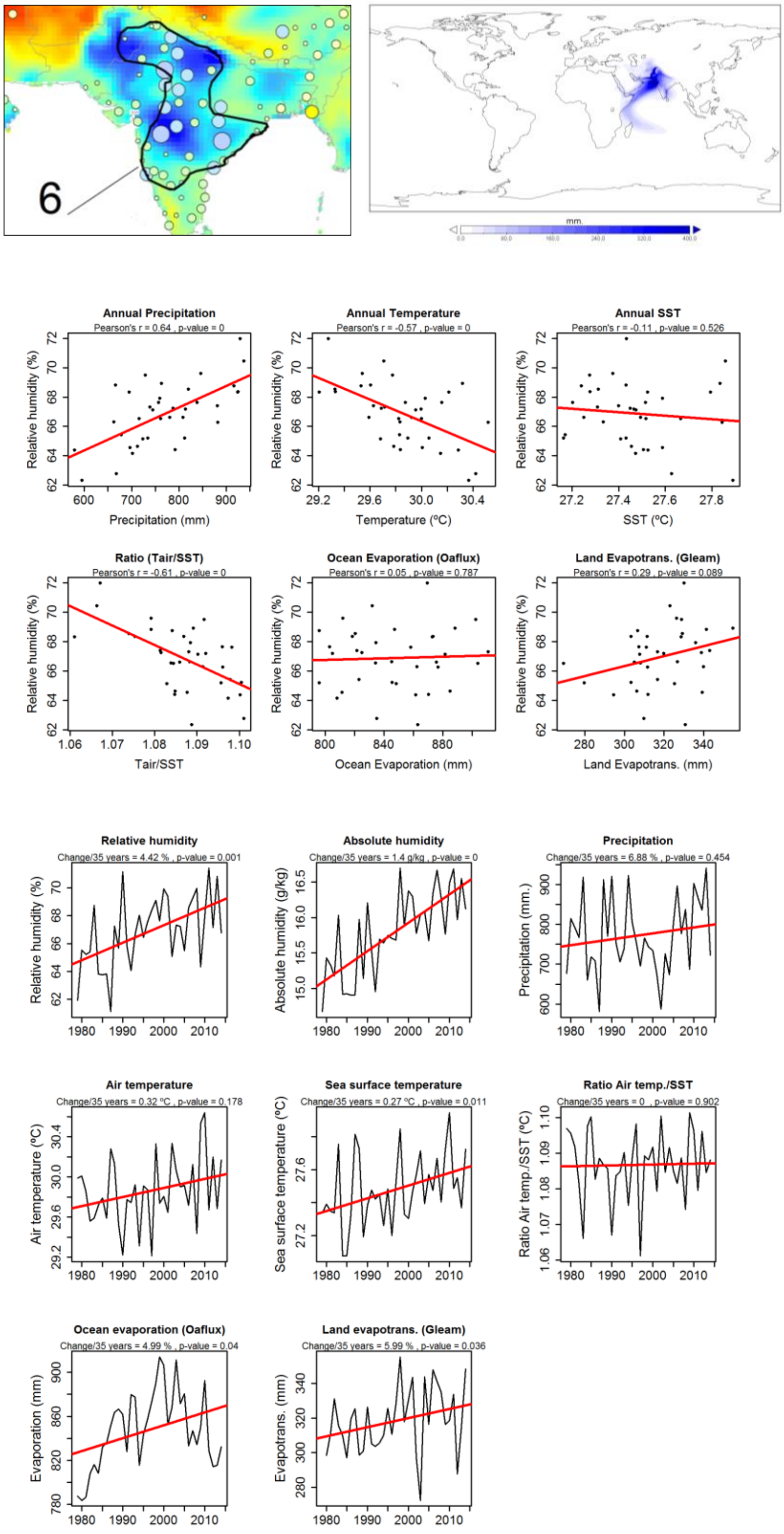

Figure S38: The same as Figure S33 but for India (region 6).

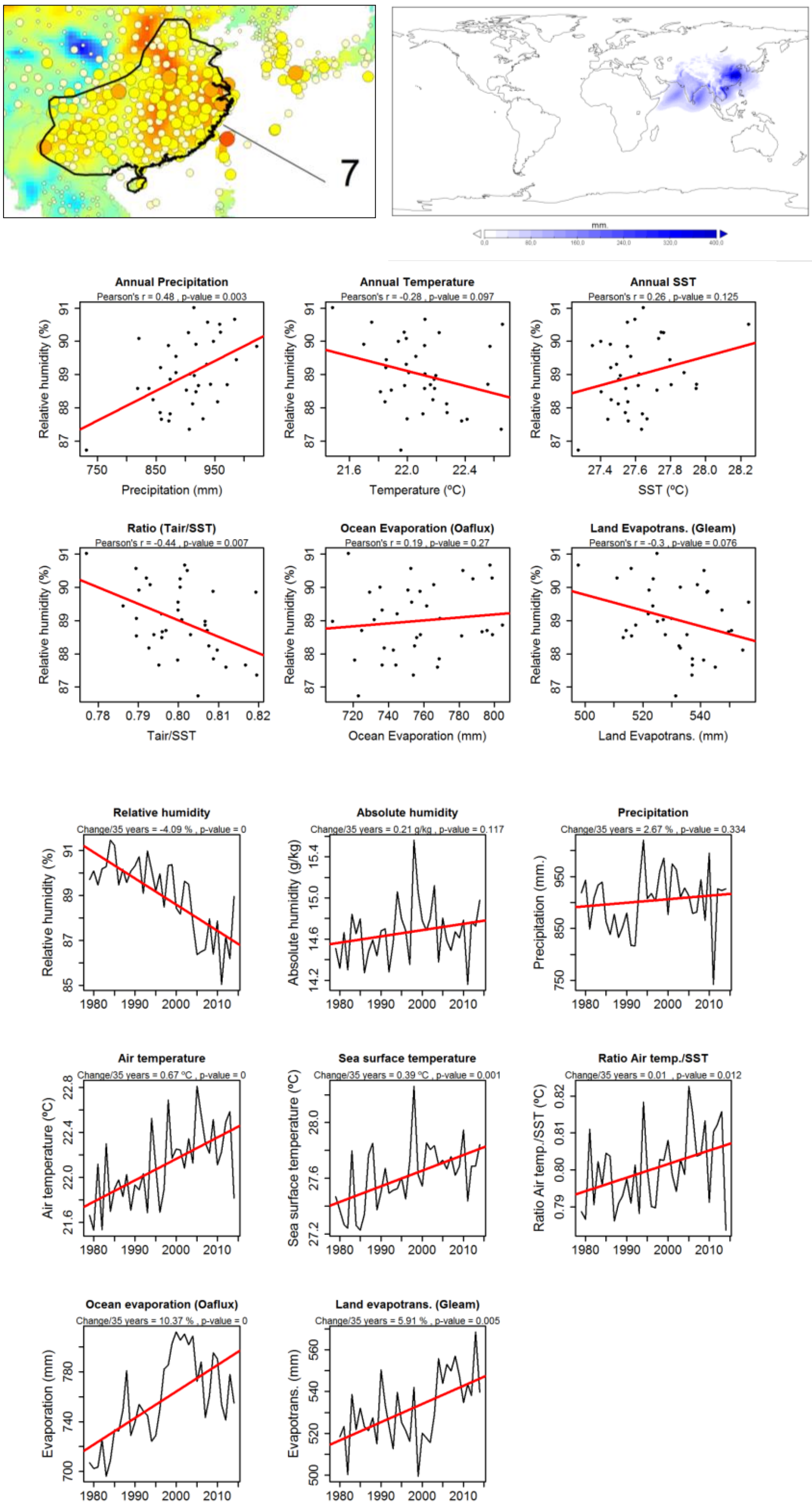

Figure S39: The same as Figure S33 but for East China (region 7).

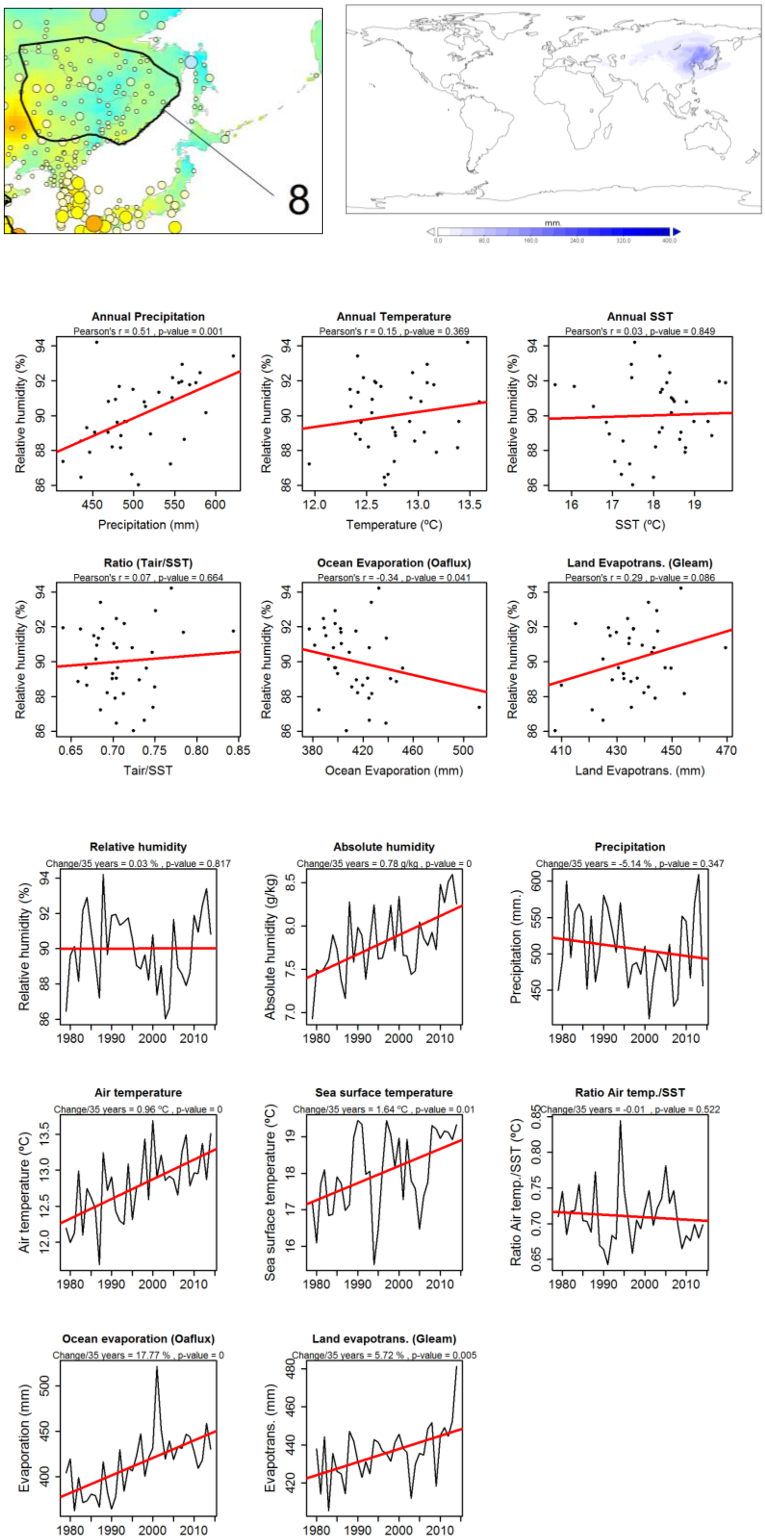

Figure S40: The same as Figure S33 but for North East Asia (region 8).

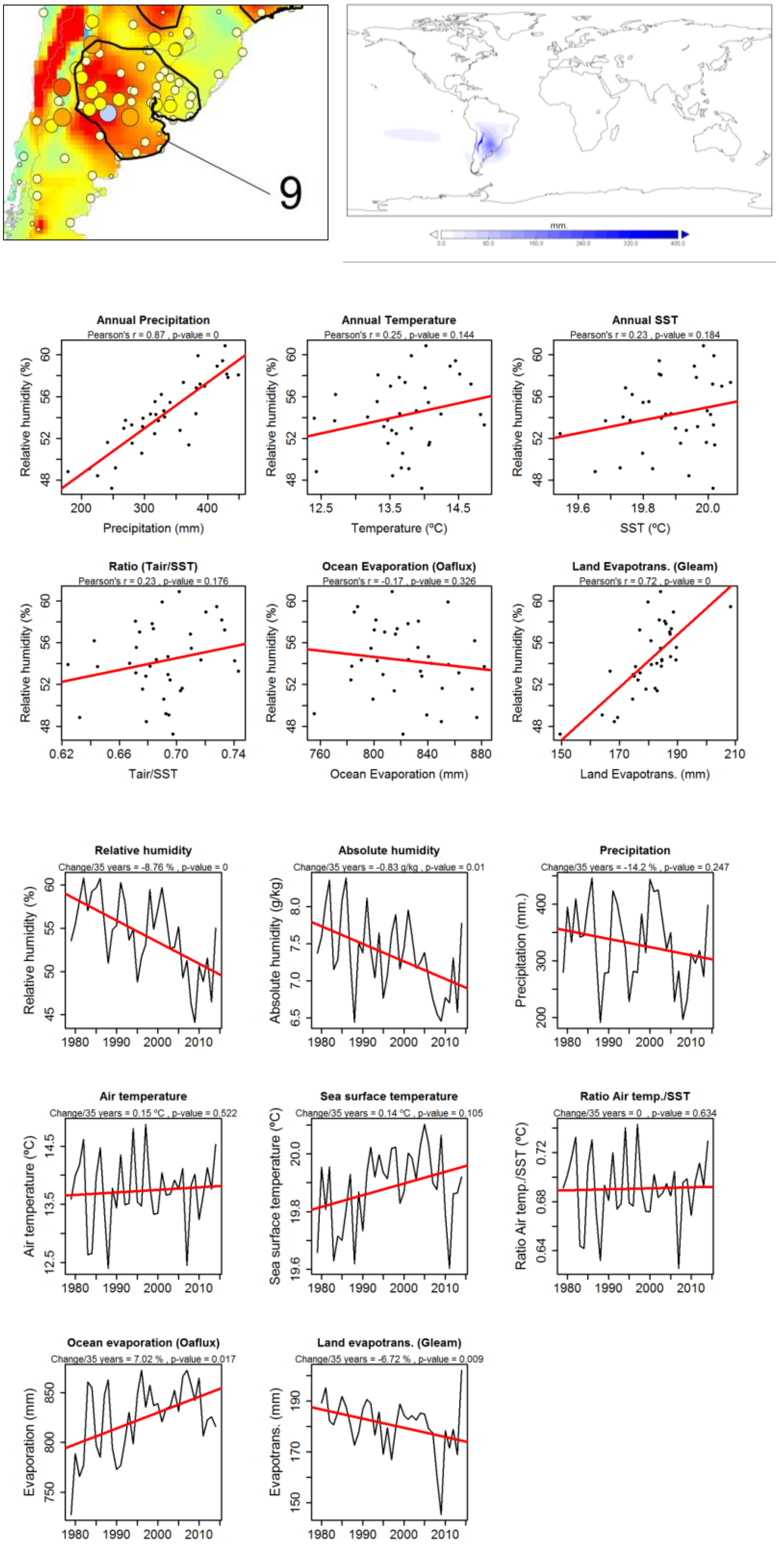

Figure S41: The same as Figure S33 but for La Plata (region 9).

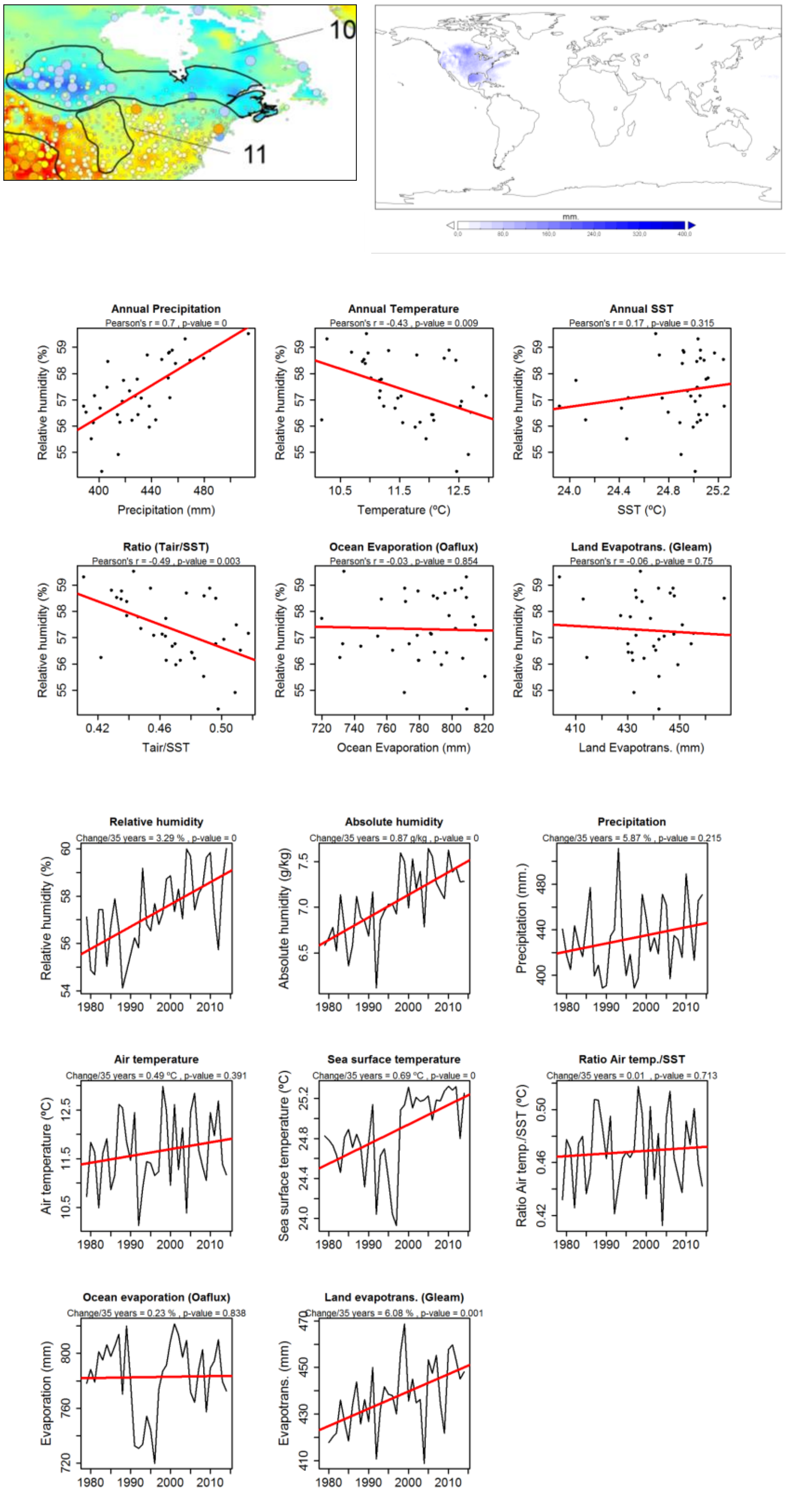

Figure S42: The same as Figure S33 but for Canada (region 10).

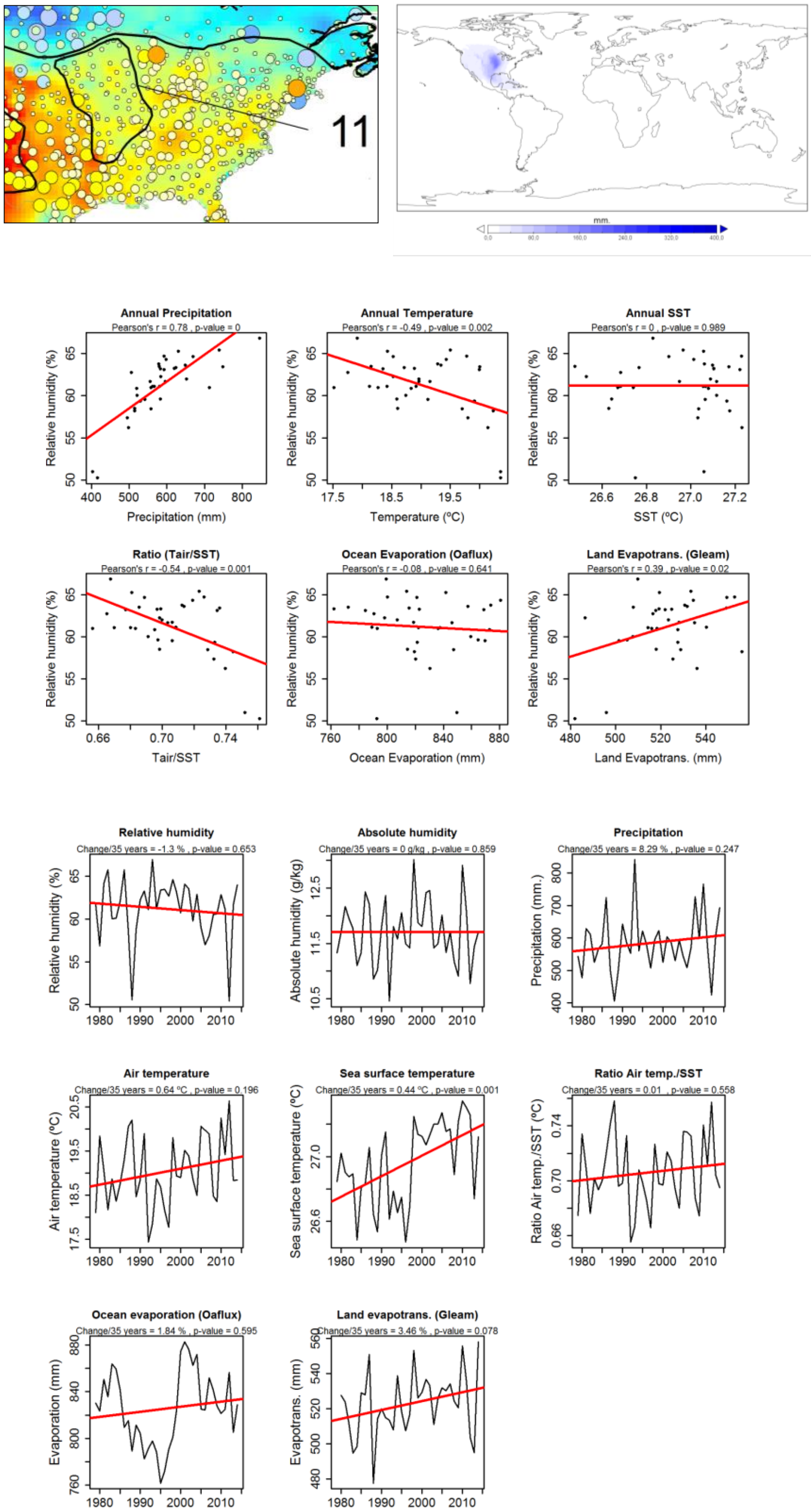

Figure S43: The same as Figure S33 but for central USA (region 11).

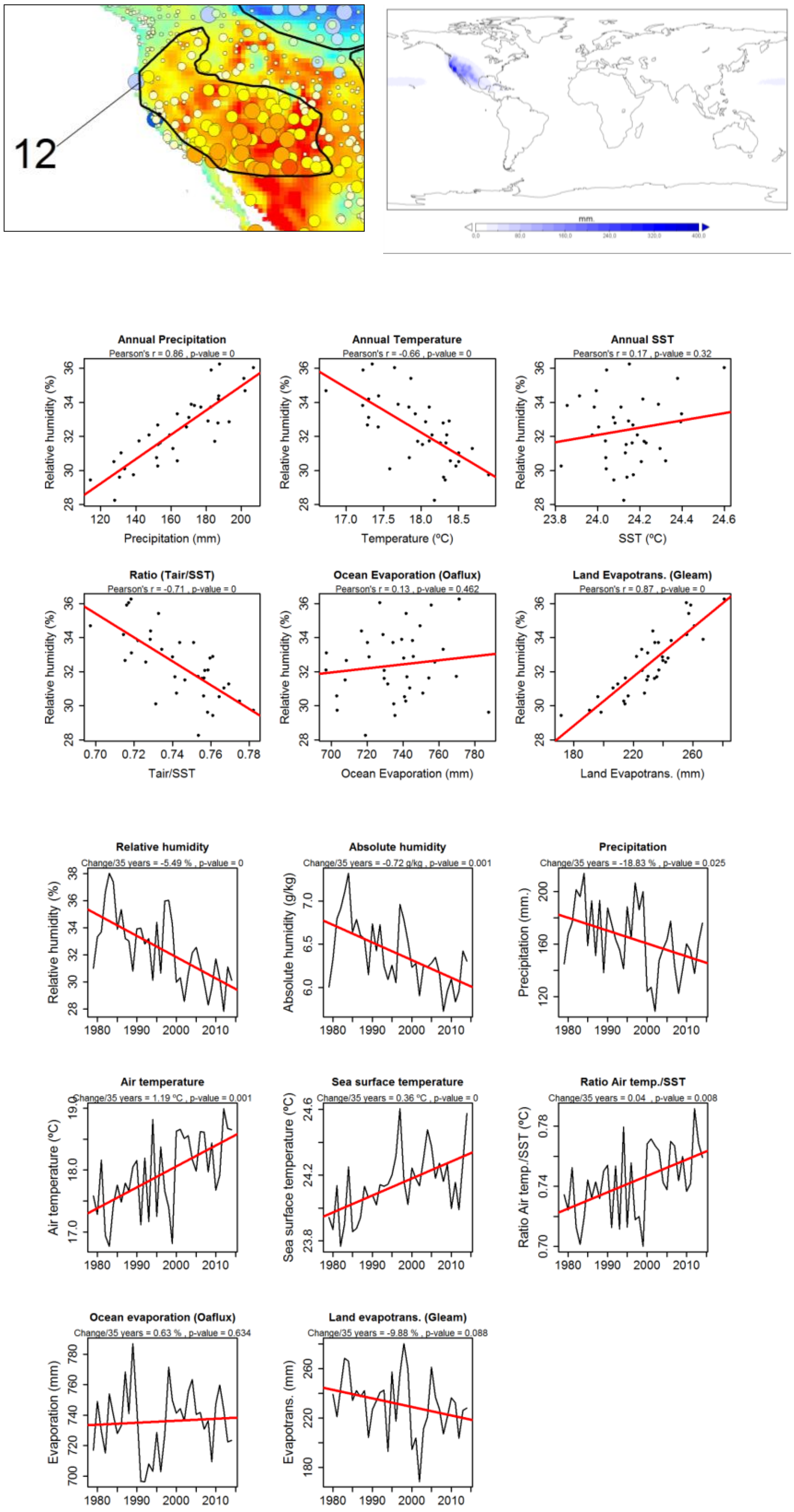

Figure S44: The same as Figure S33 but for West North America (region 12).

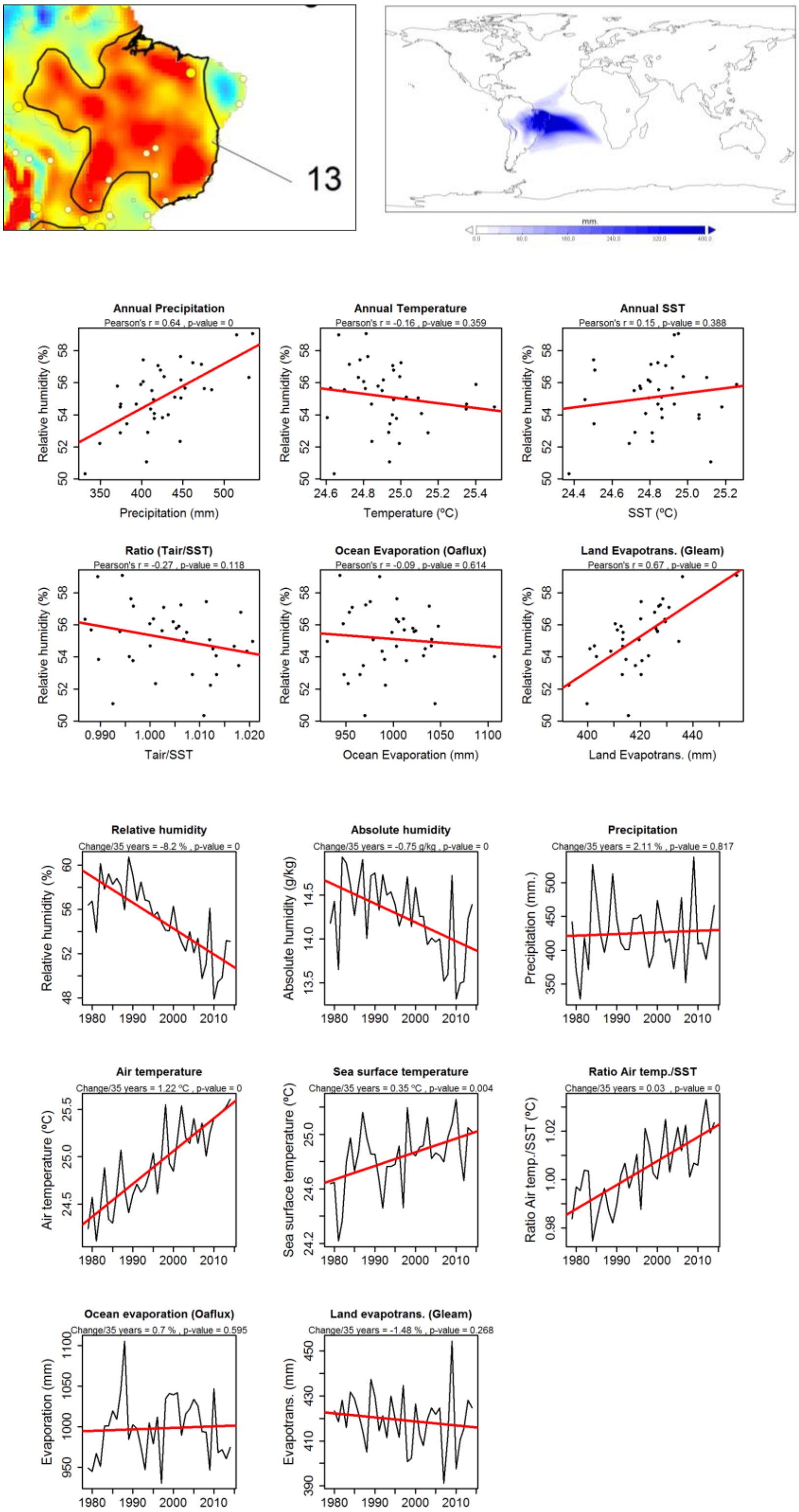

Figure S45: The same as Figure S33 but for Amazonian (region 13).

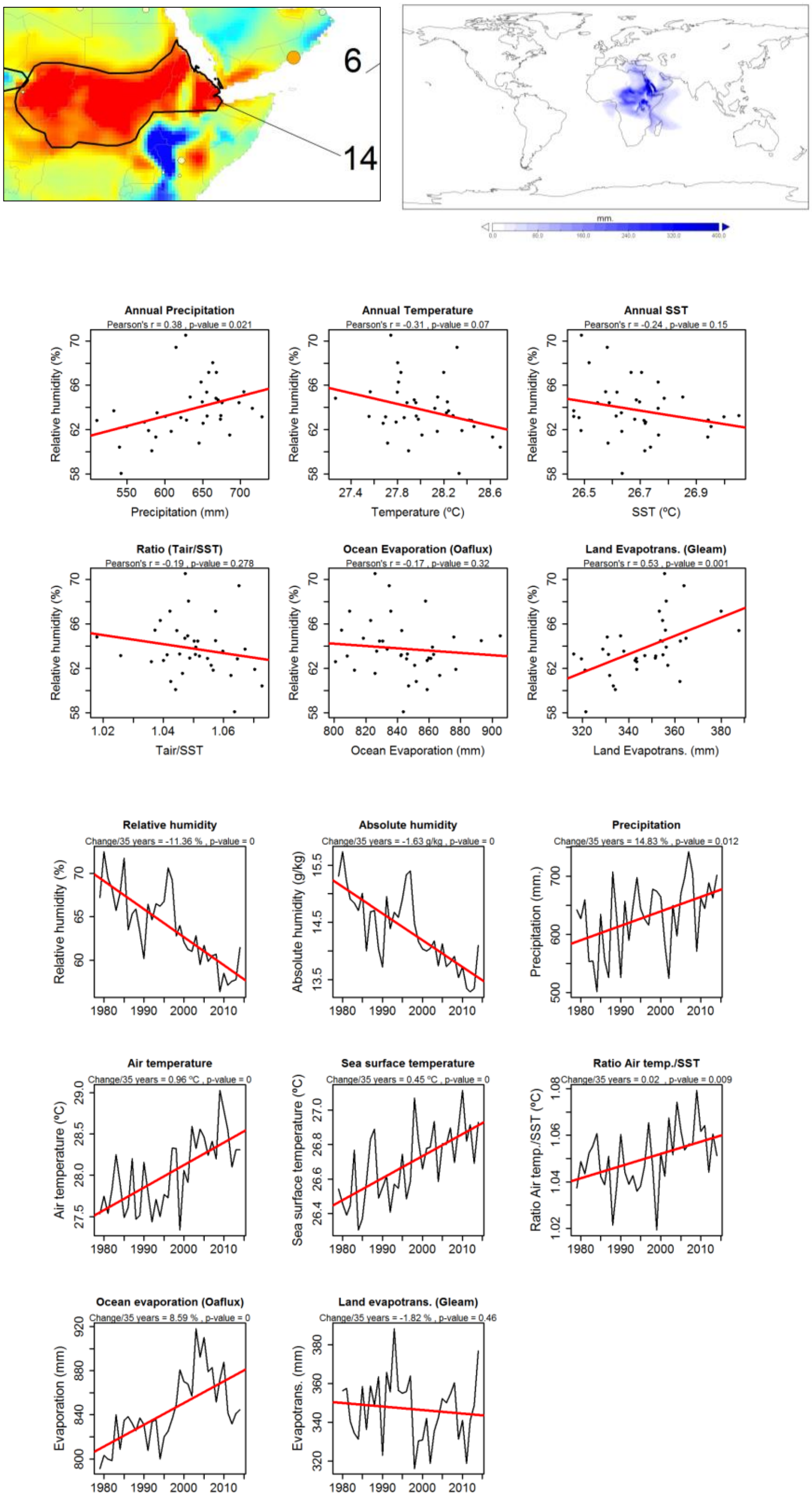

Figure S46: The same as Figure S33 but for East Sahel (region 14).

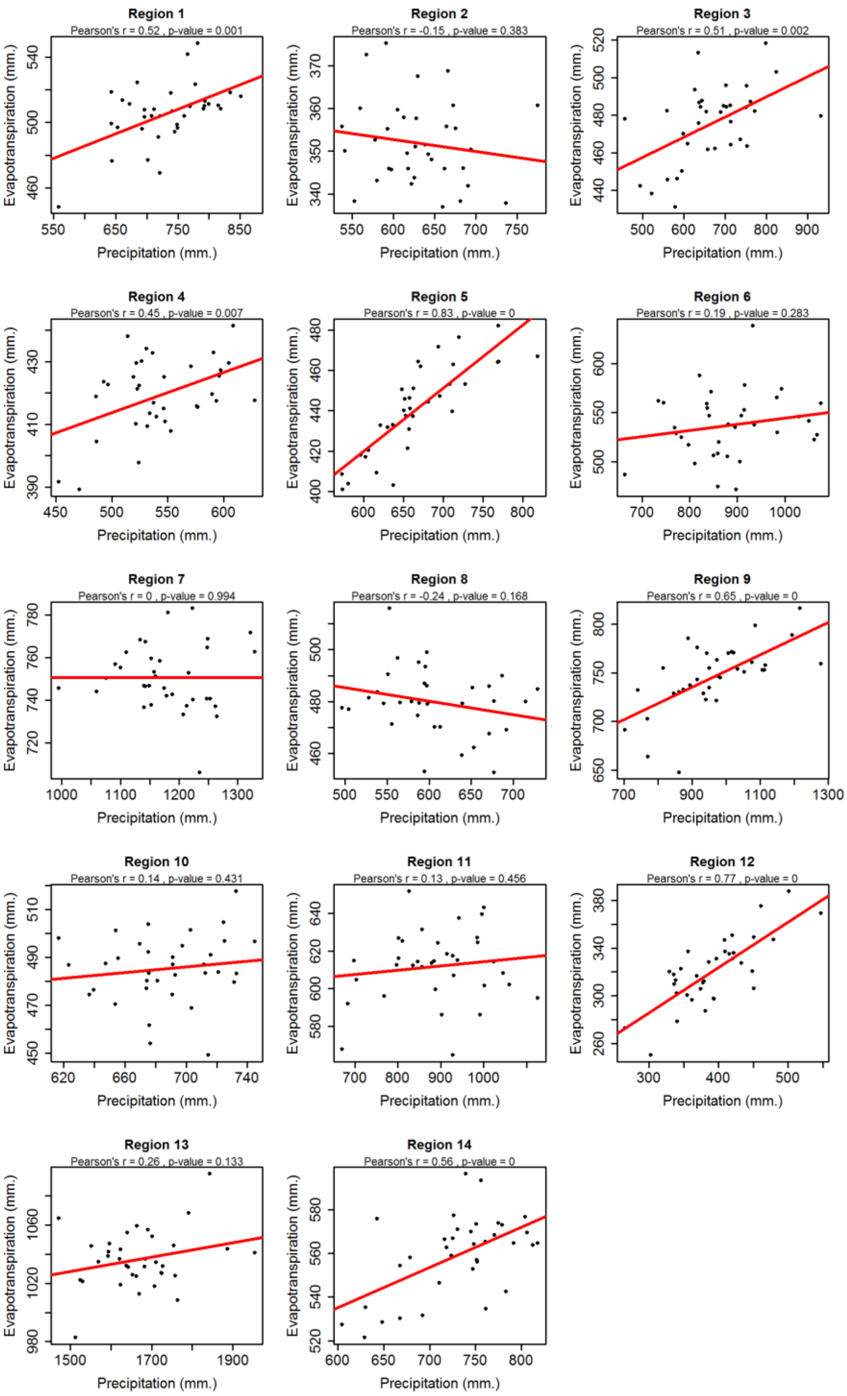

Figure S47. Relationship between the annual values of Precipitation and Land Evapotranspiration in the 14 analyzed regions.

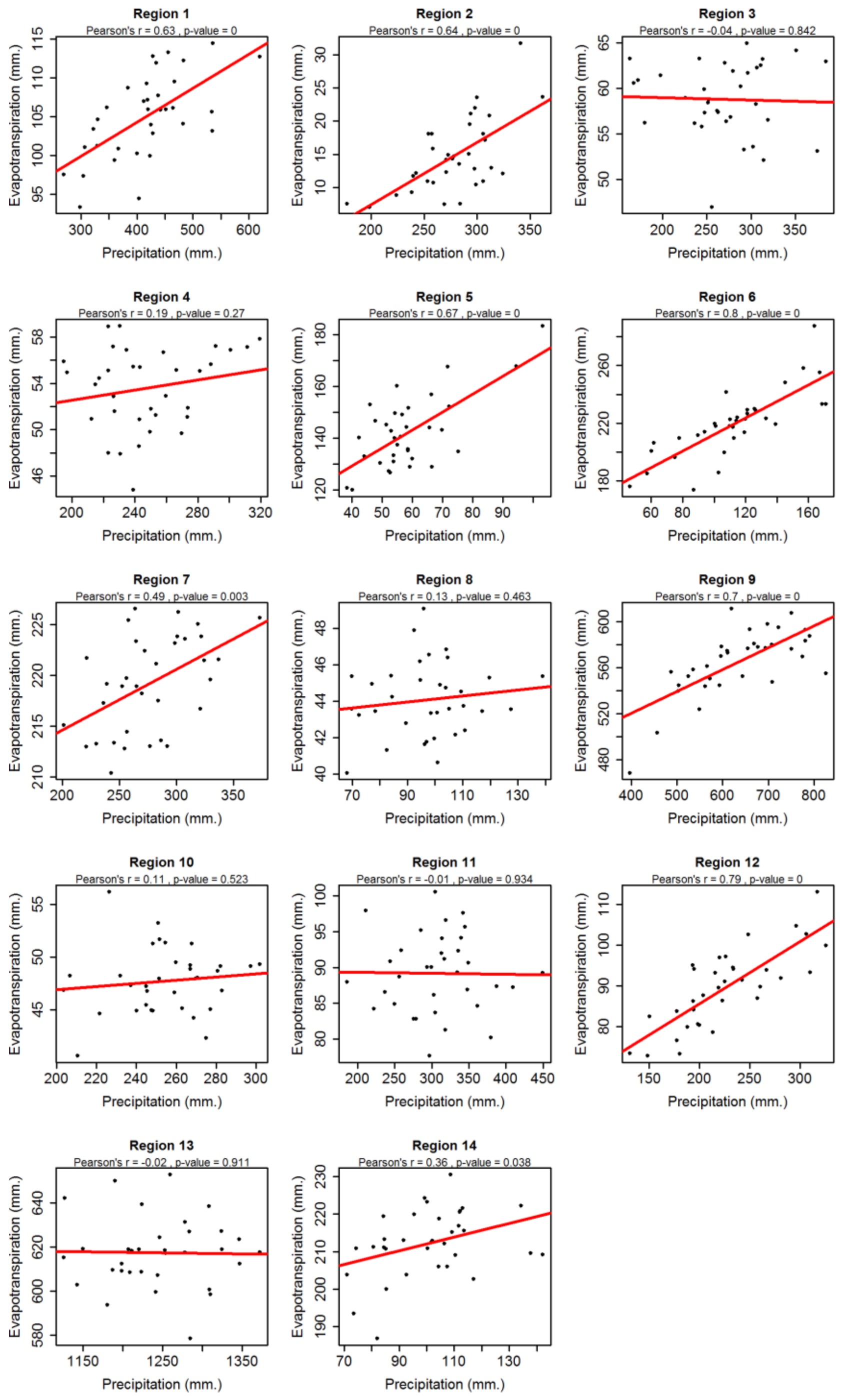

Figure S48. Relationship between the cold season values of Precipitation and Land Evapotranspiration in the 14 analyzed regions.

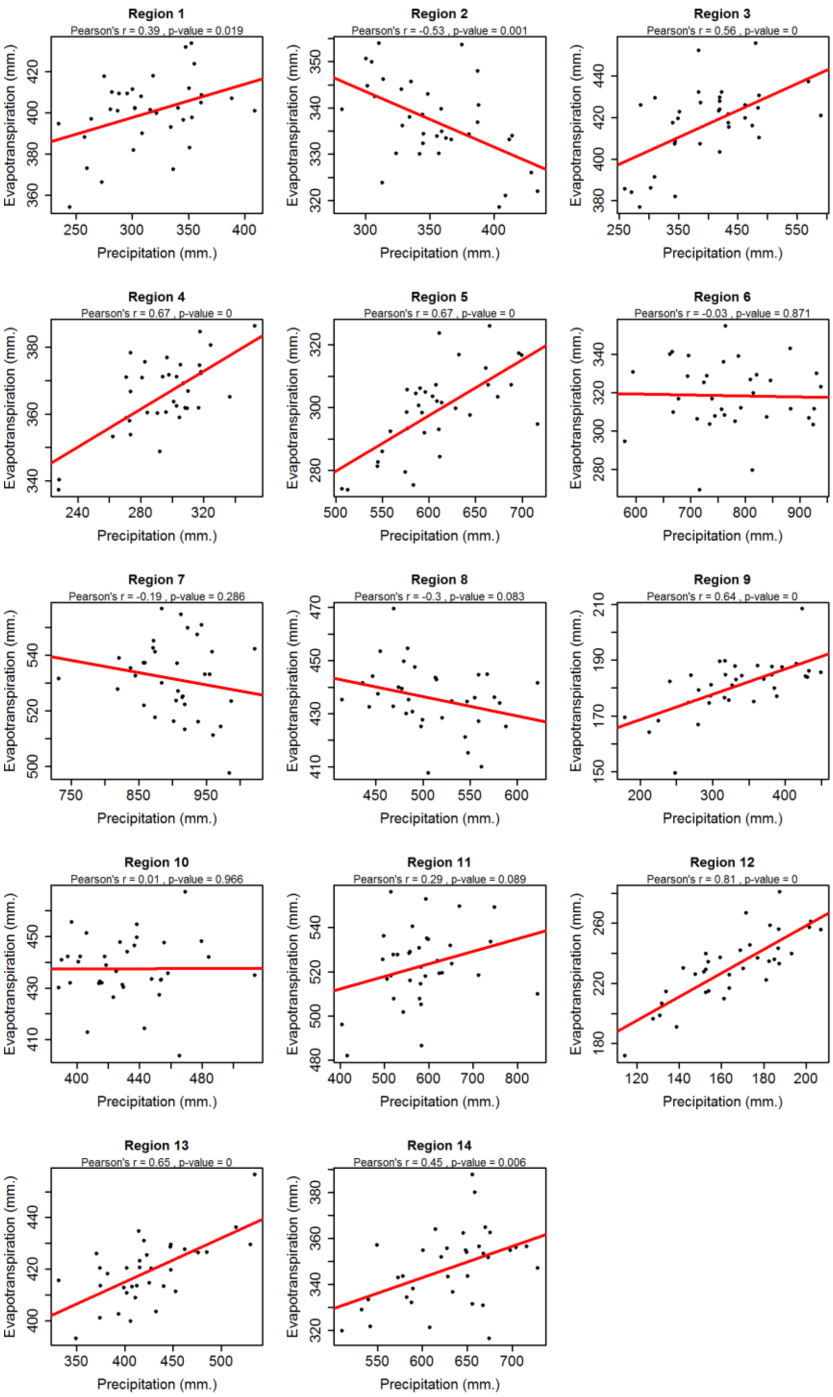

Figure S49. Relationship between the warm season values of Precipitation and Land Evapotranspiration in the 14 analyzed regions.

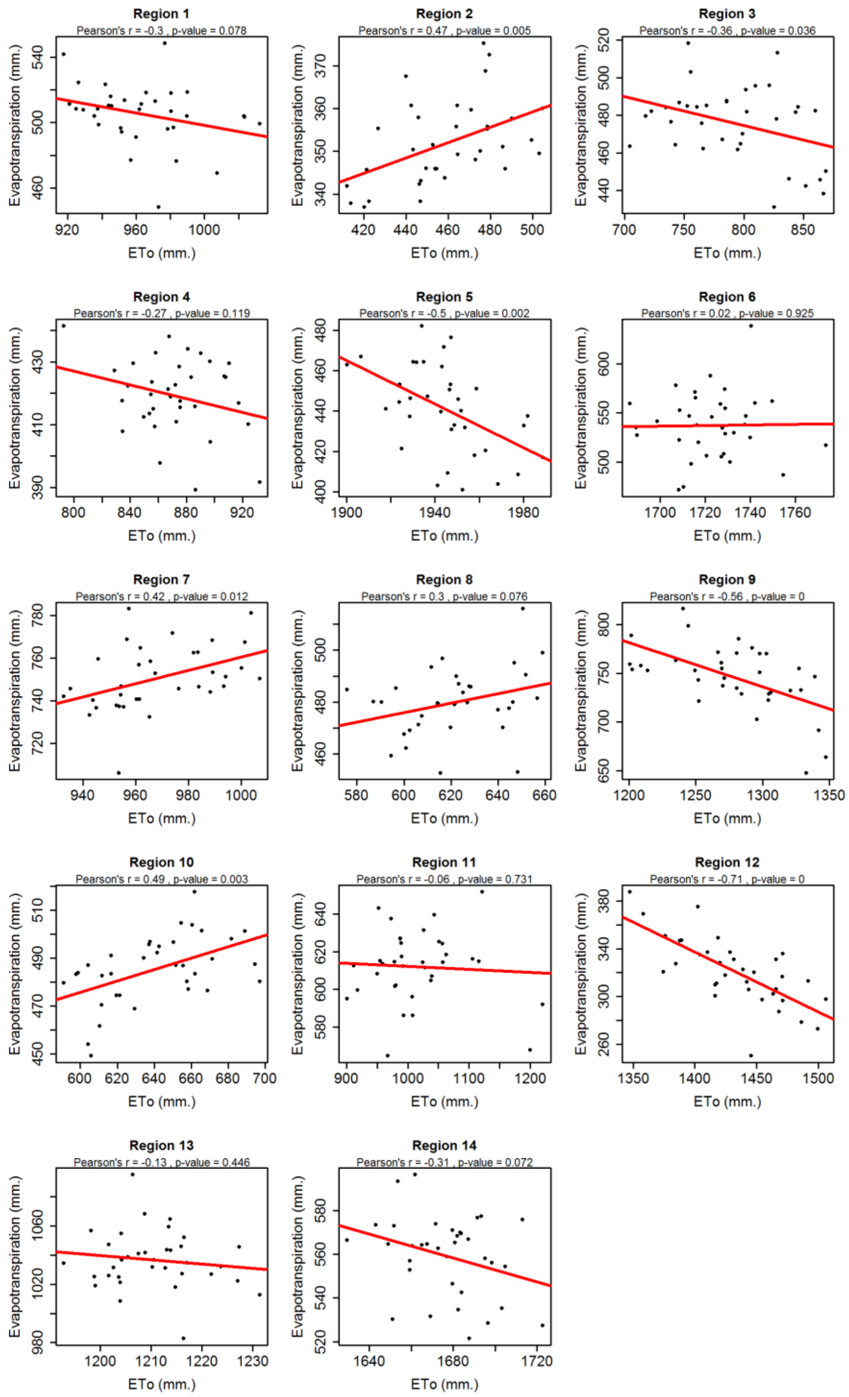

Figure S50. Relationship between the annual values of Reference Evapotranspiration and Land Evapotranspiration (ETo) in the 14 analyzed regions.

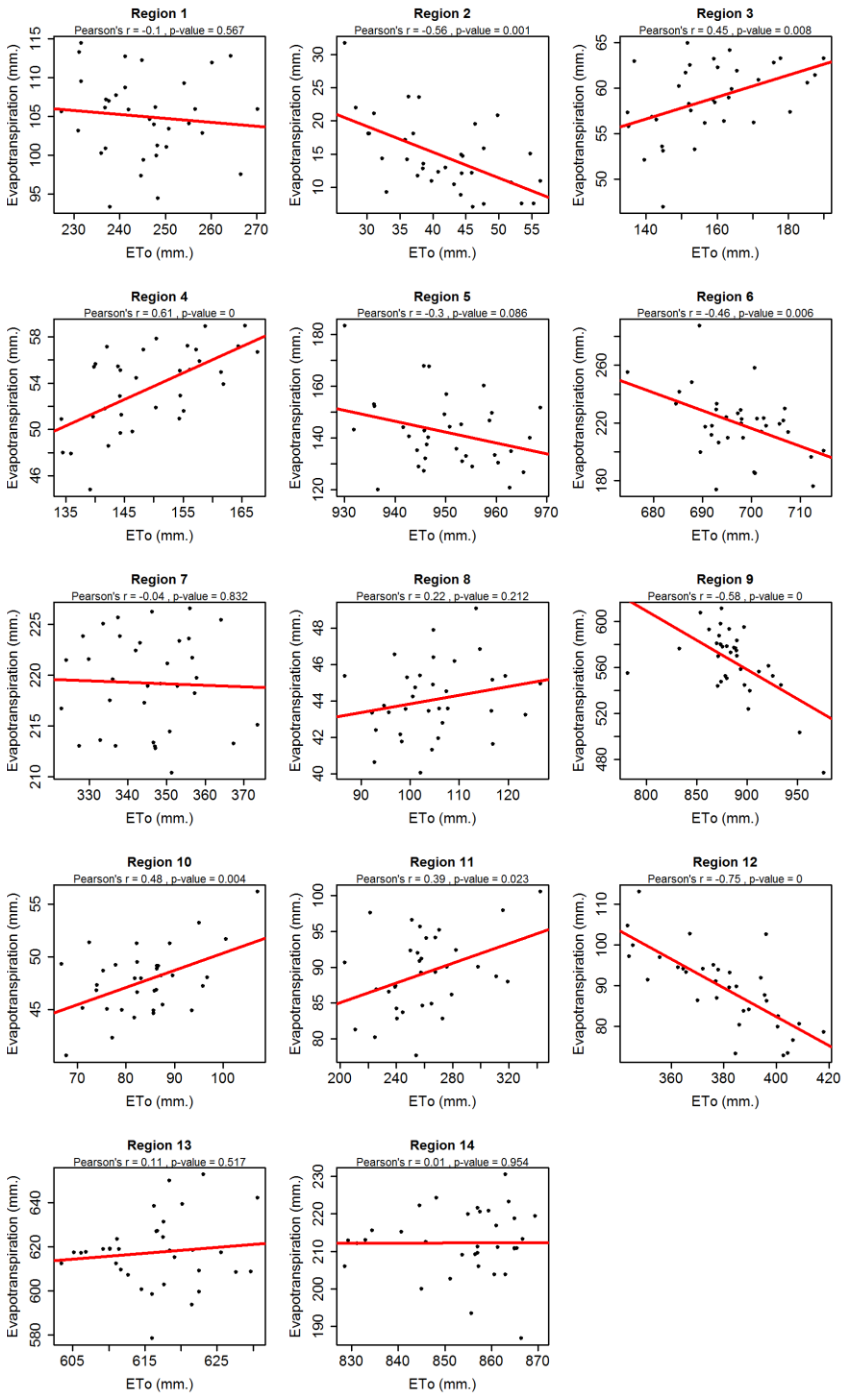

Figure S51. Relationship between the cold season values of Reference Evapotranspiration and Land Evapotranspiration (ETo) in the 14 analyzed regions.

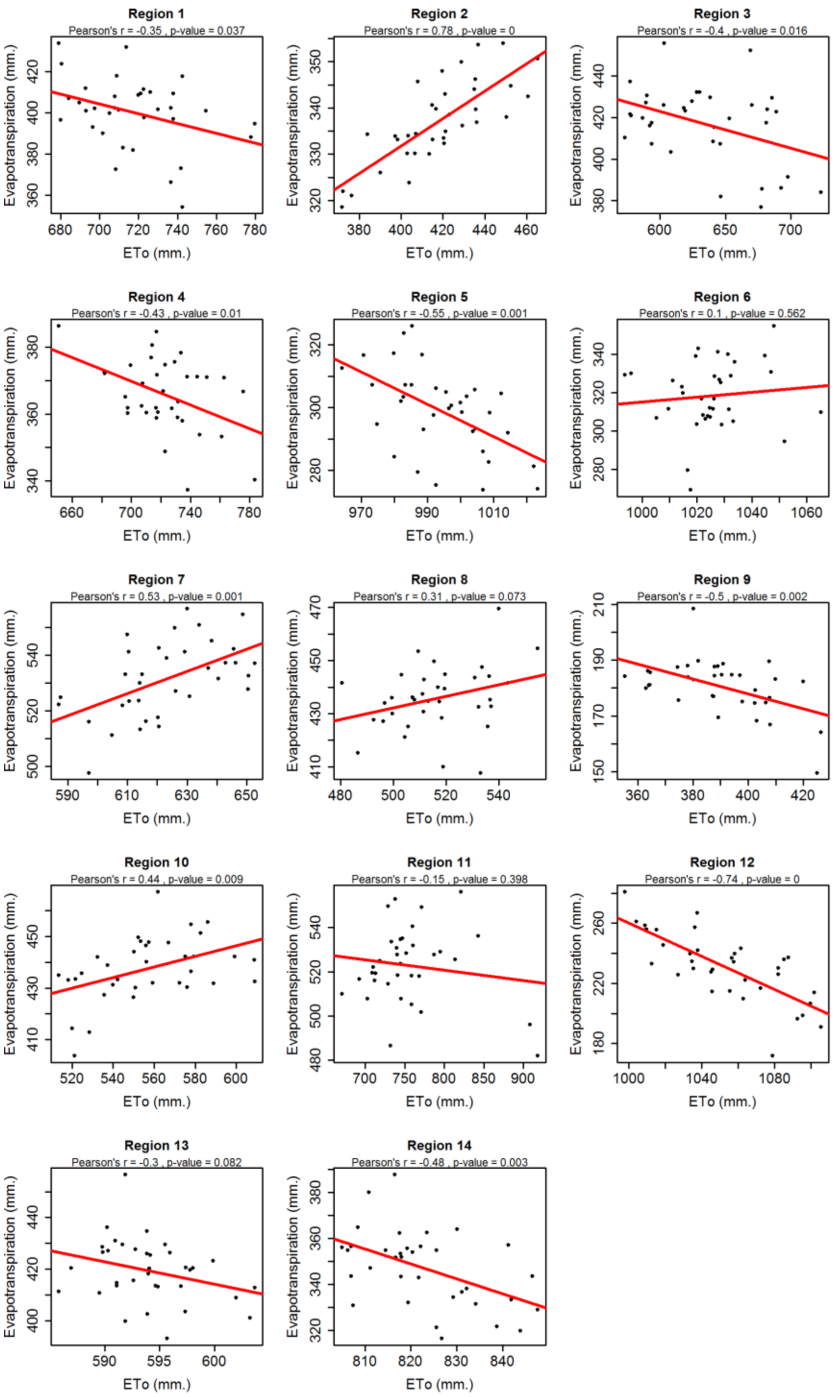

Figure S52. Relationship between the warm season values of Reference Evapotranspiration and Land Evapotranspiration (ETo) in the 14 analyzed regions.

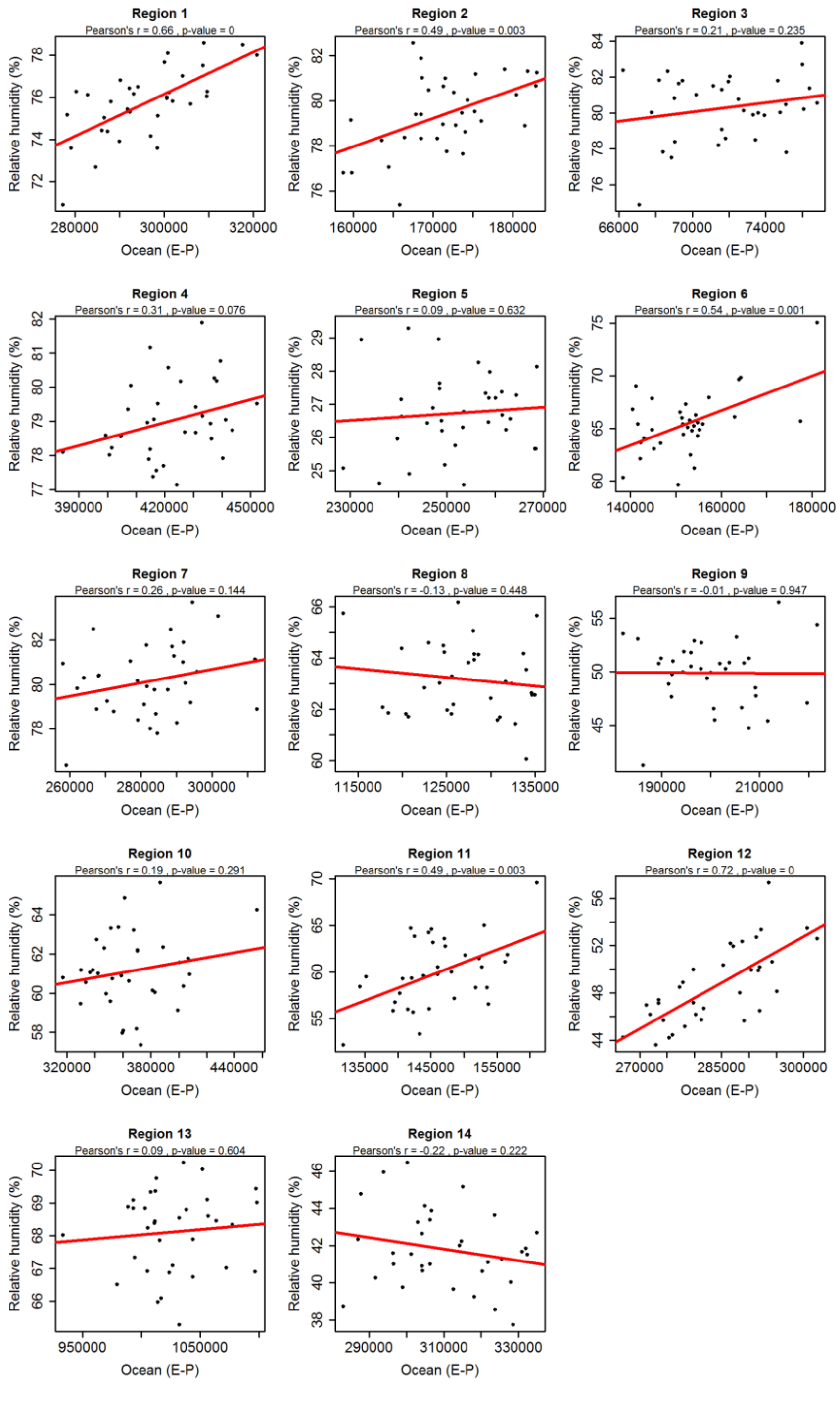

Figure S53: Relationship between the cold season ocean contribution to cold season precipitation (E-P) and the cold season RH in the target regions.

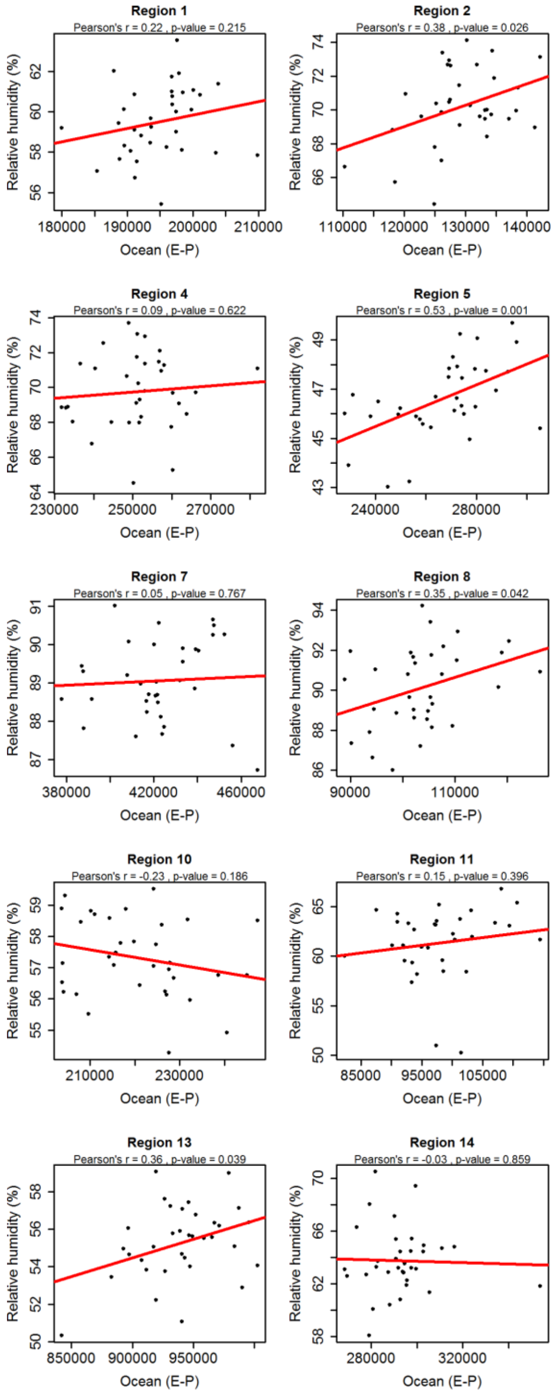

Figure S54: Relationship between the warm season ocean contribution to warm season precipitation (E-P) and the warm season RH in the target regions.

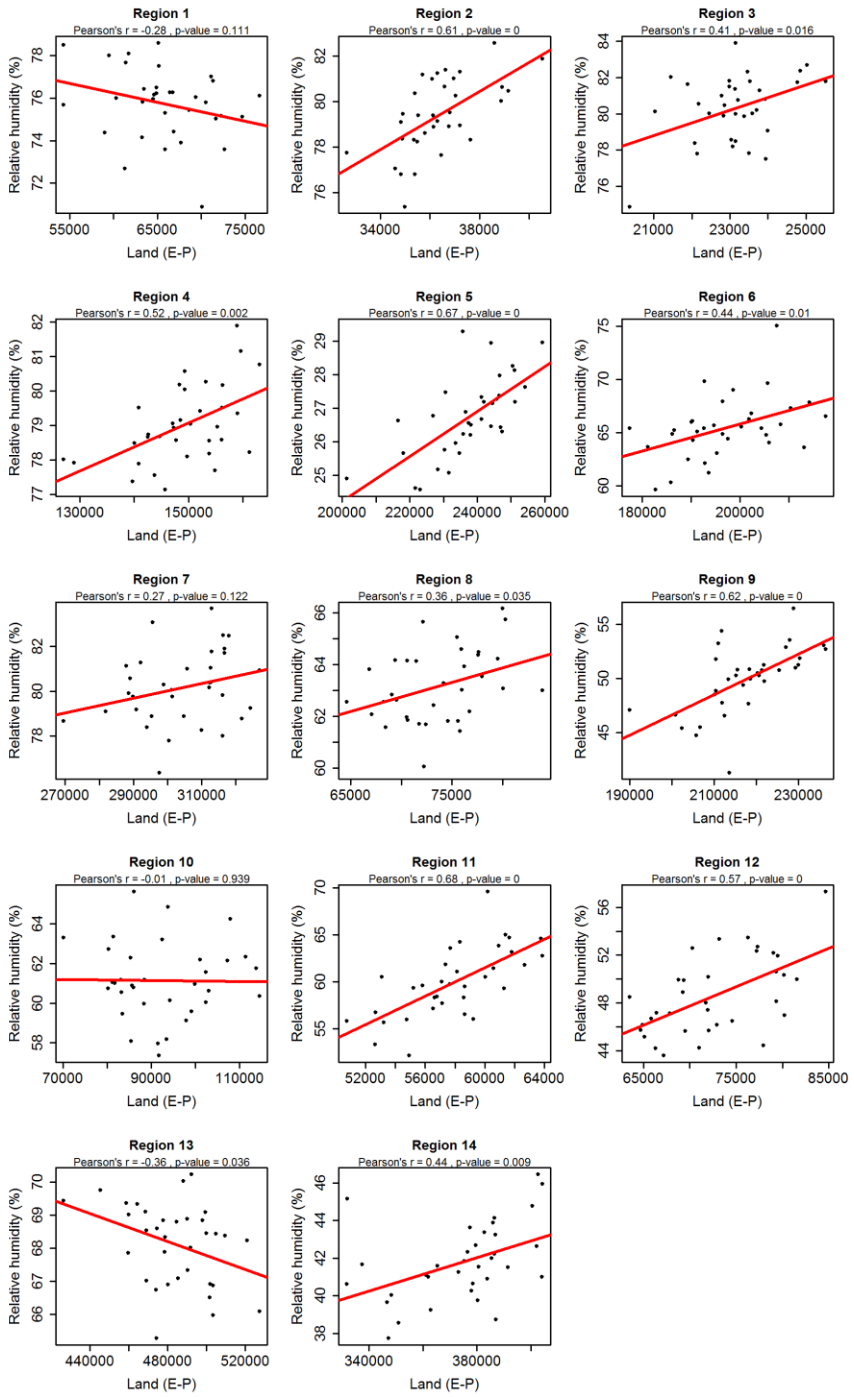

Figure S55: Relationship between the cold season land contribution to cold season precipitation (E-P) and the cold season RH in the target regions.

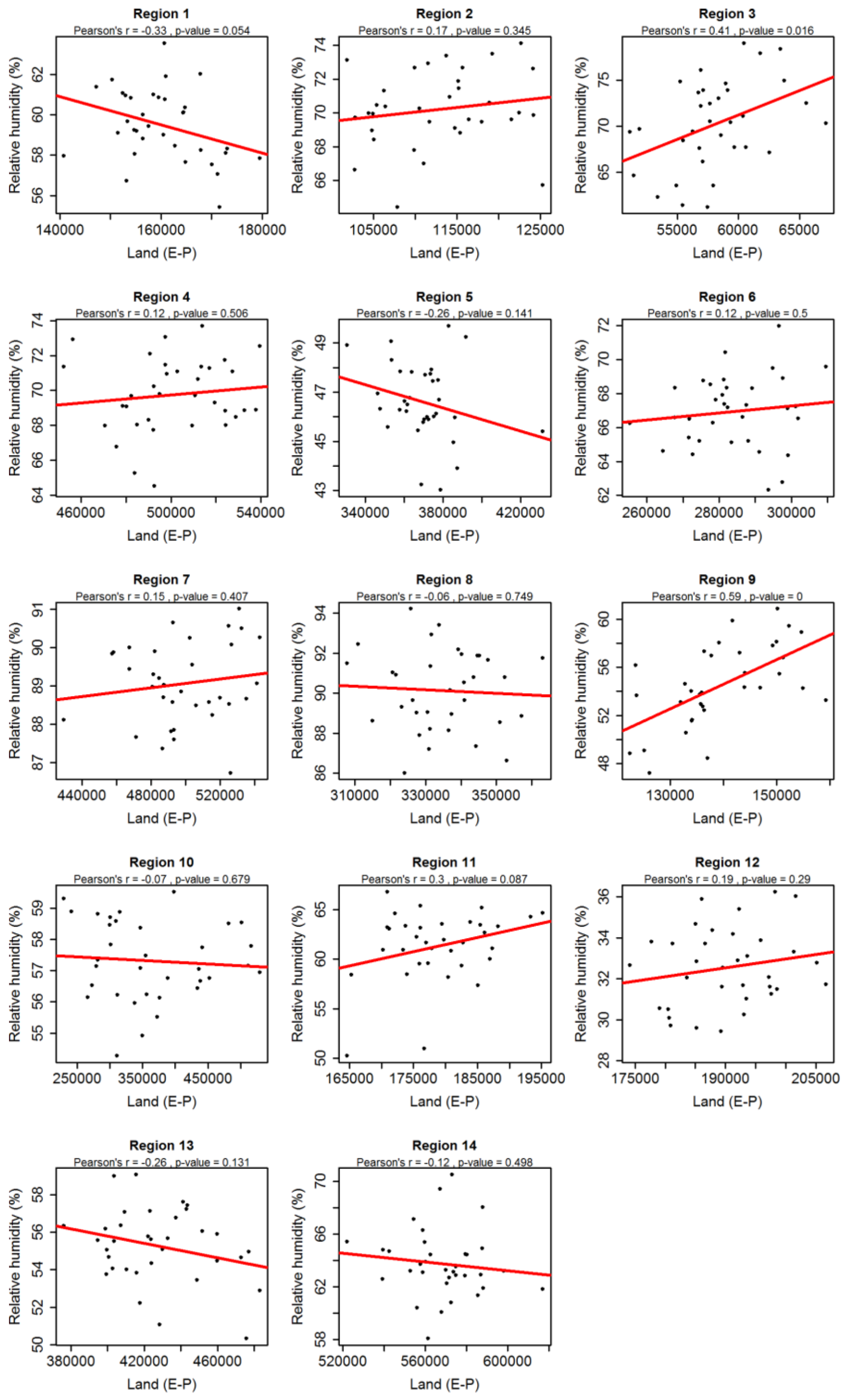

Figure S56: Relationship between the warm season land contribution to warm season precipitation (E-P) and the warm season RH in the target regions.

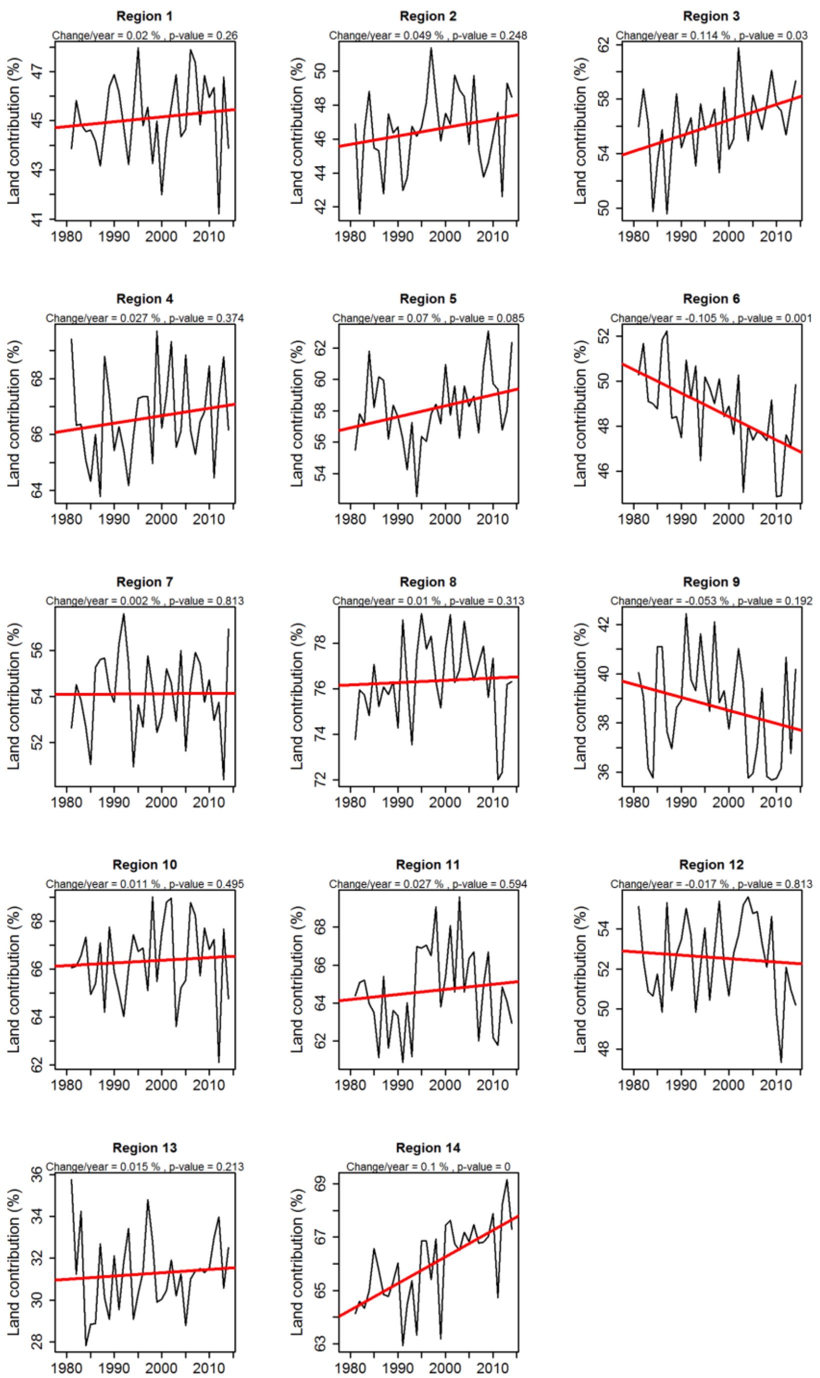

Figure S57: Evolution of the land contribution (%) to warm season precipitation in the different target regions

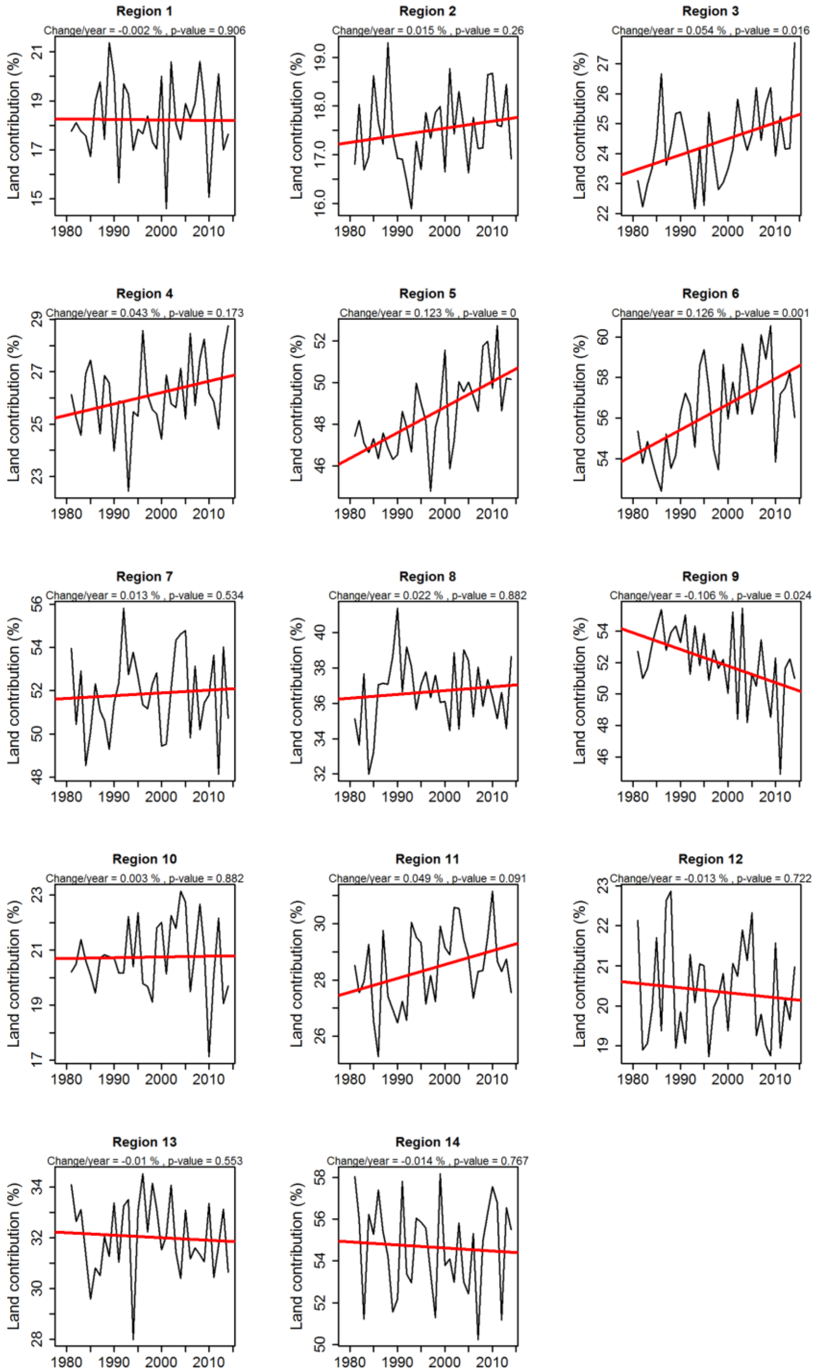

Figure S58: Evolution of the land contribution (%) to cold season precipitation in the different target regions

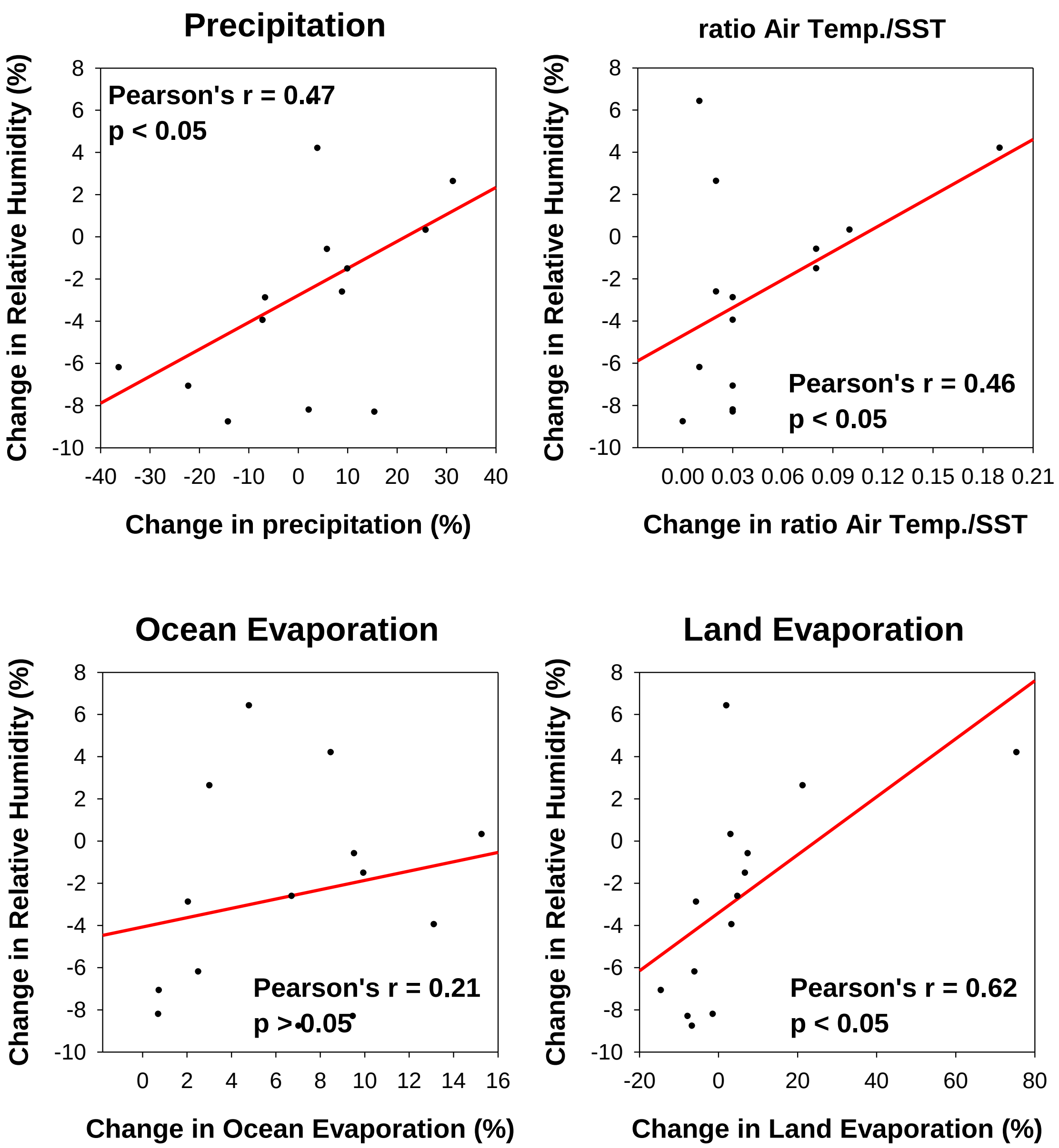

Figure S59: Relationship between the average cold season magnitude of change in RH identified in each one of the 14 analysed region and the cold season magnitude of change in precipitation, the ratio between air temperature/SST, ocean evaporation, land evapotranspiration and the ratio between the ocean evaporation and the land evapotranspiration.

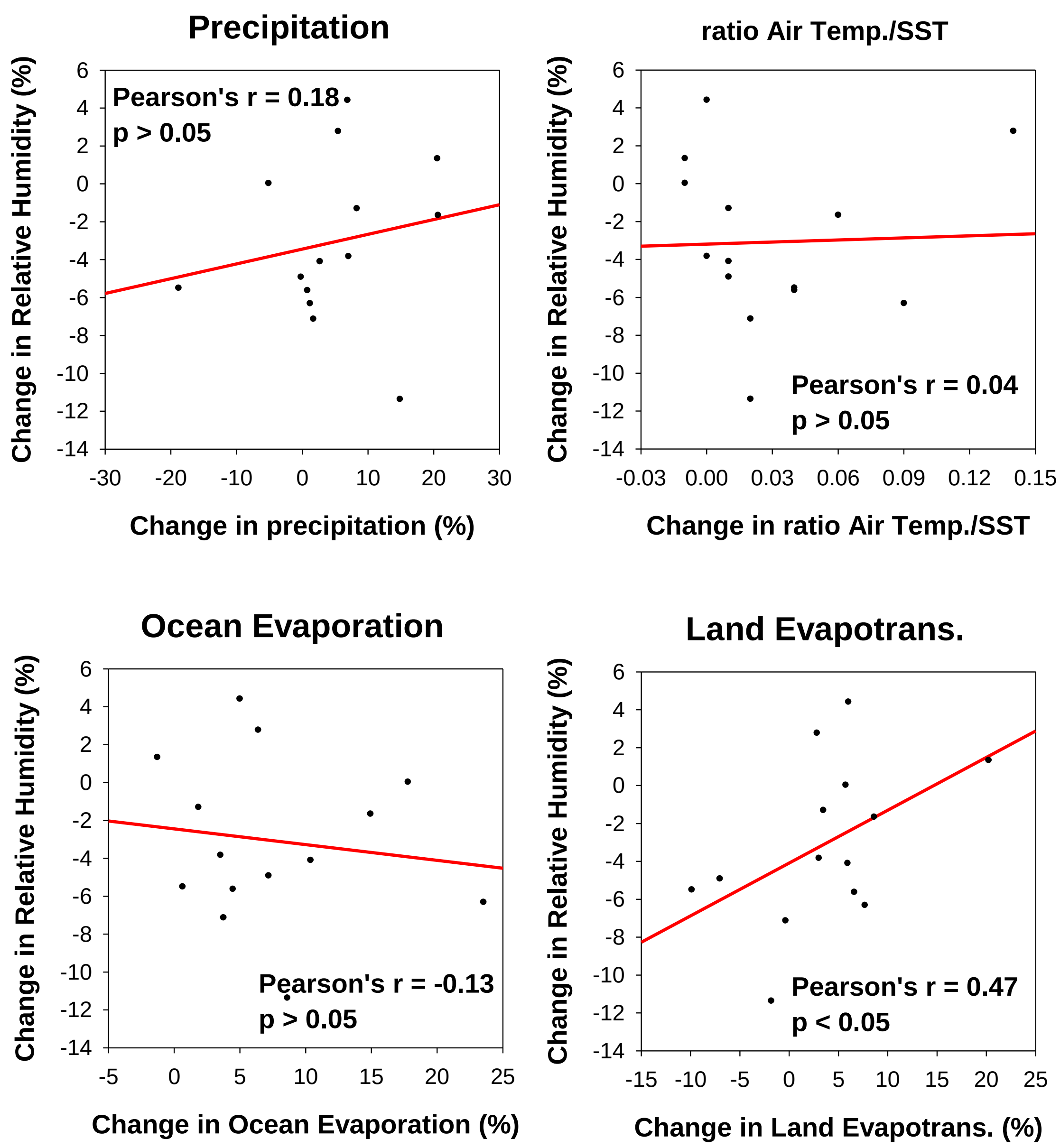

Figure S60: Relationship between the average warm season magnitude of change in RH identified in each one of the 14 analysed region and the warm season magnitude of change in precipitation, the ratio between air temperature/SST, ocean evaporation, land evapotranspiration and the ratio between the ocean evaporation and the land evapotranspiration.

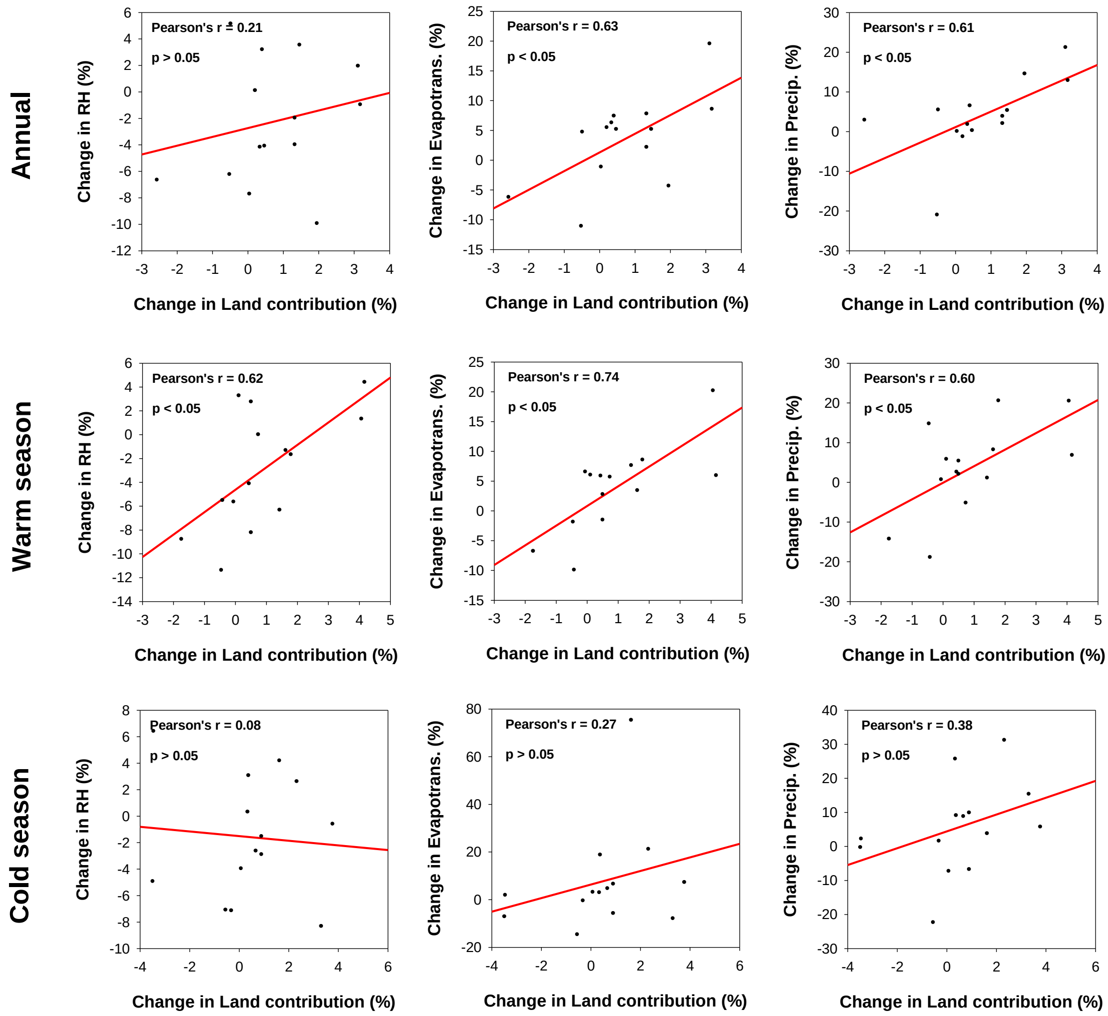

Figure S61: Relationship between the changes in annual and seasonal land contribution (%) to precipitation in the different regions and the annual and seasonal magnitude of change in RH, Evapotranspiration and Precipitation

Region	Cold season	Warm season	Annual
West Europe (region 1)	18.3	45.1	31.6
Scandinavia (region 2)	17.5	46.5	33.1
Central-East Europe (region 3)	24.5	56.2	41.1
South-East Europe and Turkey (region 4)	26.2	66.5	49.2
West Sahel (region 5)	48.6	58.1	54.0
India (region 6)	56.5	48.8	51.8
East China (region 7)	51.9	54.2	53.3
North East Asia (region 8)	36.7	76.4	64.0
La Plata (region 9)	38.7	52.1	45.9
Canada (region 10)	20.1	66.3	47.4
Central USA (region 11)	28.4	64.6	49.3
West North America (region 12)	20.4	52.6	36.7
Amazonian (region 13)	31.3	32.0	31.7
East Sahel (region 14)	54.7	66.1	61.0

Table S1: Percentage of moisture coming from the continental source in each one of the fourteen analyzed regions obtained from the FLEXPART model

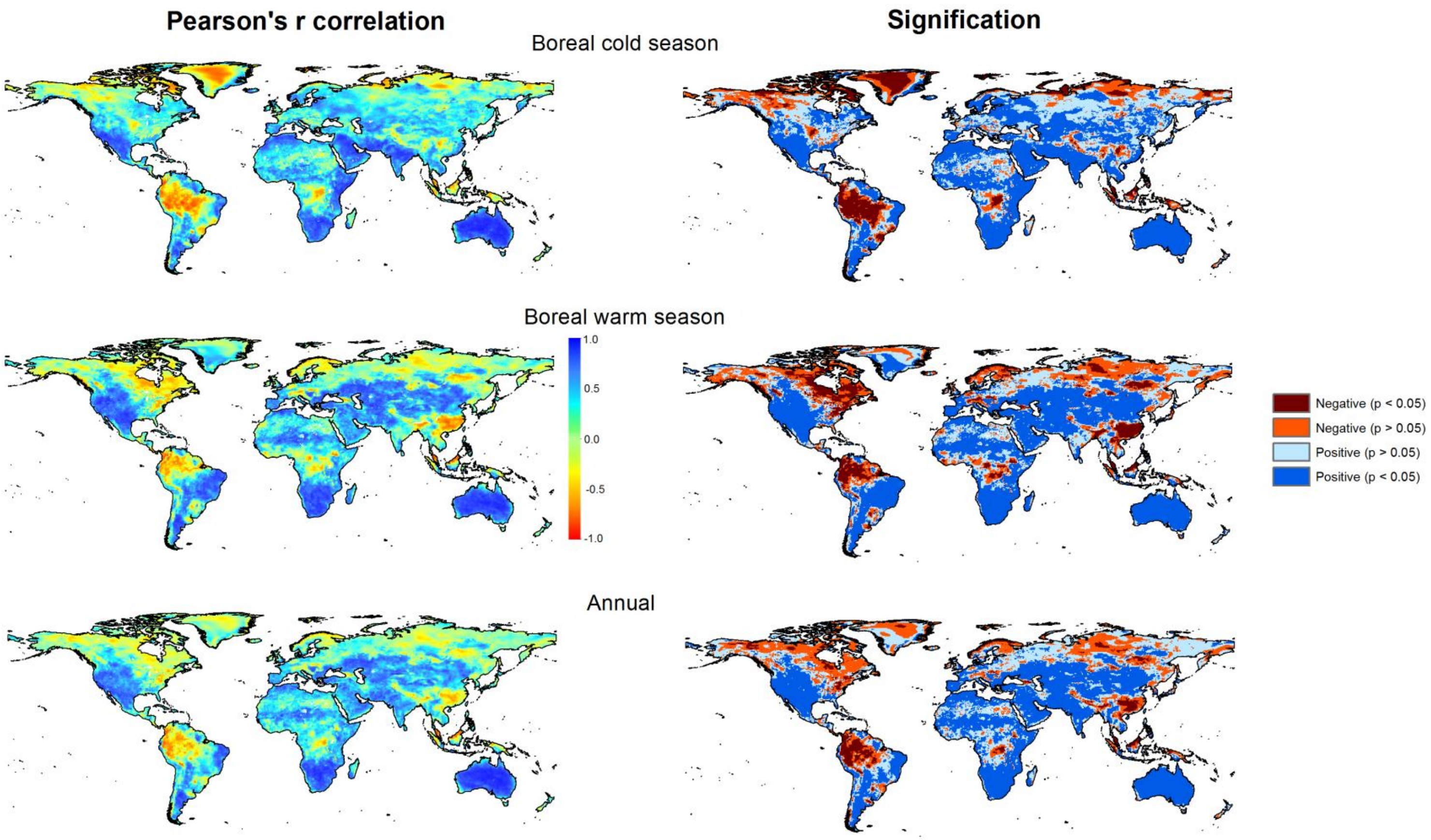

Figure S62: Spatial distribution of the Pearson's r correlations between RH and land evapotranspiration series at the annual and seasonal time scales. Note that these are local ("pixel-by-pixel") correlations and the interpretation differs from the previous analysis where RH in target regions is correlated with ET in corresponding source regions. The statistical significance of the correlations is also shown. Results reveal strong positive and significant correlations in large areas of the world. The strongest positive correlations were found in Central, West and Southwest

North America, Argentina, east Brazil, South Africa, the Sahel, central Asia and the majority of Australia. Nevertheless, there are some exceptions, including large areas of the Amazon, China, central Africa and the high latitudes of the Northern Hemisphere, where the correlations were negative. In general, the areas with positive and significant correlations between RH and land evapotranspiration corresponded to those areas characterized by semiarid and arid climate characteristics, combined with some humid areas (e.g. India and northwest North America). Nevertheless, at the global scale, the correlation between RH and land evapotranspiration shows spatial patterns consistent with those based on the correlation between RH and precipitation.

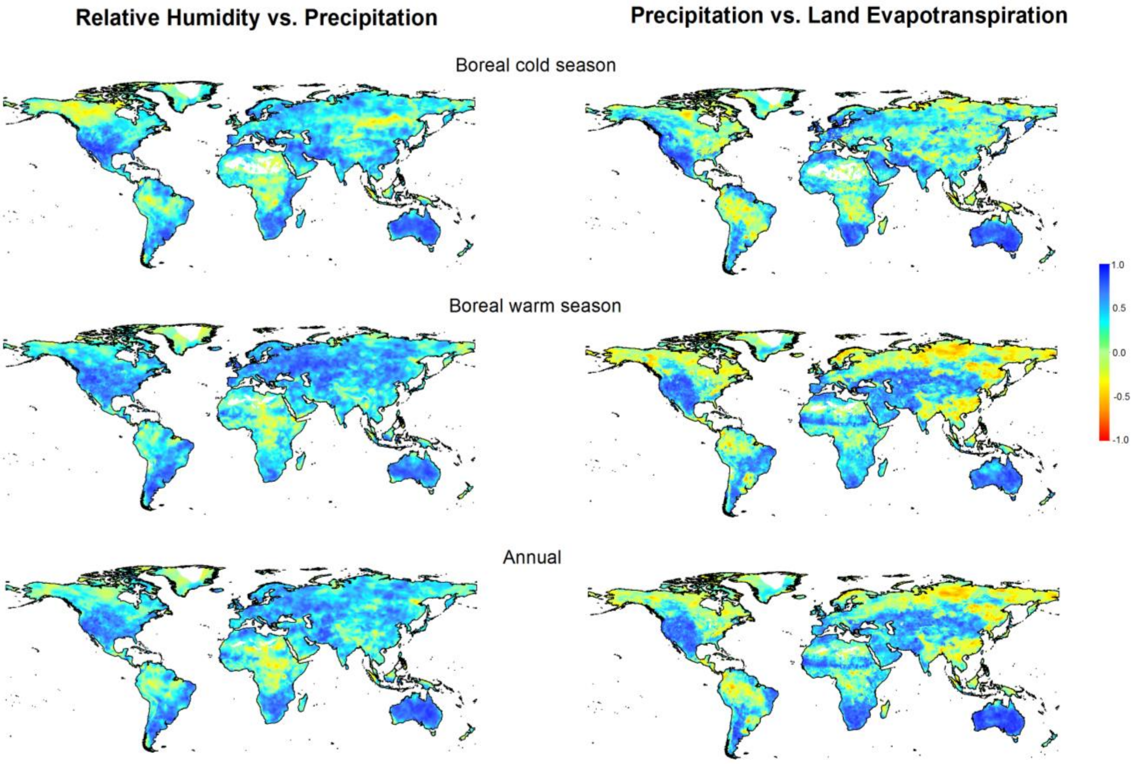

Figure S63: Spatial distribution of annual and seasonal correlations between RH and Precipitation and between Precipitation and Land evapotranspiration.

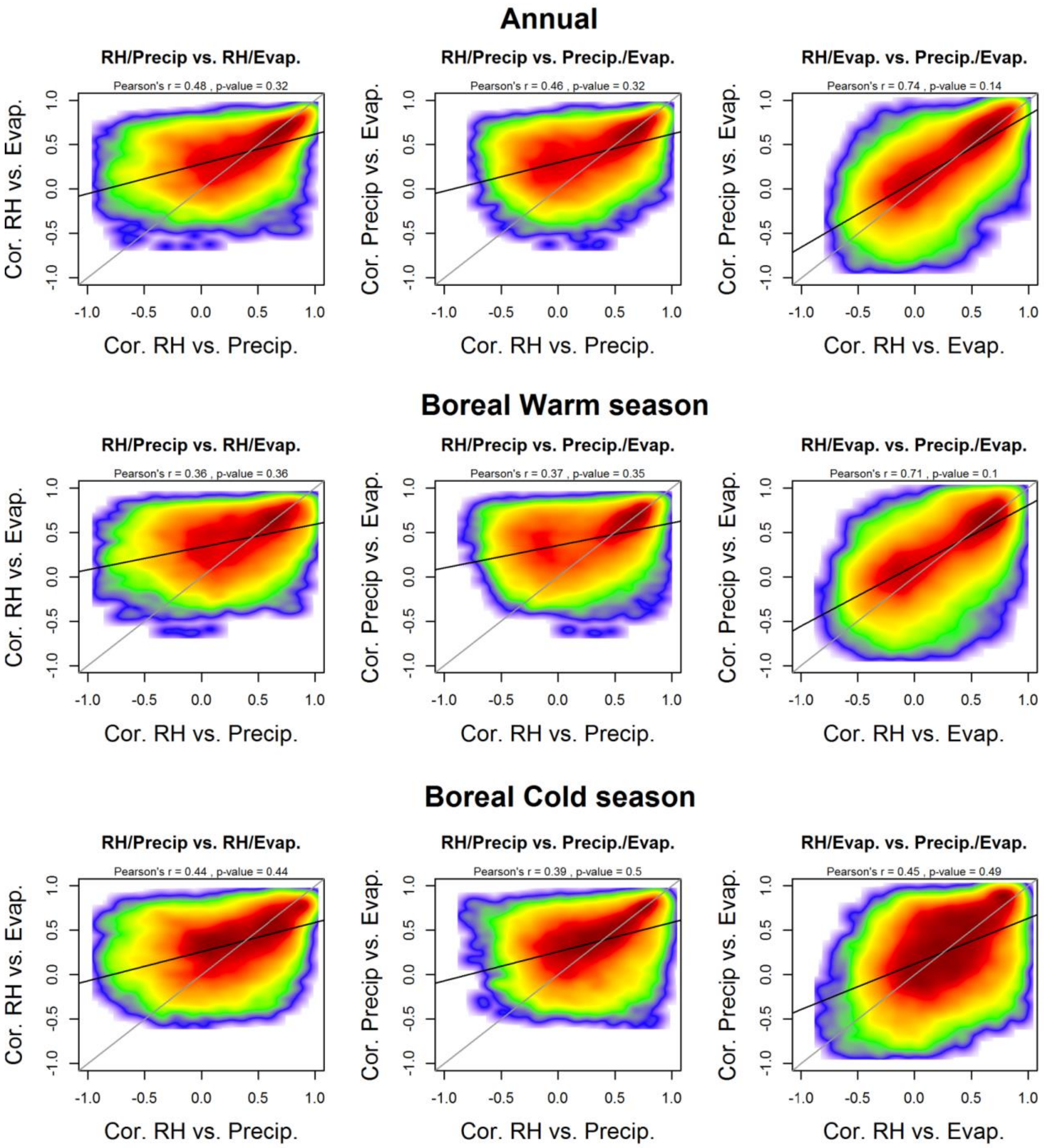

Figure S64: Relationship between the spatial pattern of correlation between RH, precipitation and land evapotranspiration at the annual and seasonal scales. Colors represent the density of points.

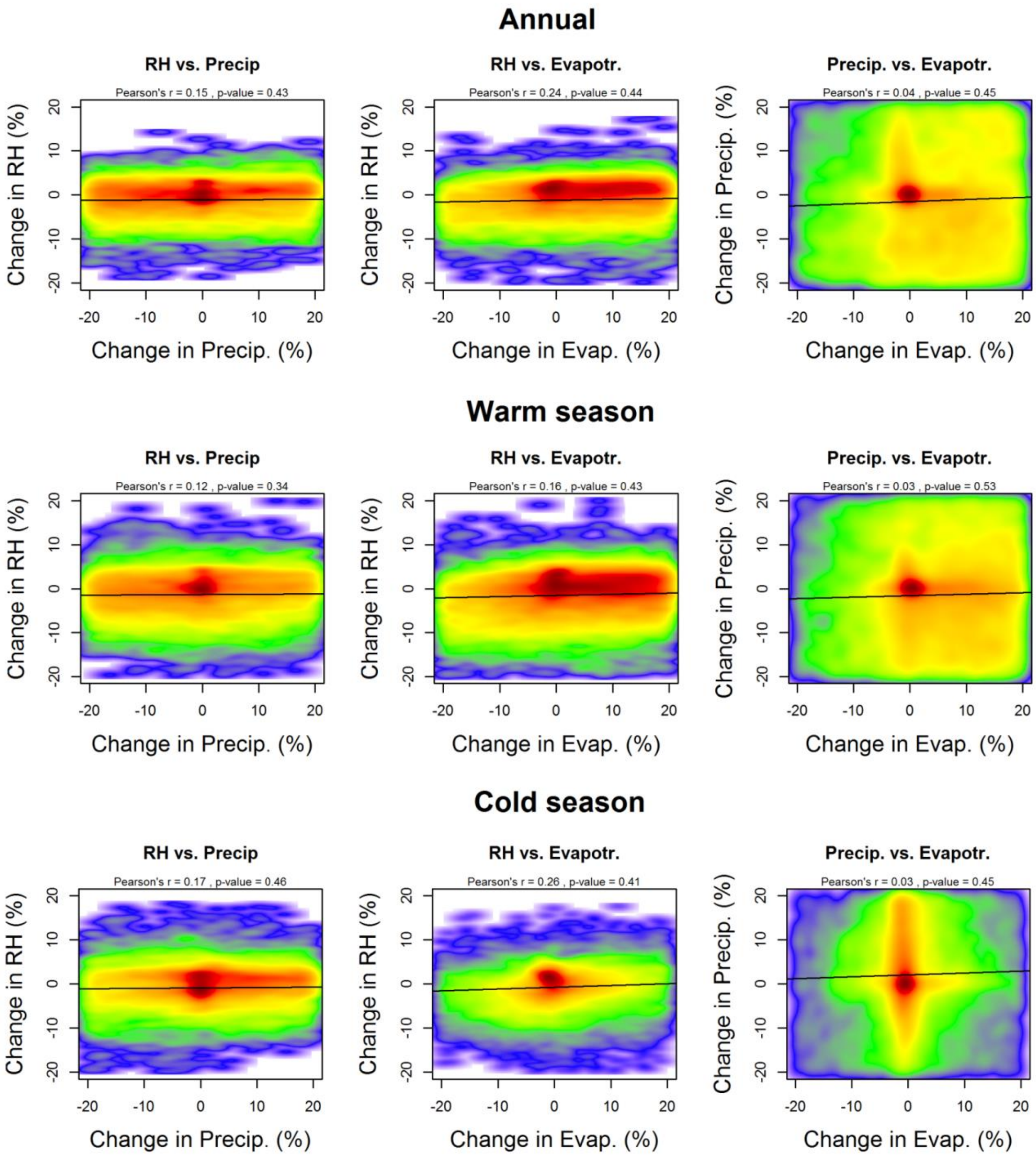

Figure S65: Relationship between the spatial patterns of the magnitude of change of RH, precipitation and land evapotranspiration at the annual and seasonal scales. Colors represent the density of points.

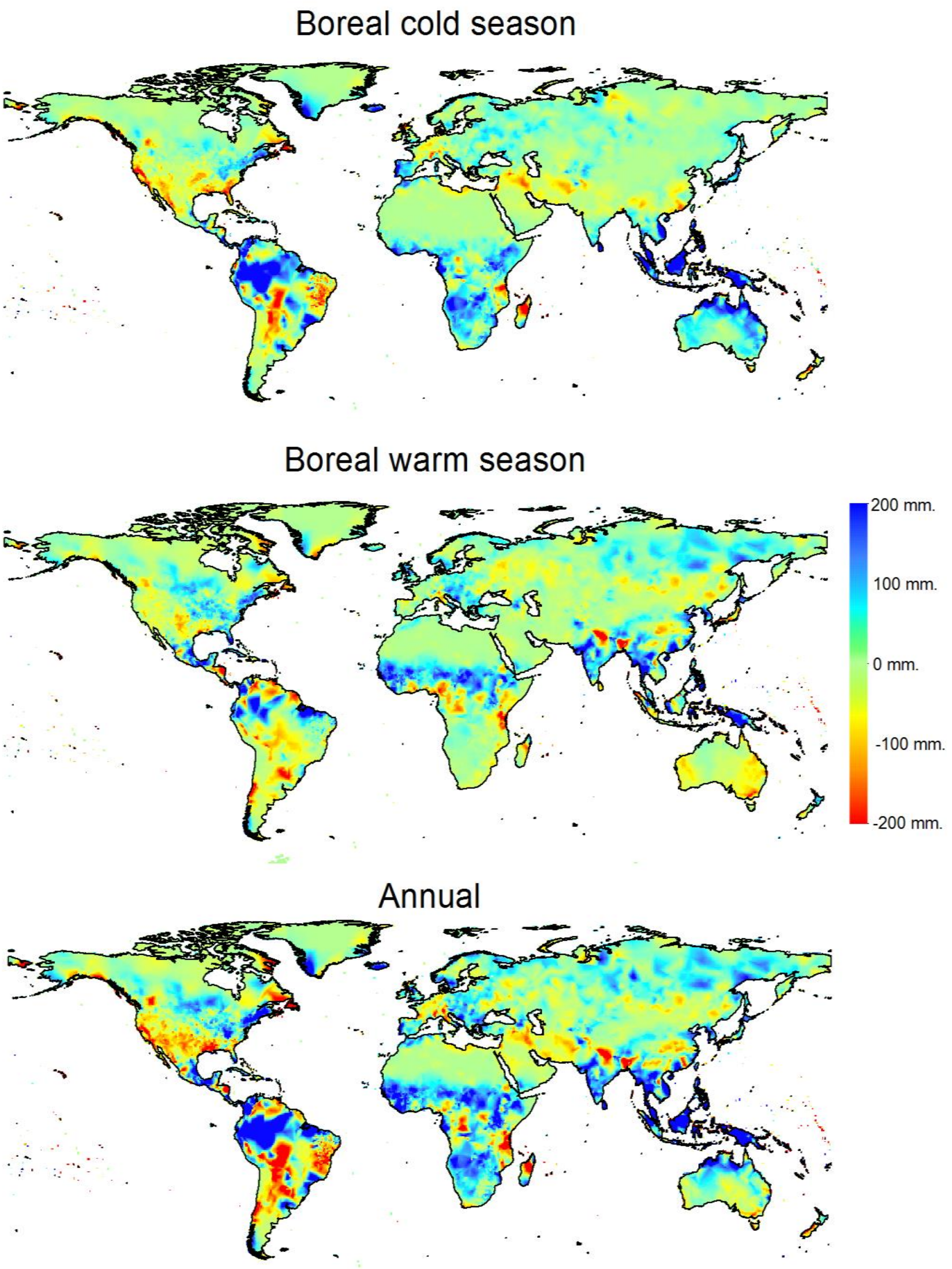

Figure S66: Spatial distribution of the magnitude of change in the precipitation (1979-2014).

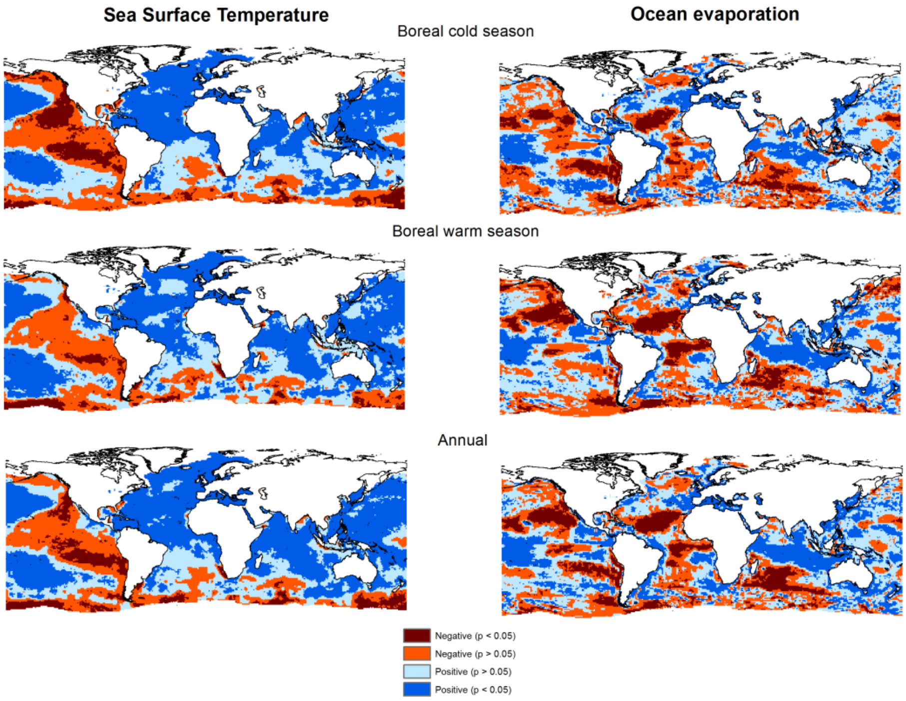

Figure S67: 1979-2014 annual and seasonal signification of trends in SST and OAFLUX ocean evaporation

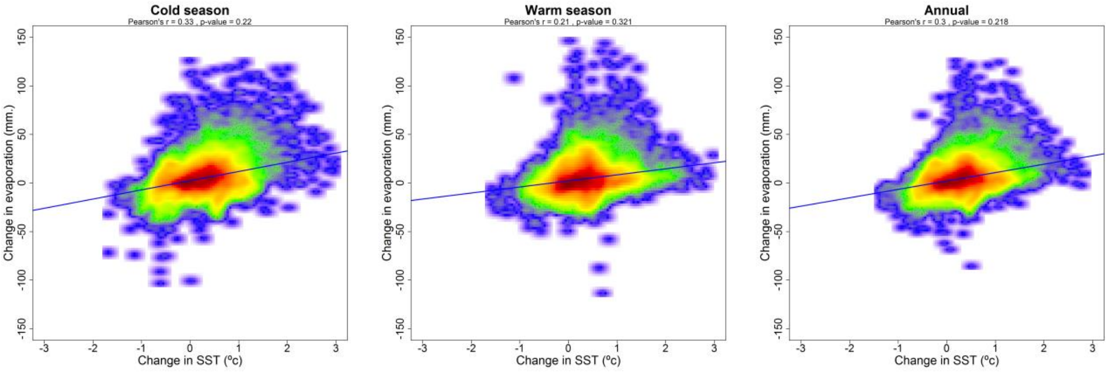

Figure S68: Spatial relationship between the annual and seasonal magnitude of change of SST and Ocean evaporation (1979-2014). Colors represent the density of points.

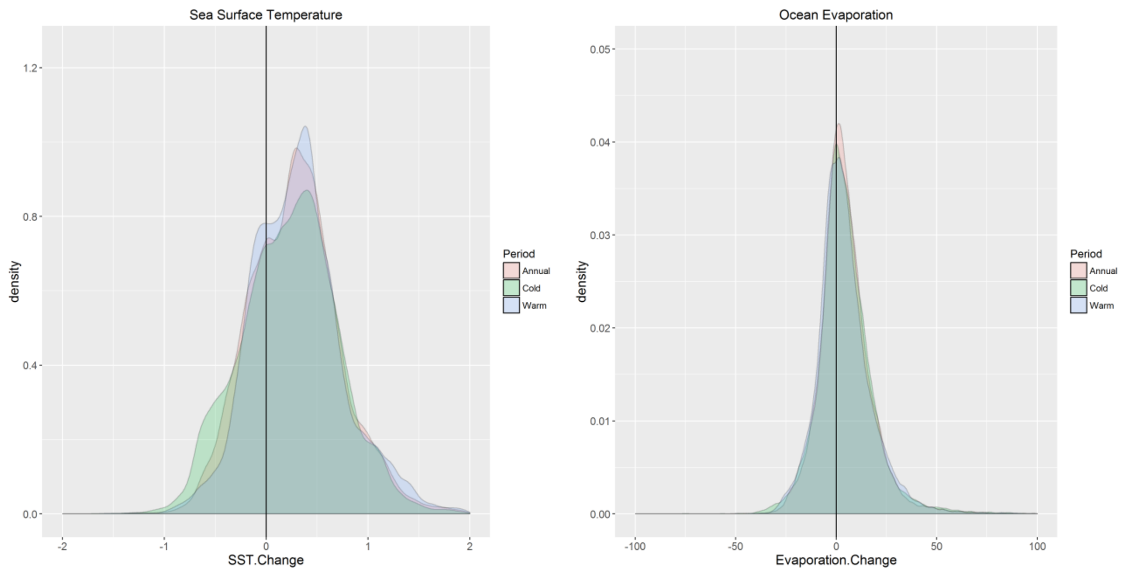

Figure S69: Density plots with the annual and seasonal magnitude of change in SST and Ocean Evaporation (1979-2014)

	Annual SST	Annual Evap.	Cold Season SST	Cold Season Evap.	Warm Season SST	Warm Season Evap.
Positive ($p < 0.05$)	48.2	28.9	40.8	25.9	46.0	23.4
Positive (n.s.)	24.4	34.1	27.4	36.6	28.6	36.0
Negative (n.s.)	19.4	24.7	23.0	27.9	21.1	28.4
Negative ($p < 0.05$)	8.0	12.2	8.8	9.6	4.3	12.1

Table S2: Percentage of Ocean areas showing positive and negative trends in annual and seasonal SST and Evaporation (1979-2014)